REPRINTS

Journal of Oleo Science
Copyright ©2014 by Japan Oil Chemists' Society
doi : 10.5650/jos.ess14071
J. Oleo Sci. **63**, *(12) 1333-1349 (2014)*

Effect of Serum, Cholesterol and Low Density Lipoprotein on the Functionality and Structure of Lung Surfactant Films

Prasant Nahak[1], Kaushik Nag[2], Ashley Hillier[2], Ravi Devraj[2], David W. Thompson[3], Kausik Manna[1], Kimiko Makino[4], Hiroyuki Ohshima[4], Hiromichi Nakahara[5], Osamu Shibata[5] and Amiya Kumar Panda[1]*

[1] *Department of Chemistry, University of North Bengal, Darjeeling, West Bengal, India*
[2] *Department of Biochemistry, Memorial University of Newfoundland, St. John's, NL, Canada.*
[3] *Department of Chemistry, Memorial University of Newfoundland, St. John's, NL, Canada*
[4] *Faculty of Pharmaceutical Sciences, Tokyo University of Science, Noda Campus, Chiba, Japan.*
[5] *Department of Biophysical Chemistry, Faculty of Pharmaceutical Sciences, Nagasaki International University, Nagasaki, Japan*

Abstract: Lung surfactant is a complex mixture of lipid and protein, responsible for alveolar stability, becomes dysfunctional due to alteration of its structure and function by leaked serum materials in disease. Serum proteins, cholesterol and low density lipoprotein (LDL) were studied with bovine lipid extract surfactant (BLES) using Langmuir films, and bilayer dispersions using Raman spectroscopy. While small amount of cholesterol (10 wt%) and LDL did not significantly affect the adsorption and surface tension lowering properties of BLES. However serum lipids, whole serum as well as higher amounts of cholesterol, and LDL dramatically altered the surface properties of BLES films, as well as gel-fluid structures formed in such films observed using atomic force microscopy (AFM). Raman-spectroscopic studies revealed that serum proteins, LDL and excess cholesterol had fluidizing effects on BLES bilayers dispersion, monitored from the changes in hydrocarbon vibrational modes during gel-fluid thermal phase transitions. This study clearly suggests that patho-physiological amounts of serum lipids (and not proteins) significantly alter the molecular arrangement of surfactant in films and bilayers, and can be used to model lung disease.

Key words: lung surfactant dysfunction, BLES, LDL, cholesterol, serum protein, Langmuir films, Raman-spectroscopy, AFM

1 Introduction

Pulmonary or lung surfactant (LS) is secreted by the alveolar type II epithelial cells[1]. From its secreted bilayer form (lamellar bodies) LS transforms into tubular myelin and gets adsorbed at the air–liquid interface to form a tightly packed monomolecular film. The film reduces the surface tension to low value as the area of the alveolar interface decreases upon expiration. The mono-molecular film becomes compressed to near 0 mN/m value and this prevents alveolar collapse and maintains air-way patency. Lipids are the main components of pulmonary surfactant. Among them, dipalmitoylphosphatidylcholine (DPPC) and phosphatidylglycerol (DPPG) are the most characterized and abundant phospholipids. While DPPC (40-50 wt% of the lipid pool) is responsible for maintaining the surface tension near zero during compression, presence of other fluid lipids are also essential in order to re-spread the compressed film easily[2, 3]. Beside the phospholipids, there are four surfactant associated proteins, SP-A, SP-B, SP-C and SP-D. While SP-A and SP-D are hydrophilic, the other two surfactant proteins (SP-B and SP-C) are hydrophobic and attenuates the surface tension of LS[4, 5]. The most abundant neutral lipid in pulmonary surfactant is cholesterol, amounting to 5-10 wt% (or 10-20 mol%) of the phospholipids[6]. Even though the presence of cholesterol in surfactant has long been recognized, however, little is known about its function[2, 6, 7]. Some studies suggests that in the presence of the hydrophobic surfactant proteins cholesterol is essential for fluidity control[6], surface tension reduction and adsorption of other phospholipids onto the monolayer[8–10].

*Correspondence to: Amiya Kumar Panda, Department of Chemistry University of North Bengal Darjeeling – 734 013 West Bengal, India
E-mail: akpanda1@yahoo.com
Accepted August 5, 2014 (received for review April 11, 2014)
Journal of Oleo Science ISSN 1345-8957 print / ISSN 1347-3352 online
http://www.jstage.jst.go.jp/browse/jos/ http://mc.manusriptcentral.com/jjocs

However previous studies also suggest that excess cholesterol also has deleterious effects, *e.g.*, it retards the achievement of minimum surface tension to near zero value during complete film compression and decrease of post collapse re-spreading[11].

In adult respiratory distress syndrome (ARDS) and acute lung injury (ALI) elevated levels of serum materials such as soluble proteins and some lipids are found in the extracted LS. These LS are also found to have reduced surface activity, although the cause for this is not clear[11]. An early study by Haas and Longmore showed that although the lung can produce cholesterol much larger in amount than its own requirement, the main mechanism used in the production of surfactant cholesterol is the use of lipoprotein cholesterol supplied form the blood, since about 2 wt% of the cholesterol is from endogenous synthesis[12]. Other studies have established that lipoproteins such as low density lipoproteins (LDL) not only supply cholesterol to surfactant but also affect the secretion of surfactant from the type-II cells[1, 6, 13].

Previous studies have shown that cholesterol present in LS in physiological amounts has no deleterious effect on LS function[9]. However in ARDS and ALI some serum materials, which leak from the capillaries into the fluid lining of the lung, inactivates LS. Most previous studies have suggested that it may be serum soluble proteins which can inactivate surfactant, however *in vitro* studies require very high amounts of proteins to provide such inactivation. It is known that some serum proteins which leak from the capillaries into the fluid lining the lungs may render LS inactive. However some recent studies have suggested that excess amounts of cholesterol or other serum lipid components are far more potent inhibitor of LS[8–10]. Previous studies on serum albumin, C-reactive protein, fibrinogen and others have shown that these proteins affect the structure-function properties of LS in very high non-patho-physiological amounts when studied *in vitro*[15–18]. However there are evidences that serum protein levels in pathophysiological lungs only increase by three folds, which cannot inactivate surfactant. In an earlier study we have shown that cholesterol levels in such lungs only increases by two fold, and completely inactivates surfactant[19]. In another study we have also observed that whole serum is a far more potent inactivator of LS than its soluble protein fraction[17].

Bovine lipid extract surfactant (BLES) a clinically used surfactant developed in Canada is used for treating patients with ARDS[11]. The material contains all surfactant lipids and proteins except the hydrophilic SP-A and SP-D, and the neutral lipid cholesterol, which are synthetically removed. This allows in vitro studies with BLES with various increments of cholesterol or serum proteins[8–11]. In a previous study we have used foetal calf serum (FCS) with BLES and have found that the serum (with its lipids and proteins) is 200 times more potent inactivator of LS than its protein component albumin[17]. FCS is very similar in composition to human serum. Human serum mainly consists of albumin, fibrinogen, CRP, globulin among other proteins, and also ions, amino acids, sugars (fructose and glucose) as well as serum lipids and lipoproteins such as LDL[20–22].

In this study we have investigated the normal and pathophysioligcal amount of FCS, and serum lipids (cholesterol and LDL) with BLES using a set of correlated biophysical and structural methods previously used to study surfactant dysfunction mainly with proteins[15–17]. Detailed Iatrascan and Matrix Assisted Laser Desorption/Ionization –Time of Flight (MALDI-TOF) suggested the exact composition of BLES and FCS lipid components. Langmuir surface balance and adsorption studies suggested the alterations of surface activity of the BLES by FCS lipids, as well as Atomic Force Microscopy (AFM) suggested the structural alteration of the gel-fluid domain distribution in such functionally altered films. Raman-spectroscopy was applied to such BLES/additive bilayer dispersions used to form such surface films, to suggest alteration of molecular packing of the surfactant phospholipid chains in such bilayers from monitoring hydrocarbon vibrational modes during thermal transitions.

2 Materials and Methods

2.1 Materials

Samples were prepared with supplied exogenous lung surfactant, Bovine Lipid Extract Surfactant (BLES®) dispersion and 10 and 20 wt% of foetal calf serum (FCS), cholesterol, and low density lipoprotein (LDL). The clinically used BLES suspension (27 mg/mL) was a generous gift from Dr. Dave Bjarnson of BLES® Biochemicals Inc. (London, Ontario, Canada) and was used without further modification. FCS (7 mg/mL), LDL (5 mg/mL), and cholesterol (crystalline form) were all purchased from Sigma-Aldrich Inc. (USA), and were used as received. HPLC grade solvents, chloroform and methanol, were purchased from Fischer Scientific (Ottawa, Ontario, Canada). Most samples were studied in the buffer using 0.15 M NaCl-Trizma®. HCl buffer at pH 7 to maintain optimum pH and ionic conditions for LS. The NaCl-Trizma®. HCl buffer used in this study was prepared by the addition of 150 mM NaCl and 5 mM (~0.08 g) Trizma hydrochloride in 1 litre of double distilled water and the pH was adjusted to 7 by titrating with 0.1M NaOH[15]. Each sample was prepared by incubating desired amount (10 and 20 wt%) of FCS, cholesterol and LDL with appropriate amounts of BLES followed by thorough mixing. Small aliquots were diluted appropriately with buffer to be used for all monolayer and bilayer model studies. This was done to ensure that the similar stock of samples was used in all experiments and to avoid heterogeneity of sample concentration and composition.

All solution preparation and experiments were conducted using double distilled water (ddH_2O). Glassware used were washed by perchloric acid followed by rinsing with ddH_2O and were dried for 2 hrs. at 180℃ to remove any organic and surface active impurities[23].

2.2 Lipid extraction of samples

While conducting the monolayer, AFM, Raman and some mass spectrometric studies on BLES and BLES + cholesterol, BLES was extracted in hydrophobic solvents from aqueous dispersions according to the Bligh and Dyer method[24]. Briefly, in this method, 0.8 mL of BLES dispersion (27 mg/mL) was mixed with 3 mL of chloroform : methanol (3:1, v/v), in a test tube and homogenized by mechanical shaking. One part of chloroform along with one part of double distilled water was added then and again vortexed to ensure uniform mixing. The mixture was then centrifuged for 2-3 minutes at 1000 rpm in order to separate the organic and aqueous layers. The organic phase at the bottom layer was carefully taken out into a glass vial with a glass pipette without disturbing the aqueous layer. This extraction process was repeated with remaining aqueous layers using 2:1 chloroform-methanol. All organic extracts were kept in a single vial. It was then placed under nitrogen gas flow to dry and kept overnight in a vacuum desiccator to make it free from trace amounts of organic solvent. Cholesterol was added to BLES and after the addition the sample was suspended in the chloroform-methanol mixed solvent, which was then dried under nitrogen gas and re-suspended in a saline buffer[17]. The BLES-cholesterol mixture was re-suspended in a saline buffer, by vortexing above 30℃, to obtain multi-lamellar vesicles as observed using electron microscopy by methods discussed elsewhere[19]. To identify the lipid components of both FCS as well as LDL, the lipid portions of each sample were extracted by using modified Bligh and Dyer method[17, 24]. The organic layer of each was dried under nitrogen and the residue was then used for analysis by Matrix-Assisted Laser Desorption Ionization-Time of Flight Mass Spectrometry (MALDI-TOF MS) using 0.5 M 2,5-dihydroxybenzoic acid (DHB) matrix.

2.3 Methods

Pure BLES as well as BLES in the presence of 10 and 20% serum or cholesterol or LDL were chosen for the present set of studies. Selections of these amounts of additives were not arbitrary since these concentrations are patho-physiologically relevant as noticed in diseased as well as in the normal lung surfactant lavages[11, 19]. Adsorption, surface tension-area isotherm and AFM measurements were performed to investigate the function and structure of monolayer films, whereas the use of Raman spectroscopy was to examine the bilayer phases. Experiments were performed at a controlled ambient temperature of 23℃, except Raman spectroscopy, which were conducted in the temperature range 10-40℃. The studies were conducted with this ambient temperature since AFM studies could not be performed at higher temperature, as well as the Langmuir surface balance had a subphase volume of 5 litre, which cannot reach higher temperature equilibrium without surface evaporation. A previous study on higher temperatures suggested that there are no major or significant differences in adsorption and surface tension changes between ambient and physiological temperatures for BLES[17].

2.3.1 Adsorption kinetics studies

Adsorption experiments were carried out by surface tension study (plate detachment method). Sample dispersions were injected thorough a rubber valve into a cylindrical teflon cup of 5 mL capacity and a surface area of 6.28 sq. cm[15]. Samples were homogenized by constant stirring and adsorption of sample to the interface was determined by the drop in surface tension, by using a Wilhelmy platinum dipping plate.

2.3.2 Langmuir Surface Balance Studies

A Langmuir-Wilhelmy balance (Applied Imaging, London, England) was used to record the surface tension (γ) – area isotherm for the adsorbed films. This balance has an initial open area of 500 cm^2, which was large enough to allow compression of films to lower γ values very close to 1 mN/m[15–17]. A motorized leak-proof rectangular teflon tape barrier was used to compress and expand the monolayer films while a platinum Wilhelmy plate hanging from a force transducer detected the change of γ[17]. Prior to beginning each experiment, the trough was thoroughly cleaned with chloroform : methanol (3:1, v/v) mixture and then with ddH_2O. Each time the interface was suctioned off and the trough was dried. The trough was filled with ddH_2O to simulate an air-water interface. BLES and BLES + 10 and 20 wt% samples of serum or LDL or cholesterol (systems) dispersions were allowed to form adsorbed films with an initial γ drop close to 60 mN/m. Compression and expansion of monolayer films were conducted at a rate of 2 mm^2/sec. Compression allowed the lipid monolayer to undergo a fluid to gel phase transition. Details of the Langmuir-Blodgett method using this trough have been previously published[15–17]. This balance was also used to deposit films using Langmuir-Blodgett transfer technique at various γ on pre-immersed freshly cleaved mica substrate for AFM studies[25, 26]. Adsorbed films were compressed to the desired γ values. Pre-immersed mica disc was then vertically lifted out off the subphase with an upstroke of 1 mm/sec in order to get the Langmuir-Blodgett films[30]. A standard surface tension vs. percent film area protocol was adopted for showing the surface tension-area isotherms data instead of the standard surface pressure-area per molecule isotherms. This was done due to technical difficulties in calculating the exact area per molecule of "ad-

sorbed" films as well as comparing the γ data with some previous studies using captive bubble methods, where surface area data are redundant and can not be calculated with accuracy[9]. The details of the techniques and physics of the Langmuir Balance and trough have been previously published[25].

2.3.3 Atomic Force Microscopy (AFM)

Langmuir-Blodgett deposits of BLES, with or without additives, were used for structural studies using AFM. A teflon dipping head with three freshly cleaved mica disks was lowered into the water subphase before the sample film was made. Compression (2 mm^2/sec) from ~60mN/m to stepwise decrease of three desired surface tensions (52, 42 and 32 mN/m, respectively) was conducted and the compression was kept stopped during each deposition. When the desired surface tension was attained, the dipping head was slowly retracted vertically at a rate of 1 mm^2/sec[17]. Monolayers were deposited on flat surfaces of mica, and were imaged with a Nanoscope IIIa atomic force microscope (AFM, Digital Instruments, CA, USA). A silicon nitride tip, attached to a cantilever was laterally moved across the surface of the deposited sample by the Nanoscope software in contact mode[25-27]. Samples were imaged within two hours from the films being deposited to prevent dehydration[17]. The images were processed using IGOR Pro software (WaveMetrics, Portland, Oregon, USA) to produce 2D, 3D and sectional images, similar to those obtained using Nanoscope IIIa software. To easily compare domain sizes and heights, each field size, Z-scale and deposited surface tensions of all samples were kept reasonably close to the best of our ability. At least 3-4 random spots were scanned for each sample and the best representative images are displayed.

2.3.4 Raman Spectroscopy

In the present study a Raman Spectral-microscope (RMS) (LABRAM confocal microscope, Horiba Jobin Yvon, Edison, NJ, USA) with a grating of 1800 grooves/mm was used. A Leica microscope with a long working distance objective (50X) attached to the spectroscope with a Peltier CCD detector allowed for direct imaging of the samples while collecting spectra at different temperatures of heating-cooling cycles. A 532nm green laser (diode pumped solid state laser) line was excited to yield the spectra. Each spectrum had an accumulation time of 6-20 seconds and was passed through the D_0 filter to find the best representative average spectrum. The shortest time (1 minute per degree) for collection was chosen to prevent sample evaporation and drying[15]. Samples were taken in a small glass cuvette and were placed in the sample chamber of the microscope. The temperature was controlled by a thermostated water bath (5-50℃), and spectrum collected for each 2℃ increments of heating or cooling to induce phase transitions. Details of similar methods have been published previously[15, 28-31].

2.3.5 MALDI-TOF MS

For Matrix Assisted Laser Desorption-Ionization time of flight mass spectrometry (MALDI-TOF MS) studies on lipid analysis an applied Biosystems voyager system 1027 (Voyager-DE™) mass spectrometer was used to analyze the lipid components of BLES, LDL and serum lipid extracts to specifically measure the difference of cholesterol and cholesterol esters in these samples, as well as some studies were followed up using Iatroscan. 100 μL of samples dissolved in chloroform: methanol (3:1, v/v) were injected in the MALDI by the methods discussed in detail elsewhere and the profiles obtained as intensity as a function of mass/charge (m/z)[32].

3 Results

3.1 Composition of Serum and Surfactant

To identify lipid components of whole FCS, both MALDI-TOF and IATRO-Scan studies were carried out. BLES extract was also used in MALDI-TOF mass spectrometry. Figure S1 shows the spectra for (a) BLES, (b) serum lipids and (c) LDL. BLES exhibits an intense peak at 735 m/z (molecular wt. of DPPC + H^+). This is the parent ion peak for DPPC, confirming that BLES contains mostly DPPC. The other peaks in 700-800 (m/z) range are for other phosphocholine classes especially the fluid 16:0/18:1 PC. In order to investigate the lipid classes comprising whole serum [Fig. S1 (a)], the spectra suggests a variety of lipids but showed the high intensity peak of cholesterol at approximately 369 m/z. Cholesterol is not detectable as a whole molecule, but detectable only upon the elimination of water as shown in Fig. S1 (b)[34]. The highest peak for LDL samples are possibly cholesterol ester fragments as shown in Fig. S1 (c). These lipids and there fragments were also previously detected by others[32, 33] and our Iatrascan results support these findings. The data from the Iatroscan of serum are

Table 1 Iatroscan data of serum: the components present in serum and their percent composition.

Lipid Classes	*Lipid Composition* (%)
Hydrocarbons	5.86
Steryl esters/wax	37.85
Ketones	2.90
Triacylglycerols	6.51
Free fatty acids	11.51
Alcohols	4.90
Sterols	6.14
Acetone mobile polar lipids	3.30
Phospholipids	21.02

also shown in Table 1 where the serum lipids were extracted from the FCS. The highest amount of lipids was stearoyl esters (37%-cholesterol ester) and phospholipids (21%). The Iatroscan method combined thin-layer chromatography and flame ionization detection[34, 35]. With this method, a lipid mixture (serum), was separated using silicic acid coated quartz rods and then quantified using flame ionization detection[35] to measure the lipid classes present[35].

3.2 Adsorption Isotherms

Adsorption isotherm of BLES in the absence and presence of serum, LDL and cholesterol is presented as a function of time (Fig. 1). Adsorption of lipids onto the air-water interface over time (seconds) was recorded by monitoring γ continuously for 300 seconds. Measurements were carried out in the presence of 10 and 20 wt% serum, cholesterol and LDL with BLES keeping the total volume constant by dilution with buffer. Each adsorption curve represents the average of three replicate experiments, with the standard deviation represented by error bars. Results are also summarized in Table 2. Pure BLES adsorbed ($\gamma \approx 20$ mN/m) within 100 seconds on to the air-water interface. With the addition of serum and LDL to BLES γ shifted to higher values and after 300 seconds observed γ value of these two systems were almost double that of pure BLES. The adsorption of BLES did not change significantly with the addition of cholesterol. These results suggest that serum and LDL did not allow BLES to be adsorbed rapidly (to equilibrium γ) to the air-water interface. It should be noted that physiological amounts of cholesterol (10 or 20%) had no significant effects on adsorption.

3.3 Langmuir Surface Balance Studies

Multiple compression and expansion cycles of the adsorbed films of BLES and BLES-serum, BLES-LDL and BLES-cholesterol was performed and compared. The same concentration of sample lipid (100 μg/mL) per group was added in each of the three trials, and the films were formed by initial adsorption of the dispersions. Compression-expansion cycles were carried out at a speed of 2 mm^2/Sec after initial equilibrium adsorption of the films to ~62 mN/m. Figure 2 compares compression-expansion isotherms of (a) BLES in buffer with (b) 10wt% serum, (c) 20 wt% serum, (d) 10 wt% cholesterol, (e) 20 wt% cholesterol, (f) 10 wt% LDL, and (g) 20% LDL. Pure BLES film, when fully compressed, could attain the γ to a minimum of near ~1 mN/m value from an initial value of 60 mN/m. Upon addition of serum to BLES, there occurred a drastic shift of the minimum surface tension to higher values (30 mN/m). Addition of LDL resulted in similar behavior as in the case of serum. No significant change was observed in presence 10wt% (physiological amount) cholesterol compared to pure BLES. But excess (20wt%) cholesterol lifted the minimum to a γ~15 mN/m. Such an observation implies

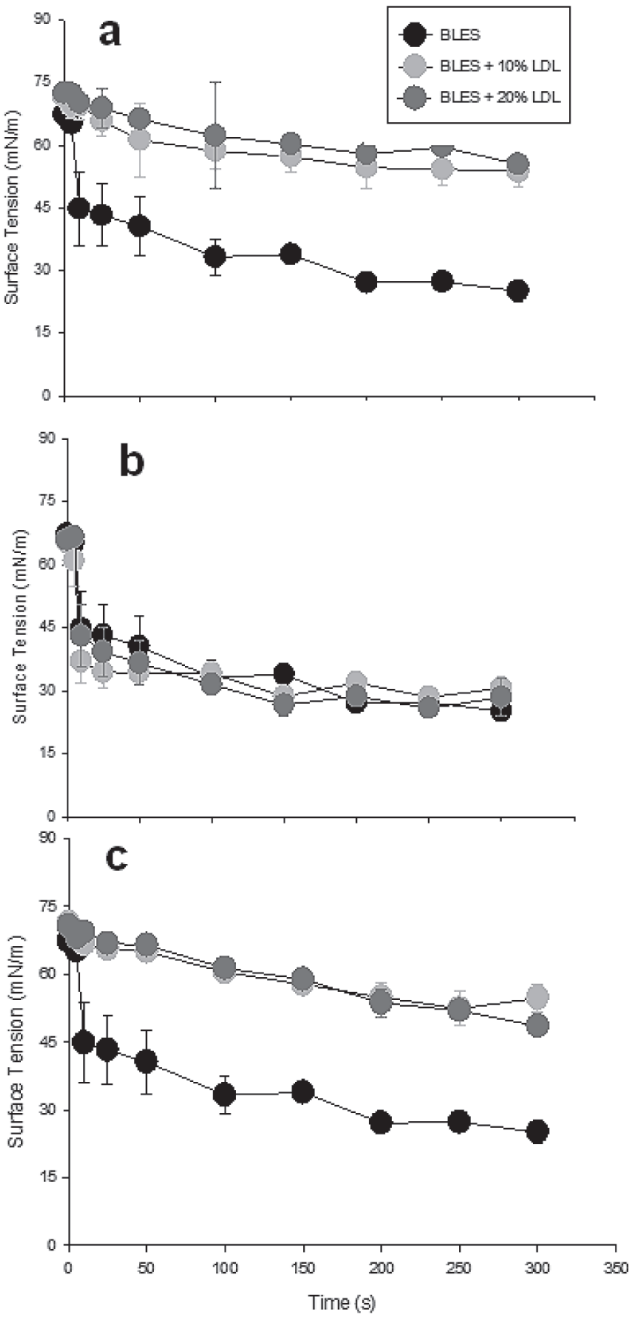

Fig. 1 Adsorption isotherms (γ *vs*. time) of BLES dispersions in the presence of 10 and 20 wt% (a) LDL, (b) cholesterol, and (c) serum at 25±1℃. Each plot is an average of 3 independent experimental sets. Standard deviation is shown by the error bars of n=3 experiments.

that excess cholesterol significantly obstructs BLES' ability to reach a low γ, but not as much as serum or LDL.

Upon addition of serum to BLES (Fig. 2(b) and 2(c)), there occurred a significant increase in the minimum γ (γ_{min}) to 30 mN/m compared to the low values for pure

Table 2 Summary of the equilibrium surface tension data for the adsorbed BLES films in the presence of different additives at 25℃.

Adsorbed sample films	*Surface tension (γ/mNm^{-1}) at 1, 150 and 300 sec of adsorption to air-water interface*		
	γ_1	γ_{150}	γ_{300}
BLES	71	35	25
BLES+10wt% Serum	73	58	53
BLES+20wt% Serum	74	61	59
BLES+10wt% Cholesterol	70	21	31
BLES+20wt% Cholesterol	65	26	27
BLES+10wt% LDL	73	59	56
BLES+20wt% LDL	72	59	50

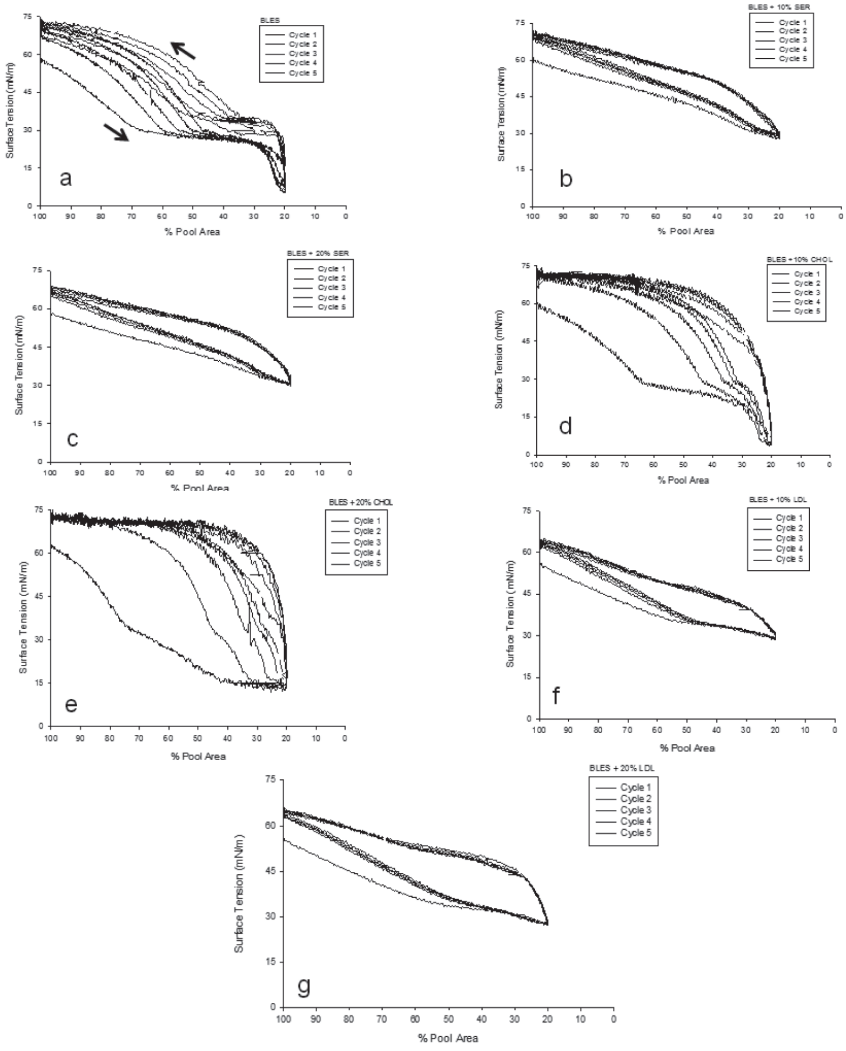

Fig. 2 Surface tension-area isotherms of 5 cycles of dynamic compression-expansion at a rate of 2 mm^2/sec for (a) pure BLES, (b) 10 wt% serum, (c) 20 wt% serum, (d) 10 wt% cholesterol, (e) 20 wt% cholesterol, (f) 10 wt% LDL and (g) 20 wt% LDL adsorbed films. Each experiment was conducted in triplicate and the best representative graph from a single experiment is shown for clarity. All isotherms were plotted as percentage of film area change versus surface tension (γ). The downward arrow shows the direction of compression and the upward of expansion.

BLES. Changes in γ_{min} were also observed upon the addition of similar amounts of LDL (Fig. 2(f) and 2(g)). Addition of cholesterol in physiological amounts (10%) resulted in γ min values comparable to BLES (γ_{min} ~1 mN/m) films, [Fig. 2(d) and 2(e)]. When cholesterol was added in excess (20 wt%) the γ_{min} could not attain low surface tension (15 mN/m). Results suggest that excess cholesterol affects BLES ability to reach a low γ, however the effect was not as dramatic as that of serum or LDL. It is evident from the results that the serum, LDL and cholesterol impair the ability of BLES films to lower γ. Isotherms of BLES + 10wt% serum and BLES + 20wt% serum are shown in Fig. 2(b) and 2(c). The inhibitory effects are clearly evident in both the cases. There occurred no change in the isotherm plateau area, suggesting that the material did not undergo 'squeeze out' phenomena and therefore could not be removed easily even after multiple cycling.

Histograms of the minimum and maximum γ that were attained during the fifth cycle of compression and expansion of monolayer films are shown in Fig. 3. Each experiment value shown in the bottom panel of Fig. 3 the average of triplicate experiments, where initial values, close to ~60 mN/m increased to ~70 mN/m after the fifth cycle. The data shown in the bottom panel of Fig. 3 suggest that upon addition of 10 and 20 wt% serum, the minimum γ increased to ~28 and ~30 mN/m respectively, clearly demonstrating that serum prevented the surface activity of BLES films to reach low γ. Figure S2(a) further shows that contrary to data obtained on serum and BLES films, addition of 10% cholesterol resulted in the appearance of a minimum γ close to that of BLES. The fact that the natural amount of cholesterol present in surfactant of the lung does not significantly alter BLES surface activity is consistent with the present experimental data. Increasing the amount of cholesterol to 20 wt% resulted in the increase of γ_{min} to ~15 mN/m, and thus rendered the BLES film inactive. However, the effect was not as significant as that of serum or LDL. A quantitative statistical analysis using the significance t-test ($p > 0.99$) indicated that the serum and LDL data were within the confidence limit to that observed for pure BLES. These data suggest that LDL and serum are extremely potent inhibitors of surfactant in adsorption and surface tension lowering ability.

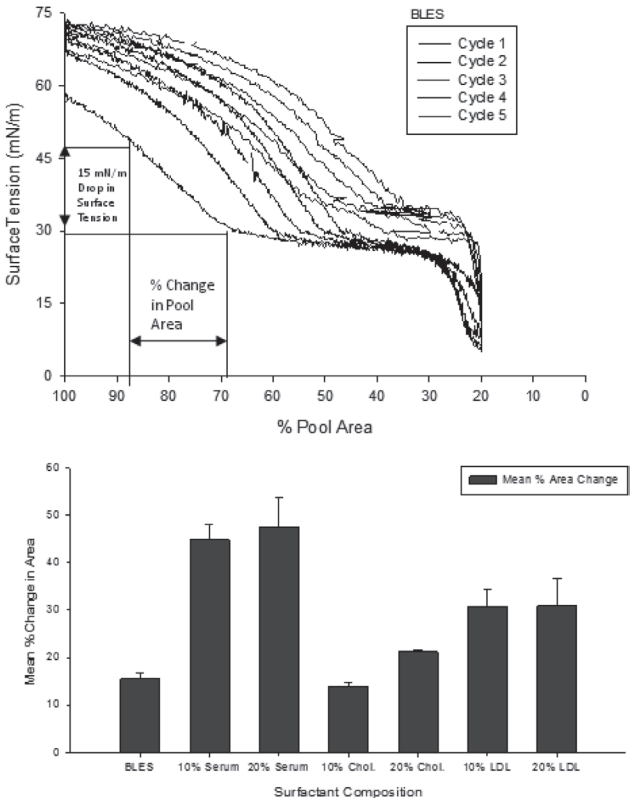

Fig. 3 Effects of serum, cholesterol and LDL on compressibility of BLES films based on mean %pool area compression required for a surface tension drop of 15 mN/m (C_{15} values). Serum and LDL had to be compressed twofold more in area than the ones of pure BLES.

Compressibility of BLES and BLES + serum or cholesterol or LDL films were calculated by obtaining C_{15} values as discussed elsewhere[15, 17, 19]. Briefly, the C_{15} values suggest the total film area (compressibility) required to drop the surface tension of the films by 15 mN/m during film compression from an initial value of 45 mN/m [Fig. 3(top)]. The greater the percent (%) area change, for the equivalent drop of γ, the more incompressible the films are. This calculation was previously applied to dysfunctional as well as normal LS films[19]. These studies had shown that for dysfunctional films of LS, large area compressions were required to drop γ compared to significantly smaller areas required for native surfactant or BLES alone[17, 19]. Requirement of large areas of compression indicates that probably materials, which inhibit LS surface activity, cannot be easily removed from the surface film either by 'squeeze-out' or by subphase vesicle formation. It was difficult to remove the serum as well as other component (cholesterol) from dysfunctional surfactant by repeated cycling and thus such films could not achieve low γ[14]. Figure 3 (top panel) shows the C_{15} values calculated from a γ change from 45 to 30 mN/m (the change of total area) since serum and LDL films could not be compressed below 30 mN/m even at maximal compression. As shown in the bar graph (Fig. 3, bottom panel), in order to lower BLES films γ by 15 mN/m, the film had to be compressed only by 15% area (highly compressible). The lowest compressibility (or highest incompressibility) was exhibited by BLES in the presence of serum and LDL where these films required 45% and 30% compression respectively. When cholesterol was added to the films, such films were found to be further

difficult to compress than pure BLES.

3.4 Atomic Force Microscopy (AFM) Studies

The samples previously used in film functionality studies were deposited on freshly cleaved mica substrates by Langmuir-Blodgett transfer technique and were examined using contact mode AFM. The images shown in Fig. 4 are representative images of BLES and BLES + 10 and 20 wt% serum or cholesterol or LDL films compressed to a surface tension of 52 mN/m prior to being deposited on mica. It is evident from the images that upon compression, the monolayer films had undergone the transition from fluid (liquid expanded) to gel (liquid condensed) phase[37]. The gel domains were formed upon compression of films at 52 mN/m. In Fig. 4(a), the BLES domains appeared brighter (or higher than surrounding phase), compact and more circular in shape. This was caused by the formation of a more compact organization of lipid molecules in the gel phase. Based on representative section analysis of corresponding figures (as shown in Fig. S3), the height of the BLES gel domain was found to be ~1.2 nm higher than the surrounding fluid phase. Comparing Fig. 6(a)-(g), it was evident that even though all the images were taken with the deposits at 52 mN/m, there appeared large differences in surface heterogeneity due to the composition of the

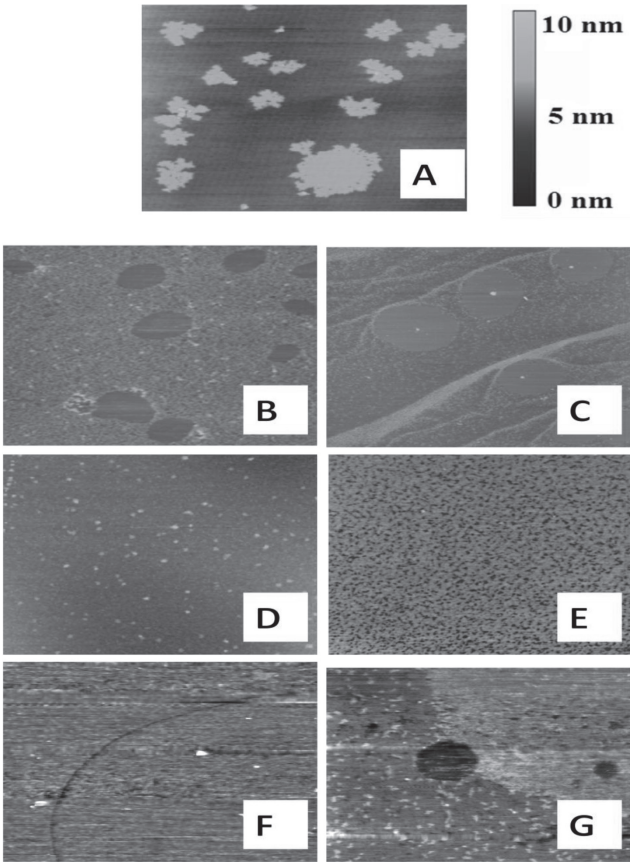

Fig. 4 Representative contact mode AFM images of Langmuir-Blodgett film deposited (imaged in air in contact mode) at equivalent γ of 52 mN/m for (a) Pure BLES, and BLES in presence of (b) 10 wt% serum, (c) 20 wt% serum, (d) 10 wt% cholesterol, (e) 20 wt% cholesterol, (f) 10 wt% LDL, and (g) 20 wt% LDL. Image field sizes shown were taken at 10 μm × 10 μm (X-Y plane) and height differences (Z plane) are shown by the 10.0 nm bar, indicated in (a). The condensed domains are about 1.2 nm above the surrounding fluid regions. The bright regions represent condensed gel domains and other structures which are 0.5-1 nm higher than the surrounding phase. Each frame represents a scan area of 10 μm × 10 μm.

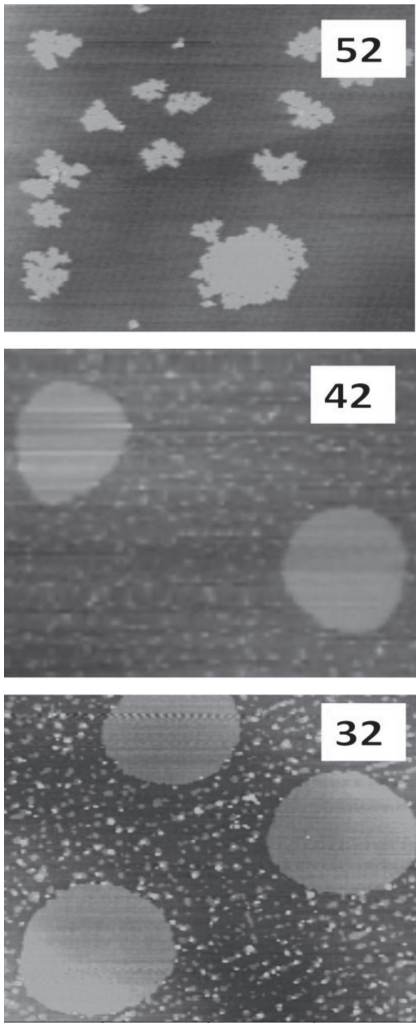

Fig. 5a Representative AFM images of films of BLES deposits taken at γ = 52, 42, 32 mN/m respectively in each vertical panel. Each frame represents a scan area of 10μm × 10 μm.

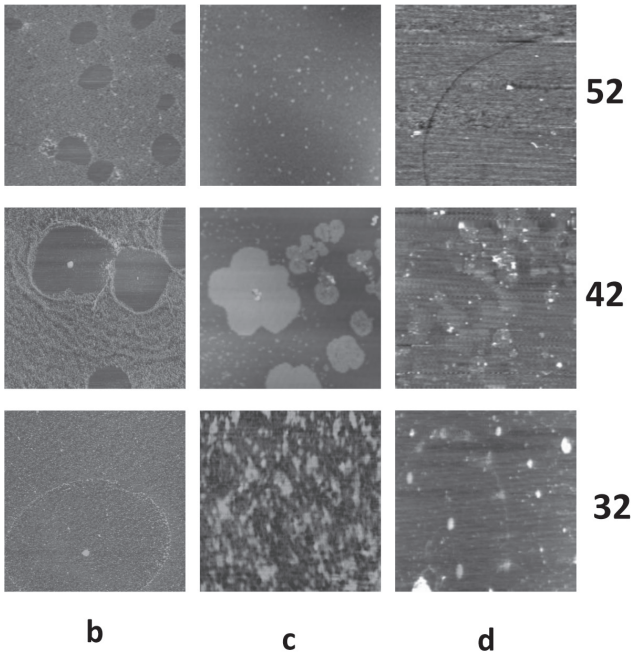

Fig. 5b-d Representative AFM images of films of BLES + 10% serum (b), 10% cholesterol (c) and 10 wt% LDL (d). Deposits were taken at γ = 52, 42, 32 mN/m respectively in each vertical panel. Upon addition of materials to BLES films, the gel domain (bright circular areas) formation is altered. Each frame represents a scan area of 10 μm × 10 μm.

films. BLES gel domains were clearly disrupted in films with the additives. As evident from Fig. 5(b) and (c) addition of serum resulted in the areas with holes as well as some areas with spiked (sharp height differences) domains in the center. Figure 5(d) shows that with the addition of cholesterol (10 wt%), small micro domains (with heights of gel phase) were also formed, which disappeared upon the addition of higher amounts (20 wt%) of cholesterol as shown in Fig. 5(e). Also as shown in Fig. 5, 10 wt% cholesterol films at further compression (γ = 42 mN/m), larger fluid like domains with spiked centers were observed. Figure 5(f) shows no gel or other domains (hole-like) structures, and the film shoed a more solid-like homogenous appearance. From Fig. 5(f) and (g), it becomes clear that higher amount of LDL (20 wt%) prevents BLES gel domain formation as well as appearance of the hole-like domains. The data collectively suggest that LDL, excess cholesterol and serum significantly perturbed the packing of gel lipids in BLES.

As shown in Fig. S3, the sections analysis of the 3D images of the films of at γ = 52, 42, and 32 mN/m respectively, the height differences in these films between domains and holes can be measured. For BLES (a), gel domains as high as 1.6 nm were formed in a continuum of

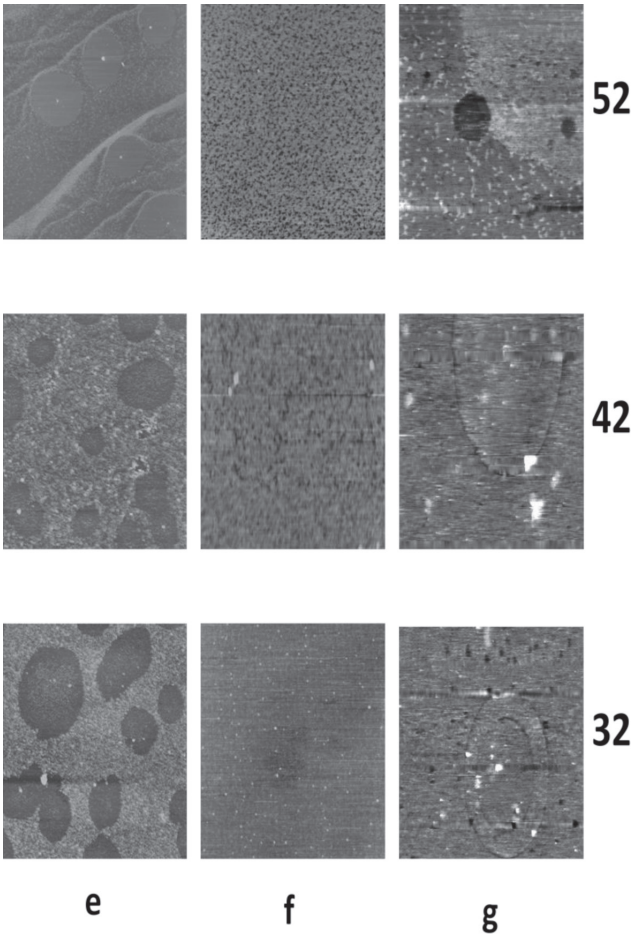

Fig. 5e-g Representative AFM images of films of BLES with 20 wt% serum (e), 20 wt% cholesterol (f) and 20 wt% LDL (g). Deposits were taken at γ 52, 42, 32 mN/m respectively in each vertical panels. Upon addition of materials to BLES films, the gel domain (bright circular areas) formation is altered. In (e) and (g) the domains formed exhibit lower height profile compared to the surrounding phase, suggesting that these circular domains may be fluid in nature. Each frame represents a scan area of 10 μm × 10 μm.

surrounding fluid phase. When serum was added to BLES, hole like structures appeared along with some spiky structures inside the domains (Fig. S3(b) and (c)). The holes are ~2 nm in depth and the spiky domains are seen to be at a height range of 4-7 nm. Upon the addition of cholesterol in smaller amounts as in (d), further micro-domains appeared and became larger upon compression. Spiky centers were formed which then disappeared upon further compression, and the film turned more homogenous upon further compression. These domains were close to about 1 nm high compared to the intermediate phase between

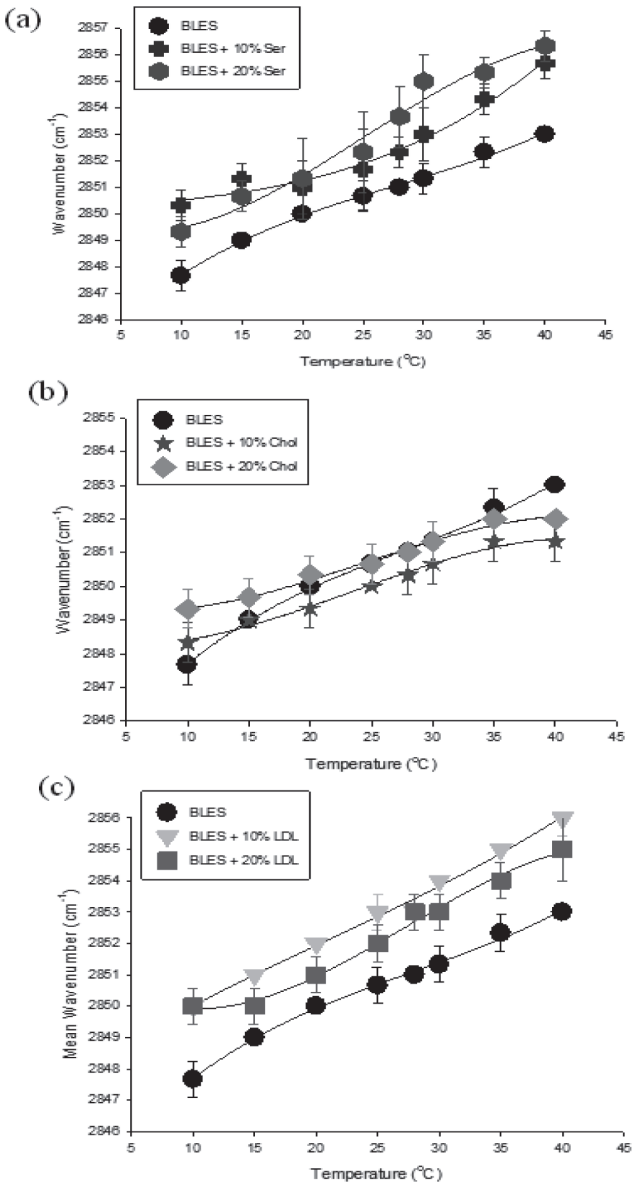

Fig. 6 Vibrational wave number shift for BLES compared to (a) BLES + serum, (b) BLES + cholesterol and (c) BLES + LDL. The temperature range was from 10-40℃ for all graphs. Each graph is the mean of wave number shifts from three independent experiments and the error bars represent the standard deviation.

them. Cholesterol, added in excess (20 wt%), prevented domain formation to occur, and the homogenous film appearance was again observed.

3.5 Raman spectroscopy studies

Raman spectroscopy can suggest specific bond vibrations in a single phospholipid system or an average of signals from specific bonds (C-H, C-C, PO_4) in a complex system such as BLES. Higher shift in wave number indicates more fluidity or increasing number of *gauche* bonds, whereas lower shift indicates more *trans* bonds or more rigidity of the hydrocarbon chains (28,31). Both serum and LDL increased fluidity of the BLES films, while cholesterol had slight fluidizing (10 wt%) and rigidifying (20 wt%) effects as shown in Fig. 6(a-c). The CH_2, CH_3, and C-C skeletal bands could clearly be defined, as well as temperature dependent shifts in some of the bands which allow for a relative measurement of the phase transition of BLES and BLES with additives could be monitored[16, 17]. This phase change monitoring allow correlating the structural features observed in films (due to the 2D lateral phase transitions induced by compression) with those that occurred in the bulk (bilayer) material with the change of temperature, since the films were formed from such bilayer dispersions. The correlations suggested significant as serum or LDL.

In the spectra of the lipid class (Fig. S3, supplementary section), the strongest peaks that were mostly evident in BLES were the bands from 2800-3000 cm^{-1}. These corresponded to the CH_2 symmetric stretching and asymmetric stretching modes at 2850 and 2890 cm^{-1} respectively. These bands were sensitive to the *trans-gauche* conformation changes in the acyl chains of lipids. Another Raman band of similar interest was that of the CH_3 symmetric stretch (2930 cm^{-1}) and asymmetric stretch (2960 cm^{-1}), as it provided information from the interior core of the bilayers. The Raman spectra of BLES and BLES + serum or cholesterol or LDL in the 2800-3000 cm^{-1} region at different temperatures are shown in Fig. S4. These Raman peaks, for specific phospholipids and their bond vibration designations, have been determined previously by others[38, 39]. As shown in Fig. S4, the symmetric CH_2 stretch (ν_s CH_2), at 2850 cm^{-1}, the asymmetric stretch (ν_{as} CH_2), at 2890 cm^{-1}, and the symmetric CH_3 stretch (ν_s CH_3), at 2930 cm^{-1} were prominent for BLES and BLES + 10 wt% serum, 10 wt% cholesterol and 10 wt% LDL systems. For BLES, in (a), the ν_{as}, showed a trend for a broadening of the ν_{as} CH_2 band with the increase in temperature from 25-40℃. For temperatures lower than 25℃, narrowing of the band was observed. Another trend was the shift in wave number of the ν_{as} CH_2 peak with the increase in temperature, as shown in Fig. S4(b)-(d). It was also evident from the intensity of the ν_{as} CH_2 peak compared to the ν_s CH_2 peak. At higher temperature intensity of ν_{as} CH_2 was less than ν_s CH_2 and it increased with decreasing temperature. The ν_s CH_3 peak at 25℃ was less intense than that of the ν_{as} CH_2 peak, and as the temperature increased, so did the ν_s CH_3 intensity.

These trends were consistent with a change in conformation of the lipids as a function of temperature, where an increased fluidity of the hydrocarbon chain or gauche conformation had been observed at higher temperatures. At lower temperatures (10-25℃) however, the hydrocarbon

chains were more "gel-like" or rigid with *trans*- conformation[9, 15]. The effects of serum, cholesterol, and LDL on BLES however were not seen quite clearly from Fig. S4, due to high noise or low signal/noise ratio ascribed to protein auto-fluorescence expected from the serum soluble proteins or from apoproteins of LDL. Also any clear cut peaks from pure serum and LDL were not observed due to their high protein content. By plotting the shift of the wave number of the ν_s CH_2 peak versus temperature, small changes in conformation were seen, as shown in Fig. 6. The wave number of the ν_s CH_2 (2850 cm^{-1}) was plotted against temperature for the average of three independent experiments and the error bars represent standard deviation. These plots can suggest the order parameters of the phospholipid chains as discussed in details elsewhere[9, 15]. A shift in wave number towards higher frequency side indicated more fluidity or higher number of *gauche* bonds, whereas lower shift indicated more *trans* bonds or more rigidity. The temperature induced changes in the wave number of the ν_s CH_2 band of BLES + serum, BLES + cholesterol and BLES + LDL are shown with those of BLES in Fig. 6. For the BLES curve, a more sigmoid shaped plot was obtained which might be attributed to a broad phase transition observed between 10-40℃, the midpoint of the transition being about 27℃, which was previously measured by differential scanning calorimetry (DSC)[15].

Figure 6(a) and (c) describe the fluidizing effects of serum and LDL, respectively, on BLES. The fluidizing effects were reflected from the increase in shift to higher wave numbers for all points on the curve throughout the temperature range. Upon addition of cholesterol however, the shifts of wave numbers were not so significant compared to BLES alone. A slight shift to higher wave numbers were resulted in the 20 wt% cholesterol system, however the effects were not significant, suggesting cholesterol might have rigidified as well as fluidized the system depending on the temperature. The systems containing LDL (Fig. 6(c)), as well as the ones with serum (Fig. 6(a)), clearly show a shift of all wave numbers of higher values suggesting a fluidizing effect of the BLES system with these additives. Therefore it could be concluded that both serum and LDL fluidized the bilayer, which in turn prevented the formation of gel domains in films formed from such bilayers, and this might have affected LS function. Cholesterol seemed to increase fluidity of the gel phase at lower temperatures and to rigidify the fluid phase at the higher temperatures. The Raman studies directly showed that serum and LDL affected surfactant molecular packing in bilayers.

4 Discussion

Studies published, over the last three decades, on the surfactant inhibition by serum proteins have been conducted using mainly surface tension measurements. These studies suggest that inhibition by soluble serum proteins such as albumin, fibrinogen, C- reactive protein (CRP) and others may be the major factors in surfactant inactivation in ARDS[18, 36–41]. These proteins have been shown to inhibit surfactant function by inhibiting adsorption and ability of such surfactant films to reach low γ using various surface analytical techniques[37–41]. However studies have also shown that the protein mediated inhibition is concentration dependent as in the case of albumin, and that such inhibition can be overcome by an increase in surfactant to protein ratio[38–42]. However some recent studies including ours clearly suggest that the serum lipids are far more potent inhibitors of surfactant, at pathophysiological levels or those that are found in ARDS[32, 42, 44].

4.1 Cholesterol and Lung Surfactant

Previous studies have shown that cholesterol is an integral component of LS, found between 7-15% in various mammalian systems[9, 10, 39, 43, 44]. However, the physiological role of cholesterol is not clear to date, since the source of the material as well as its delivery route in LS has not been firmly established. Previous studies also indicated that radio labelled cholesterol and LDL is taken up by type II pneumocytes, however its insertion in the secreted surfactant pool is complex. Some authors have shown that LDL cholesterol is mainly enriched in the outer lamella body limiting membrane, and this membrane does not reach the secreted surfactant pool during exocytosis[5, 12]. There are also reports which suggest that cholesterol is segregated into two types of domains in combination with the porcine surfactant proteins SP-B and SP-C[43]. It is not clearly known what the major role of the lipid is in LS function, let alone in dysfunction. In the studies by Gunasekara *et al.*[9], it has clearly been shown that a normal amount of cholesterol does not affect the surface activity of LS. Others have shown that cholesterol actually allows the formation of a specific monolayer to bilayer squeeze-out phases[9], as well as allowing the function of surfactant proteins SP-B and SP-C by forming lipid-raft like structures[43]. Some of our previous studies agree with the structure-function changes induced by normal cholesterol[23], however, whether cholesterol mainly deactivates BLES is still an open question, since there are some differences in the interaction of LDL and whole serum with BLES compared to cholesterol with BLES.

With the present level of knowledge it is also uncertain about the source of extra cholesterol from LDL and serum. The mass spectral data (Fig. S1) do not provide any clear idea about excess cholesterol. The bulk of cholesterol in LDL and probably in serum is supposedly to be found as cholesterol esters, the MALDI-TOF data shows that some of the cholesterol is mainly detected in its free form in the

serum lipid extract as well as LDL. The main peak in the mass spectra (Fig. S1) at 369 m/z is possible either the fragmented form of cholesterol ester or free cholesterol from some other source. Previous mass spectral study of LDL (33) also suggests that the 369 m/z peak is a deoxygenated cholesterol, [molecular wt, M.W., of cholesterol – OH = 386 – O (16) = 370 or cholesterol + H^+], and is the major peak. The other major peak at 496 could possibly be fragments of cholesterol ester[33, 34]. The calculated number for complete cholesterol ester peak at 671 m/z is very small as well as contained an Na^+ ion and was difficult to detect in MALDI-TOF of LDL[33]. A more recent study has shown that cholesterol esters are more potent inhibitors of BLES than free cholesterol[45].

4.2 Serum Lipids and Proteins

As our earlier studies suggest, serum has been proved to be a more (~200 times more) potent inhibitor than its constituent proteins[17]. The concentration of serum as little as 2 wt%, added to BLES dispersions, could inactivate BLES in ways that would take tenfold soluble protein concentrations or 500-1000 wt%[15, 16, 22]. This gave some credence to the idea that there may be some other factors in serum that cause such potent inhibition, perhaps a lipid-like, nonprotein material. Another study by Panda *et al.*[19] has focused on the alterations of lung surfactant composition as well as surface activity that occurred during lung injury. Not only were protein levels increased three fold but levels of cholesterol were also increased about two fold in such surfactant. Other studies confirmed this and showed that an elevated level of cholesterol from 10 to 20 wt% completely inactivates surfactant such as BLES[9, 11].

Adsorption occurs when there is a propensity for the more hydrophobic regions on the outer surface of a molecule to repel from interaction with the aqueous environment towards the air, while the hydrophilic portion would be drawn towards the aqueous environment[4, 5, 41, 47, 49, 58]. Adsorption studies were conducted to determine the exact mechanism in which BLES surface activity is compromised by serum and its components. Adsorption of BLES and BLES + additive mixtures (Fig. 1) showed that BLES + serum and BLES + LDL samples had prevented adsorption of the BLES film to an equilibrium value (~25 mN/m). For these samples γ values could not go below 50 mN/m. However BLES + cholesterol samples, on the other hand, were able to reach equilibrium γ in a short time of adsorption, with very little effect compared to BLES alone.

The inhibition of LDL and serum could perhaps be explained by competitive adsorption of specific components of serum or by prevention of the specific BLES lipids to be able to absorb[48]. Since the Raman studies show that the bilayers of BLES were directly affected by serum and LDL, we would rather assume the latter idea. However, since the AFM studies show that serum and LDL caused dramatic changes in BLES film structure, it is reasonable to assume that some of the additive components could have competitively adsorbed on the surface from such bilayers. Serum derived proteins as well as cellular lipids are normally surface active and can also adsorb onto the air-water interface, forming films, just like LS. These materials are known to impair LS through specific biophysical interactions as suggested above. An earlier study by Holm *et al.*[18], showed that albumin and fibrinogen, by way of competitive adsorption, interfered with the adsorption of specific surfactant components to the air-water interface. A recent study of ours showed that fibrinogen adsorbs competitively to the air-water interface, as well aggregate the gel domains in BLES films[15]. Competitive adsorption described serum proteins that formed a film or parts of the film at the air-water interface and prevents or delays surfactant adsorption by occupying space in films or the air-water interface and preventing the surfactant aggregates from reaching the interface due to lack of space[18]. The results from an *in vitro* study suggests such a mechanism[15]. Using Wilhelmy balance and pulsating bubble surfactometer studies to measure adsorption, Holm *et al.*[18] measured the attenuation of the overall γ with surfactant alone or with the addition of inhibitors. It was found that albumin competed with LS for the air-water interface during adsorption when simultaneously added with the surfactant.

Some conflicting results have been experienced in a study by Gunasekara *et al.* in 2008[39]. They examined two different mechanisms of surfactant inhibition: i) competition of the air-water interface and ii) impairment of the surfactant film by itself. They studied serum proteins, albumin and fibrinogen, in concentrations similar to those in diseased lungs and when additives were added before or after formation of BLES films. In their study, minimal delay or rapid adsorption was noticed in BLES film formation with the presence of a pre-formed protein film. They concluded that surfactant inhibition was likely caused by a dysfunctional film instead of inhibition by way of competitive adsorption of the serum proteins[39]. This contradicted the previously reported result[11, 17]. This may be due to different surfactant concentrations used in the studies as well as insertion of the proteins in the surfactant dispersions by different methods. However unlike these proteins, cell membrane lipids and free fatty acids, such as oleic acid, are shown to also readily adsorb and penetrate the films and form mixtures with lung surfactant lipids[22, 29, 33, 46]. Previous study on the effects of lysophosphotidylcholine (LPC) on lung surfactant show that, LPC-induced inhibition of LS due to interactions within the surfactant film during compression. LPC was shown to readily adsorb and penetrate the film and efficiently mix with the film itself[46]. In this study, it was mentioned that due to its conical or 'wedged' shape, LPC possibly perturbed the packing of the disaturated phospholipids (DPPC) and thus prevented the low

surface tension values being achieved as in normal surfactant films. This may be a possible mechanism by which cholesterol or its ester may interact with gel lipids in BLES.

4.3 Cholesterol and Structural Organization

As mentioned above, the effect of cholesterol on BLES adsorption was minimal. It has been previously shown that enhancement of adsorption rate of surfactant phospholipids occurs to the equilibrium γ, by physiological levels of cholesterol. This is credited to fluidizing effects of cholesterol on phospholipid mixtures high in DPPC content[11, 23]. It was suggested however, that this fluidity of the phospholipid may disrupt such films from reaching low γ upon compression[11]. However, Vockerath *et al.*[41], showed that normal cholesterol present in the surfactant can lower surface tension more efficiently than those seen in its absence.

In the present study, it is possible that excess cholesterol could not affect the adsorption rate but the ability of such surfactant films to reach low γ is significantly affected. This may have been with an increase in the fluidity of bilayer dispersions that would help in the rapid spreading of surfactant but would also make the LS film too fluid to lower γ upon compression as evident from the experimental results. In another previous study no difference in the behaviour of surfactant containing various amounts of cholesterol with respect to adsorption (film formation) was noted[9]. This study pointed out that both the normal and dysfunctional surfactants are able to reduce the γ to equilibrium, but only a fully functional surfactant can achieve very low surface tension values upon compression. However most studies have shown that excess cholesterol can slightly impede surfactant adsorption rate[7–10].

Figure 2 showed the compression-expansion isotherms for BLES and BLES + additive films. As evident from the plots, all materials except 10% cholesterol prevent the BLES films reaching close to 1 mN/m surface tension. When 10% cholesterol films are further compressed, there occurs indeed the formation of gel type domains along with some other 'spiky' centre. In a previous study we suggested that these spikes may also be possibly cholesterol crystals squeezing-out of the films in air, and this may be a mechanism of small amounts of cholesterol remaining in the film upon expansion[23, 25]. Somehow serum, cholesterol and LDL interact with the BLES lipids to prevent complete compression of the monolayer and also interact with the gel lipids to prevent LS films to reach a low γ. Cholesterol may somehow bind to some of the lipid components in the monolayer which in turn prevents the LS monolayer from fully functioning and the LS from reaching a low surface tension. Multiple compression-expansion cycles, on BLES (Fig. 2(a)) shows that the plateau region changes with increasing number of cycles. This suggests that materials from films probably were 'squeezed out' and caused film refining with specific surfactant components as suggested by others[1, 2, 37, 47]. The term 'squeeze out' refers to the removal of material above or below the plane of the air-water interface. It was proposed that this 'squeeze out' process allows the removal of the non-lipid or other fluid phospholipid constituents off the lipid monolayer, thus allowing for the enrichment of DPPC in such films. As more compression-expansion cycles are preformed, the more enriched with DPPC the monolayer becomes which allows the surfactant monolayer to achieve low γ values[23, 37].

In comparison, Fig. 2(d), BLES + cholesterol (10%) shows different isotherms than those with 20% (Fig. 2(e)). With BLES + 10% cholesterol (as shown in Fig. 2(d)), a low γ value could be achieved, which agrees with the fact that the 10% physiological amount of cholesterol naturally found in the LS, does not affect the film's ability to reach very low γ. The plateau region for BLES + 20% cholesterol (Fig. 2(e)) is, however different, since there appears no significant plateau (squeeze-out) region. This is due to the fact that when excess cholesterol is added, this excess cholesterol could not have been 'squeezed out' as easily as those of other components of LS. The attainment γ_{min} for BLES + 10% cholesterol (Fig. 2(d)) is ~5 mN/m, which is almost the same as for BLES alone, and lower than that for BLES + 20% cholesterol (Fig. 2(e)) which had a minimum γ of ~15 mN/m. This trend is also evident in Figs. 2(f) and 4(g) with the addition of both 10% and 20% LDL to BLES. These results suggest that serum and LDL materials can uniformly mix well with the BLES lipids in films and cannot be easily removed. These results are in agreement with those found in a previously conducted study[6], where a captive bubble surfactometer (CBS) was used to investigate the effects of addition of 10% (healthy lung) and 20% (injured lung) by wt of cholesterol to BLES[11]. It was found that with 10% cholesterol added to BLES films, a low (close to 1 mN/m) value of surface tension, similar to normal LS, could have been sustained for a period of time. Samples that contained BLES + 20% cholesterol however could not attain a low γ[11, 19].

Cholesterol and LDL are difficult to remove since they are lipids. Cholesterol also has a high affinity for DPPC[23]. The phospholipid DPPC having two saturated palmioyl chains can pack tightly in films (and thus produces gel domains) due to their chains being in the all-trans conformation[48, 49]. Cholesterol will normally fluidize these chains or cause packing perturbation and such films would not be expected to reach low γ[7, 9, 23]. However, when present in physiological amounts, they may also rigidify the fluid chains of fluid phospholipids such as 16:0/18:1 (palmitoyl-oleyl-PC) which are also present in significant amounts in BLES (Fig. S1(b)). This balance of rigidity of chains in LS may be overturned by excess cholesterol, mainly since cholesterol is difficult to remove from the lipid environment either by increasing compression or multiple cycling

as evident from Fig. 3(a). These effects are far more evident and dramatic for serum and LDL, suggesting possibly cholesterol may not be the only factor in surfactant inhibition. Their inability to be removed would interfere with the tight packing of DPPC lipids as well as the DPPC gel domain formation in the surfactant monolayer. Previously hole-like domains and the absence of gel domain structure has been observed on dysfunctional surfactants which had about twice the amount of normal cholesterol and prevented films from reaching low γ[19].

By examination of the C_{15} values as seen in Fig. 3, it was evident that the compressibility of BLES films got dramatically altered when serum or LDL were added. This might have been due to the competition of these materials with BLES for the formation of the monolayer or some portions of these materials may have somehow bound to BLES molecules and thus prevents the formation of a surface active film. Since serum and LDL contains proteins, it is possible that there may be a twofold mechanism of surfactant inhibition.

4.4 Structure and Dysfunction

Atomic force microscopy (AFM) is a useful tool in imaging the structure(s) of biological systems, mostly due to its nano-scale resolution. Various previous studies have used the method to study lipid films as well as those with serum proteins[7, 11, 15, 16, 27]. Our study examined the effects of serum or serum components in the formation of BLES domain. It was concluded that serum materials separately or in conjunction with one another can prevent BLES domain formation by interacting with the DPPC lipids or forming their own monolayer film. Deposits of the same samples used in the monolayer studies were taken at γ 52, 42, and 32 mN/m, respectively. Representative AFM images have been presented in Fig. 4. Prevention of BLES domain formation was seen in all but the 10% cholesterol deposit γ = 42 mN/m. This was likely to do with the physiological amount of cholesterol that was found in the lung somehow helping to form these domains, such as lipid rafts in cell membranes. Evident from Fig. 4, serum and LDL were able to form areas of holes and also their own domains. The domains in the holes were due to components of serum and LDL preventing surface active components of LS to adsorb so that they could not form a surface active film. The hole-like areas were perturbed DPPC gel domain remnants or separate domains of serum components (possibly cholesterol esters) or a combination of both of both[17].

The 'spiky' area seen in the various samples, especially BLES + 10% cholesterol, could possibly be the cholesterol domains, or in other cases, some combination of perturbant and BLES lipids. Previous studies with low amounts of cholesterol (2-8 wt %) in DPPC and BLES films, suggested that the lipid remains in the films at high compression by a unique mechanism rather than being directly removed from the film by squeeze-out to the subphase[23, 25], By AFM and fluorescence, it was observed that cholesterol in highly compressed films form multi-layer structures, as well a possibly crystallizes into solid forms, above the plane of the monolayer. Upon expansion these structures are re-adsorbed or dispersed back in the films[23, 25].

Domain height is due to the tilting of the DPPC fatty acid chains in gel phase, more perpendicular with respect to the plane of the monolayer, compared to those in the fluid phase as shown in Fig. S3(a). Cholesterol when added in excess completely abolished any domain formation. This was due to the fact that when cholesterol exceeds the DPPC concentration, the sterol may start to interact with the unsaturated lipids and thus completely keep the monolayer in a fluid state[11]. Previous AFM and fluorescence studies suggest that normally soluble proteins or other bulky perturbants were preferably adsorbed in the fluid phase of lipid films because of the loose packing of the lipids in that phase[15, 17]. This most often resulted in decreased size and amount of gel or condensed domains as the addition of the perturbant increased. An earlier study using fluorescence microscopy showed that high concentrations of serum had caused the formation of smaller BLES domains possibly due to its presence in the fluid phase which inhibited DPPC lipids to segregate into gel domains upon compression[17]. Also in the present case the domains that were not probed, may have been formed by serum component. In agreement with these findings, an even earlier study showed how injuriously ventilated lungs, similar to diseased lungs, showed increases in serum protein and cholesterol[19]. Detail mechanisms for the formation of different types of domains in these "diseased" lungs was proposed in that study. In the present case, very few, if any, DPPC-rich domains were present at low surface tension (more compressed films) and these domains are noticeably smaller and covered less of the total surface area, despite similar DPPC content. These intermediate domains were found to contain areas of some fluidity seen from non-exclusion of fluorescent probes[19]. This is viewed as different types of domain height differences between the two phases in AFM (25). The larger heights of the gel domains (circular areas) are due to tilting of the fatty acyl chains of the PLs in gel phase when there occurs a tighter packing induced by lateral compression of the films as well as due to the molecules' orientation being more perpendicular to the air-water interface[11, 25].

4.5 Bilayer Phase Changes

Raman spectroscopy is a very useful technique to study various materials because it is a non-invasive method. It does not require the use of a probe, intensive sample preparation, as well as its low intensity laser prevents samples from local heating or photo degradation. Raman spectroscopy involves the study of vibrational modes of a system. It

can be used to study solids and even liquids and solutions because water is Raman inactive unlike Fourier transform infrared spectroscopy (FTIR) where water vibrations at 3000 cm^{-1} and H-bonding suppress the hydrocarbon vibrations peaks at the 2000-3000 cm^{-1} range[28-31]. Figure 6 describes the variation in the Raman shift for adsorbed BLES film in the absence and presence of different additives. It is noted that there occurs an upshift in the ν_s CH_2 peak position with an increase in temperature. The shift in wave number in higher numbers implies an increase in the fluidity of the system. Since the fluidity of BLES bilayers gets directly affected by additives, it is assumed that the films formed from such bilayers would also lead to an increase in fluidity[48, 49]. Serum and LDL addition seem to cause a more fluid bilayer at all temperatures and it is probably due to this fluidity that prevention of BLES domains formation occur in the films, thereby inactivating a functioning surfactant or by the lipids ability to be tightly packed.

The bilayer phase changes observed from the order parameter profiles (Fig. 6) from the Raman spectra suggest that LDL and serum alters the fluidity of such membranes, however excess cholesterol does not show any significant effects. It is also puzzling to notice how the cholesterol or its ester in LDL directly affects the BLES bilayers, since the esterified form of cholesterol in LDL (or in serum LDL) cannot directly enter BLES bilayers simply by lipid exchange, since in normal situations these are entered into type II cells by the receptor mediated pathway. Whatever be the case, certain materials from LDL and serum seem to cause fluidity changes of bilayers as detected in the Raman spectroscopy, and this causes possible structure-function changes in the films being adsorbed from such bilayers. Previous studies had shown that cholesterol can interact with SP-B and SP-C in LS bilayers which were present in BLES[43]. Other studies using NMR and X-ray diffraction show cholesterol to slightly increase the order parameter of BLES bilayer in the gel phase albumin to induce specific fluid-like domains in such bilayers[48, 49]. Although these studies do not suggest any clear cut mechanism of bilayer interactions of LDL and serum with BLES, our Raman data clearly suggest possibilities of different modes of interaction of these serum materials with BLES compared to cholesterol in normal or excess amounts. It is possible that the apo-proteins present in LDL as well as serum soluble proteins such as albumin and others could have probably interacted with SP-B/SP-C present in BLES and thus causes the changes in BLES bilayers, other than the effects already induced by cholesterol or its esters[45]. There may possibly be a dual mechanism involved here requiring further investigation with serum or LDL protein components. This could be considered as the future perspective.

5 Summary and Conclusions

Complete physicochemical studies involving the composition, functionality and structure of the adsorbed BLES films in the absence and presence of three additives, viz., cholesterol, serum and LDL were performed. The study includes the patho-physiological amounts of these materials found in lungs in disease. The additives altered the bilayer and film packing, surface activity and structures of surfactant, suggesting possible molecular rearrangement and disordering of surfactant in disease. Since excess cholesterol or its esters may actually arrive inside the lung through LDL transport, it is cholesterol that is the most potent inactivator of LS, than leaked soluble serum proteins, since lipids are far more hydrophobic and more difficult to remove from films during dynamic cycling. Whole serum, serum proteins and its lipid components may specifically interact with the surfactant films and bilayers by either separate mechanisms, or synergistically. In future studies, specific lipid components of serum such as HDL, One of the major studies requires the specific separation of serum lipid and serum protein fractions and observing their structure-function correlations in inactivating surfactant, is currently undergoing in our laboratory. The specific molecular re-arrangements observed in our study of domains in films need to be further explored in detecting the exact composition of the variety of domain structures using possibly fluorescently labelled LDL, cholesterol and serum proteins. However these studies need to be conducted in a manner using similar sets of biophysical methods which yield structure-function correlates of bilayers and films, as well as uses patho-physiological amounts of materials, so that an over-simplification of the models in previous studies can be rectified.

Acknowledgements

K. N. and D. T. sincerely acknowledges operating research funding from NSERC and CIHR, Canada. The authors acknowledge the generous gift of BLES from Dr. Dave Bjarnson of BLES® Biochemicals Inc. (London, Ontario, Canada). AKP sincerely acknowledge the receipt of a visiting fellowship under the DST-JSPS Exploratory Visit Program. R. D. and A. H. great fully acknowledges graduate fellowships from the School of Graduate Studies of Memorial University. P.N. acknowledges the receipt of a research fellowship from the University Grant Commission, New Delhi under the Rajiv Gandhi National Fellowship for disabled (No. F./2012-13/RGNF-2012-13D-GEN-CHH-51106/ 31-Oct-2013).

Supporting information

This material is available free of charge via the Internet at http://dx.doi.org/jos.63.10.5650/jos.ess.14071

References:

1) Clements, J. A. Pulmonary Surfactant. *Am. Rev. Respir. Dis.* **106**, 984-990(1970).
2) Creuwels, L. A. J. M.; Van Golde, L. M. G.; Haagsman, H.P. The pulmonary surfactant system: Biochemical and clinical aspects. *Lung* **175**, 1-39(1997).
3) Nag, K.(Ed)Lung Surfactant Function and Disorder. Taylor & Francis, Boka Raton, FL.(2005).
4) Possmayer, F.; Nag, K.; Rodriguez, K.; Qanbar, R.; Schurch, S. Surface activity in vitro: Role of surfactant proteins. *Comp. Biochem. Physiol. : A Mol. Int. Physiol.* **129**, 209-220(2001).
5) Perez-Gil, J.; Keough, K. M. W. Interfacial properties of surfactant proteins. *Biochim. Biophys. Acta* **1408**, 203-217(1998).
6) Daniels, C. B.; Orgeig, S.; Sullivan, L. C.; Ling, N.; Bennett, M. B.; Schurch, S.; Val, A. L.; Brauner, C. J. The origin and evolution of the surfactant system in fish: Insights into the evolution of lungs and swim bladders. *Physiol. Biochem. Zool.* **77**, 732-749(2004).
7) Nag, K.; Fritzen-Garcia, M. F.; Devraj, R.; Hillier, A.; Rose, D. Phase transitions, cholesterol and raft structures in films and bilayers of a natural membranous sytem. in Structure and Dynamics of Membranaous Interfaces,(Ed. K. Nag)Chapter 15, John Wiley & Sons, NJ.(2008).
8) Panda, A. K.; Nag, K.; Harbottle, R. R.; Possmayer, F.; Peterson, N. O. Thermodynamic studies of bovine lung surfactant extract mixing with cholesterol and its palmitate derivative. *J. Colloid Interface Sci.* **311**, 551-555(2007).
9) Gunasekara, L.; Schürch, S.; Schoel, W. M.; Nag, K.; Leonenko, Z.; Haufs, M.; Amerin, M. Pulmonary surfactant function is abolished by an elevated proportion of cholesterol. *Biochim. Biophys. Acta* **1737**, 27-35 (2005).
10) Leonenko, Z.; Gill, S.; Baoukina, S.; Monticelli, L.; Doehner, J.; Gunasekara, L.; Felderer, F.; Rodenstein, M.; Eng, L. M.; Amrein, M. An Elevated Level of Cholesterol Impairs Self-Assembly of Pulmonary Surfactant into a Functional Film. *Biophys. J.* **93**, 674-683 (2007).
11) Keating, E.; Rahman, L.; Francis, J.; Petersen, A.; Possmayer, F.; Veldhuizen, R.; Petersen, N. O. Effect of Cholesterol on the Biophysical and Physiological Properties of a Clinical Pulmonary Surfactant. *Biophys. J.* **93**, 1391-1401(2007).
12) Hass, M. A.; Longmore, W. J. Regulation of lung surfactant cholesterol metabolism by serum lipoproteins. *Lipids* **15**, 401-406(1980).
13) Voyno-Yansenetskaya, T. A.; Dobbs, L. G.; Erickson, S. K.; Hamilton, R. L. Low density lipoprotein-and high density lipoprotein-mediated signal transduction and exocytosis in alveolar type II cells. *Proc. Natl. Acad. Sci. USA.* **90**, 4256-4260(1993).
14) Bailey, T. C.; Da Silva, K. A.; Lewis, J. F.; Rodriguez-Capote, K.; Possmayer, F.; Veldhuizen, R. A. W. Physiological and inflammatory response to instillation of an oxidized surfactant in a rat model of surfactant deficiency. *J. Appl. Physiol.* **96**, 1674-1680(2004).
15) Devraj, R.; Nag, K.; Nahak, P.; Manna, K.; Fritztn-Garcia, M.; Thompson, D. W.; Makino, K.; Ohshima, H.; Nakahara, H.; Shibata, O.; Panda, A.K. Impairing effetc of fibrinogen on the mono/bilayer form of bovine lung surfactant. *Colloid Polym. Sci*. 2014(DOI 10.1007/s00396-014-3319-4).
16) Nag, K.; Vidyashankar, S.; Devraj, R.; Fritzen-Garcia, M.; Panda, A. K. Physicochemical studies on the interaction of serum albumin with pulmonary surfactant extracts in films and bulk bilayer phases. *J. Colloid Interface Sci.* **352**, 456-464(2010).
17) Nag, K.; Hillier, A.; Parsons, K.; Fritzen-Garcia, M. Interactions of serum with lung surfactant extract in the bronchiolar and alveolar airway models. *Respir. Physiol. Neurobiol.* **157**, 411-424(2007).
18) Holm, B. A.; Wang, Z.; Notter, R. H. Multiple mechanisms of lung surfactant inhibition. *Ped. Res.* **46**, 85-93 (1999).
19) Panda, A. K.; Nag, K.; Harbottle, R. R.; Rodriguez-Capote, K.; Veldhuizen, R. A. W.; Petersen, N. O.; Possmayer, F. Effect of acute lung injury on structure and function of pulmonary surfactant films. *Am. J. Respir. Cell. Mol. Biol.* **30**, 641-650(2004).
20) Durrington, P. Dyslipidaemia. *Lancet* **362**, 717-731 (2003).
21) Ockene, I.; CDESIIIE, J. Seasonal variation in serum cholesterol levels: Treatment implications and possible mechanisms. *Arc. Int. Med.* **164**, 863-870(2004).
22) Gunther, A.; Ruppert, C.; Schmidt, R.; Markart, P.; Grimminger, F.; Walmrath, D.; Seeger, W. Surfactant alteration and replacement in acute respiratory distress syndrome. *Resp. Res.* **2**, 353-364(2001).
23) Worthman, L. A. D.; Nag, K.; Davis, P. J.; Keough, K.M.W. Cholesterol in condensed and fluid phospholipid monolayers studied by epifluorescence micorsocpy. *Biophys. J.* **72**, 2569-2580(1997).
24) Bligh, E. G. A rapid method of total lipid extraction and purification. *Can. J. Biochem. Physiol.* **37**, 911-917(1959).
25) Nag, K.; Fritzen-Garcia, M.; Devraj, R.; Panda, A. K. Interfacial organization of gel phospholipid and cholesterol in bovine lung surfactant. *Langmuir* **23**, 4421-

4431(2007).
26) Ekelund, K.; Sparr, E.; Engblom, J.; Wennerstrom, H.; Engstrom, S. AFM study of lipid monolayers. 1. Pressure-induced phase behavior of single and mixed fatty acids. *Langmuir* **15**, 6946-6949(1999).
27) Bringezu, F.; Ding, J.; Brezesinski, G.; Waring, A. J.; Zasadzinski, J. A. Influence of pulmonary surfactant protein B on model lung surfactant monolayers. *Langmuir* **18**, 2319-2325(2002).
28) Dluhy, R. A.; Ping, Z.; Faucher, K.; Brockman, J. M. Infrared spectroscopy of aqueous biophysical monolayers. *Thin Solid Films* **327-329**, 308-314(1998).
29) Vincent, J. S.; Revak, S. D.; Cochrane, C. D.; Levin, I. W. Interactions of model pulmonary surfactants with a mixed phospholipid bilayer assembly: Raman spectroscopic studies. *Biochemistry* **32**, 8228-8238(1993).
30) Spiker, R. C.; Levin, I. W. Raman spectra and vibrational assignments for dipalmitoylphosphatidylcholine and structurally related molecules. *Biochim. Biophys. Acta* **388**, 361-373(1975).
31) Wong, P. T. T. Raman Spectroscopy of Thermotropic and High-Pressure Phases of Aqueous Phospholipid Dispersions. *Anal. Rev. Biophys. Bioeng.* **13**, 1-24 (1984).
32) Harbottle, R.; Nag, K.; McIntyre, S.; Possmayer, F.; Petersen, N. O. Molecular organization revealed by tume of flight secondary ion mass spectrometry of a clinically used extracted pulmonary surfactant. *Langmuir* **19**, 3698-3704(2003).
33) Rodriguez-Capote, K.; Manzanares, D.; Haines, T.; Possmayer, F. Reactive oxygen species inactivation of surfactant involves structural and functional alterations to surfactant proteins SP-B and SP-C. *Biophys. J.* **90**, 2808-2821(2006).
34) Schrijver, R.; Vermeulen, D. Separation and quantitation of phospholipids in animal tissues by latroscan TLC/FID. *Lipids* **26**, 74-76(1991).
35) Crane, R. T.; Goheen, S. C.; Larkin, E. C.; Rao, G. A. Complexities in lipid quantitation using thin layer chromatography for separation and flame ionization for detection. *Lipids* **18**, 74-80(1983).
36) Dastis, M.; Rojo, N.; Alsina, M. A.; Haro, I.; Panda, A. K.; Mestres, C. Study in mono and bilayers of the interaction of hepatitis G virus(GBV-C/HGV)synthetic antigen E2(99-118)with cell membrane phospholipids. *Biophys. Chem.* **109**, 375-385(2004).
37) McEachren, T. M.; Keough, K. M. Phosphocholine reverses inhibition of pulmonary surfactant adsorption caused by C-reactive protein. *Am. J. Physiol. Lung Cell. Mol. Physiol.* **269**, L492-L497(1995).
38) Lu, K. W.; Perez-Gil, J.; Echaide, M.; Taeusch, H. W. Pulmonary surfactant proteins and polymer combinations reduce surfactant inhibition by serum. *Biochim. Biophys. Acta* **1808**, 2366-2373(2011).
39) Gunasekara, L.; Schoel, W. M.; Schürch, S.; Amrein, M. W. A comparative study of mechanisms of surfactant inhibition. *Biochim. Biophys. Acta* **1778**, 433-444 (2008).
40) Fuchimukai, T.; Fujiwara, T.; Takahashi, A.; Enhorning, G. Artificial pulmonary surfactant inhibited by proteins. *J. Appl. Physiol.* **62**, 429-437(1987).
41) Bernhard, W.; Gebert, A.; Vieten, G.; Rau, G. A.; Hohlfeld, J. M.; Postle, A. D.; Freihorst, J. Pulmonary surfactant in birds, Coping with surface tension in a tubular lung. *Am. J. Physiol. - Reg. Int. Comp. Physiol.* **281**, R327-R337(2001).
42) Seeger, W.; Gunther, A.; Thede, C. Differential sensitivity to fibrinogen inhibition of SP-C- vs. SP-B-based surfactants. *Am. J. Physiol. Lung Cell. Mol. Physiol.* **262**, L286-L291(1992).
43) De La Serna, J. B.; Perez-Gil, J.; Simonsen, A. C.; Bagatolli, L. A. Cholesterol rules: Direct observation of the coexistence of two fluid phases in native pulmonary surfactant membranes at physiological temperatures. *J. Biol. Chem.* **279**, 40715-40722(2004).
44) Laing, C.; Baoukina, S.; Tieleman, D.P. Molecular dynamics study of the effect of cholesterol on the properties of lipid monolayers at low surface tensions. *Phys. Chem. Chem. Phys.* **11**, 1916-1922(2009).
45) Panda, A. K.; Nag, K.; Harbottle, R. R.; Possmayer, F. Thermodynamic studies of bovine lung surfactant extract mixing with cholesterol and its palmitate derivative. *J. Coll. Interf. Sci.* **311**, 551-555(2007).
46) Cockshutt, A. M.; Possmayer, F. Lysophosphatidylcholine sensitizes lipid extracts of pulmonary surfactant to inhibition by serum proteins. *Biochim. Biophys. Acta* **1086**, 63-71(1991).
47) Panda, A. K.; Nag, K.; Harbottle, R. R. Possmayer, F.; Petersen, N. O. Thermodynamic studies on mixed molecular langmuir films: Part 2. Mutual mixing of DPPC and bovine lung surfactant extract with long-chain fatty acids. *Colloids Surf. A* **247**, 9-17(2004).
48) Larsson, M.; Nylander, T.; Keough, K. M. W.; Nag, K. An x-ray diffraction study of alterations in bovine lung surfactant bilayer structures induced by albumin. *Chem. Phys. Lipids* **144**, 137-145(2006).
49) Nag, K.; Keough, K. M. W.; Morrow, M. Probing perturbation of bovine lung surfactant extracts by using DSC and ^{2}H-NMR. *Biophys. J.* **90**, 3632-3642(2006).

(a)

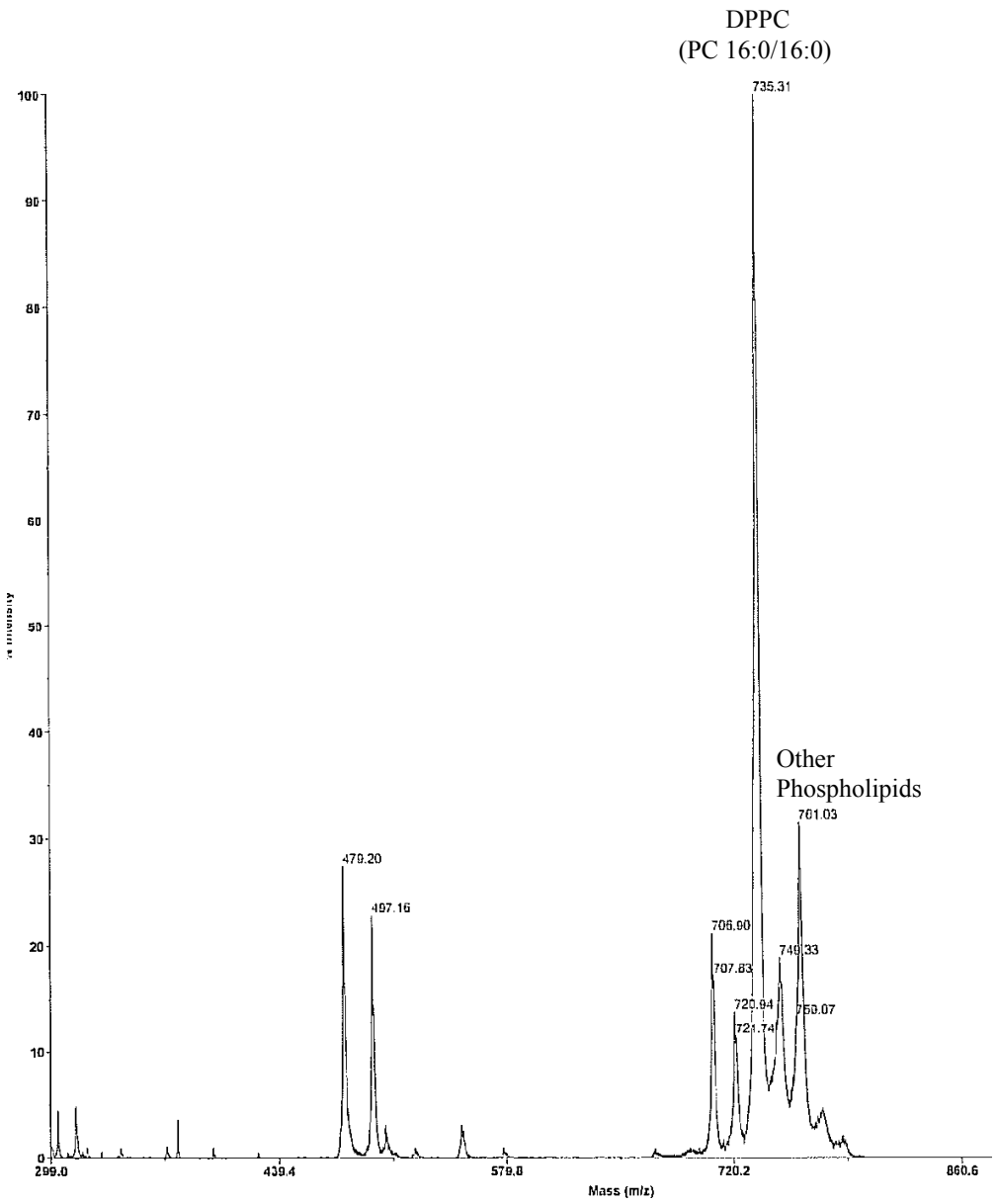
DPPC
(PC 16:0/16:0)
735.31
Other
Phospholipids
761.03
479.20
497.16
706.90
707.83
720.94
721.74
749.33
750.07
100
90
80
70
60
50
40
30
20
10
0
299.0
439.4
579.8
720.2
860.6
Mass (m/z)

(b)

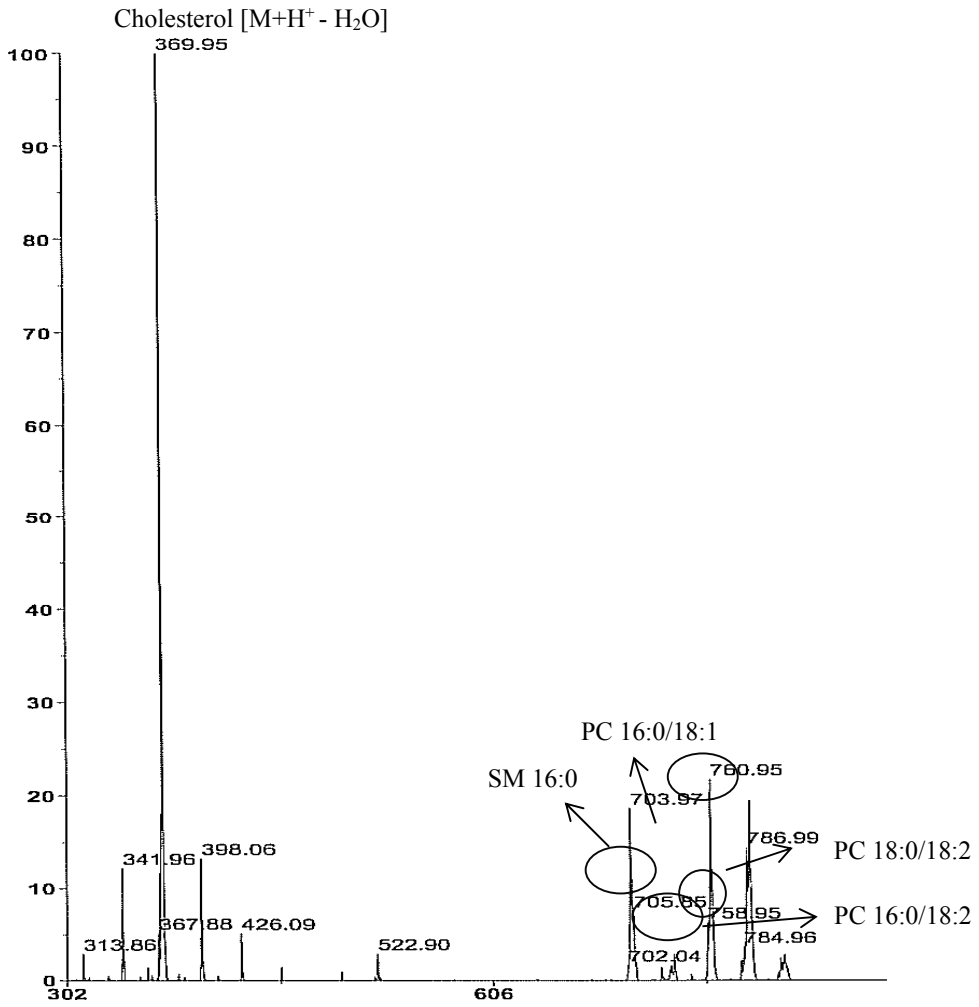
Cholesterol [M+H+ - H2O]
369.95
100
90
80
70
60
50
40
30
20
10
0
302
606
341.96
398.06
313.86
367.88
426.09
522.90
PC 16:0/18:1
SM 16:0
780.95
703.97
786.99
PC 18:0/18:2
705.85
758.95
PC 16:0/18:2
784.96
702.04

(c)

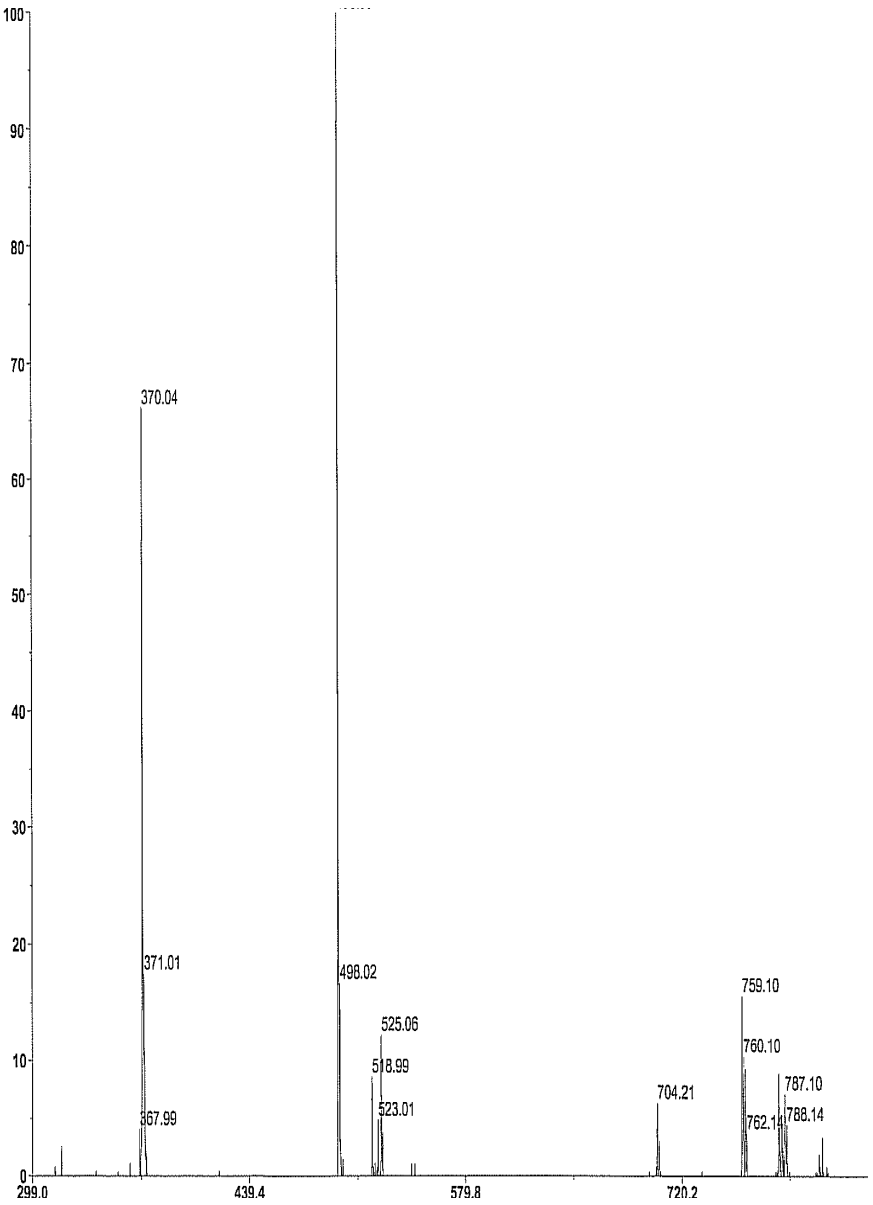

Figure S1: MALDI-TOF mass spectrometry spectra of (a) BLES and (b) serum lipids (c) LDL and (d) table of serum lipids by Iatroscan. For the BLES sample, DPPC was the most abundant. As for the serum lipid extract, cholesterol was the most abundant. Several other phospholipid classes are detected in the 700+ m/z range.

(a)

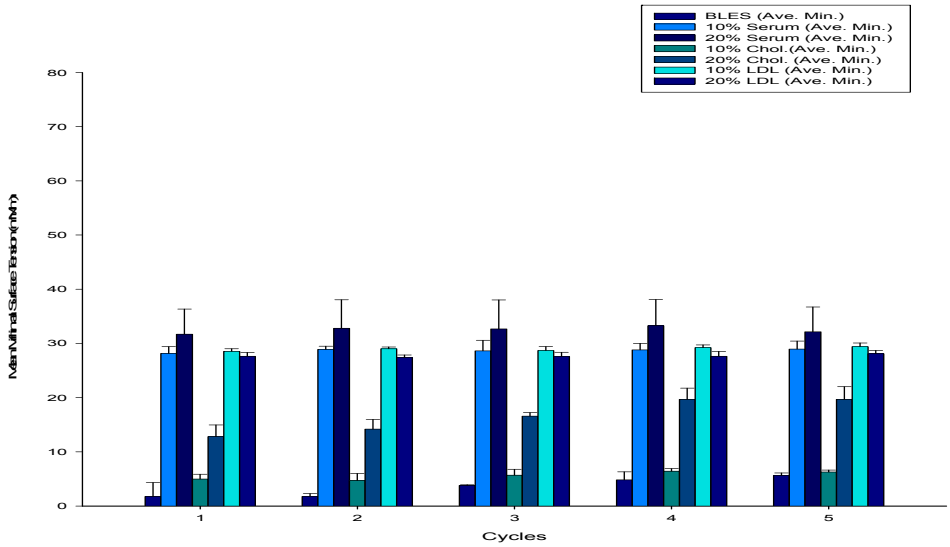

(b)

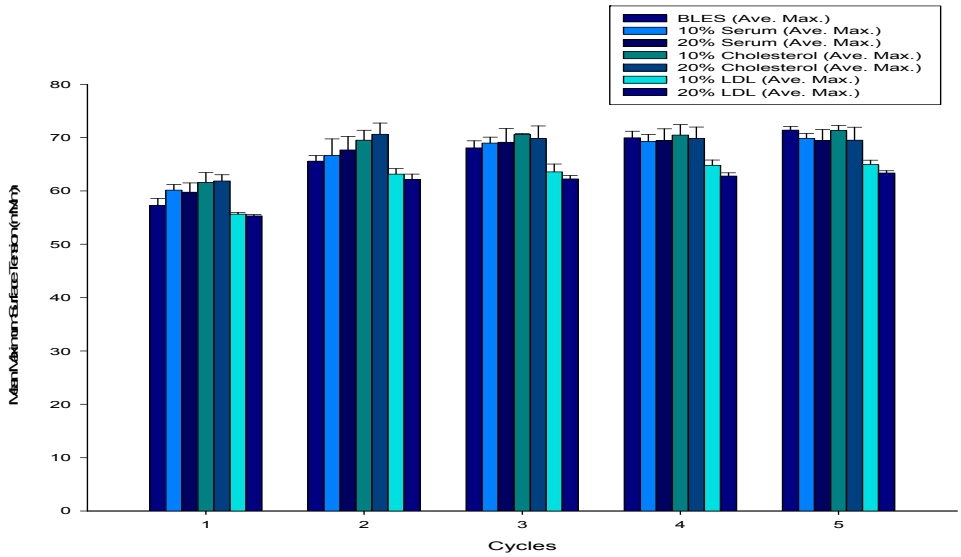

Figure S2. Effects of serum, cholesterol, and LDL on (a) minimum and (b) maximum surface tension achieved by BLES films for 5 cycles of compression-expansion. Three sets of independent experiments were performed and the graphs are indicative of the mean of each sample (n=3, error bars are standard deviation of the mean). The standard deviation is represented by error bars.

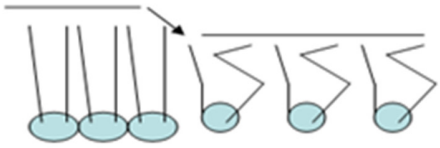

(a) BLES

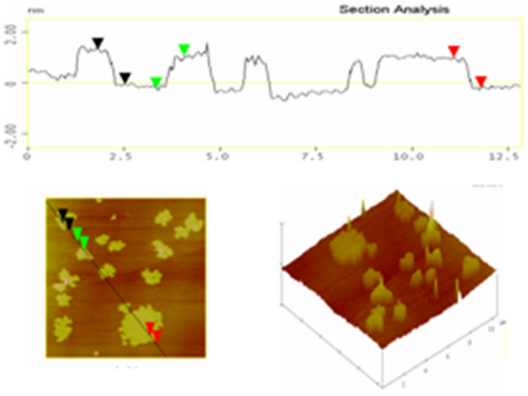

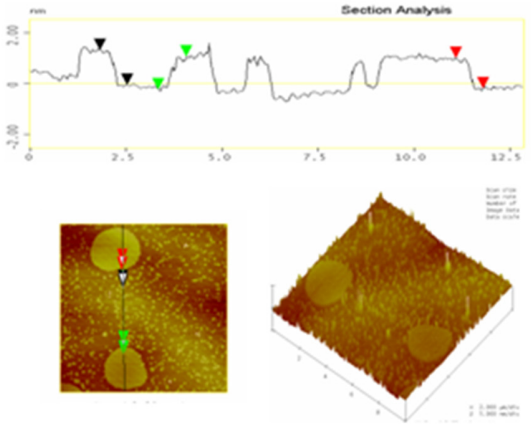

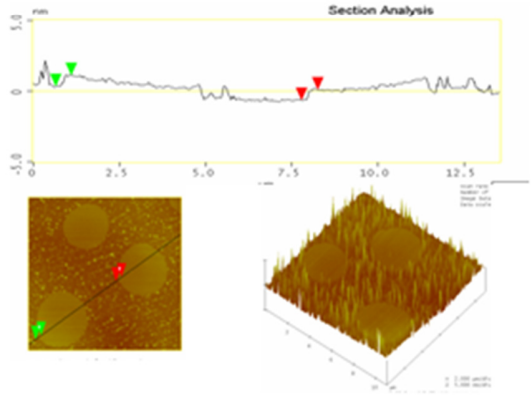

(b)

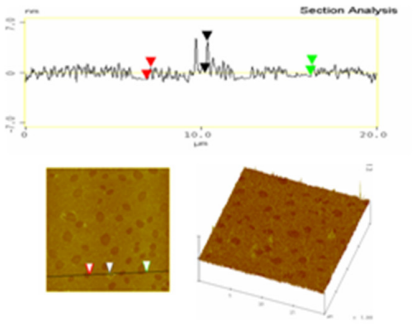

(c)

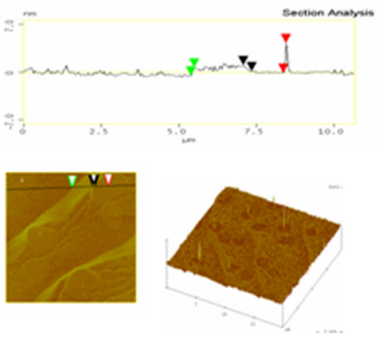

52 mN/m

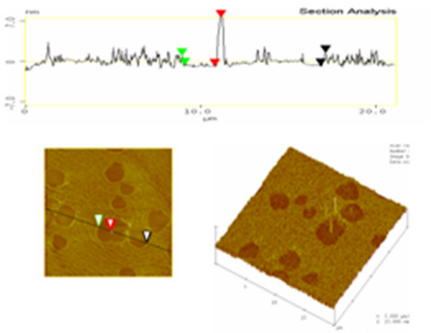

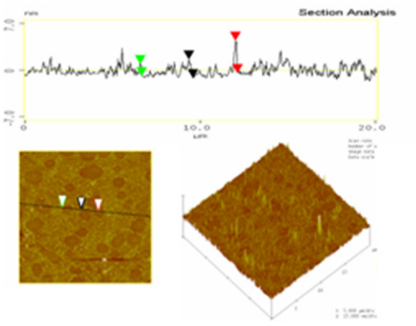

42 mN/m

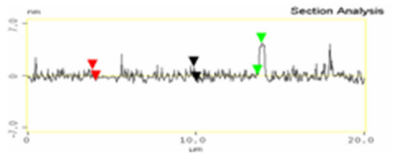

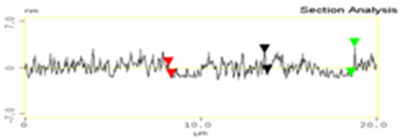

32 mN/m

(d)

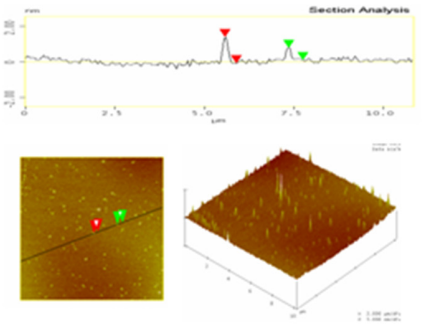

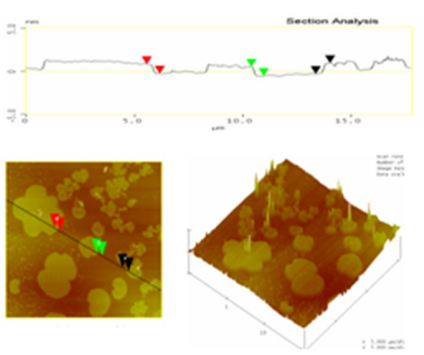

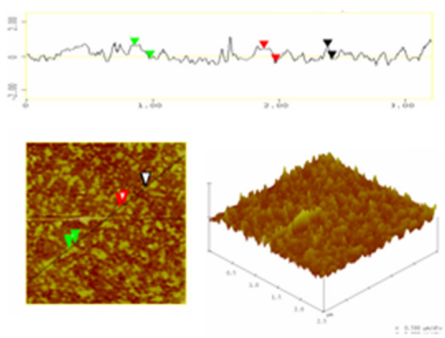

(e)

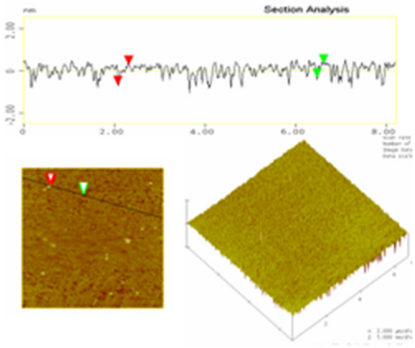

52 mN/m

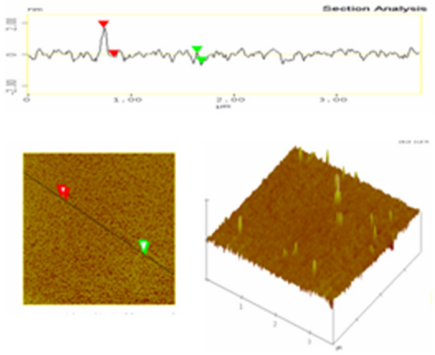

42 mN/m

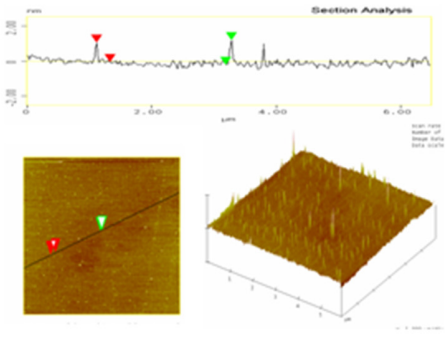

32 mN/m

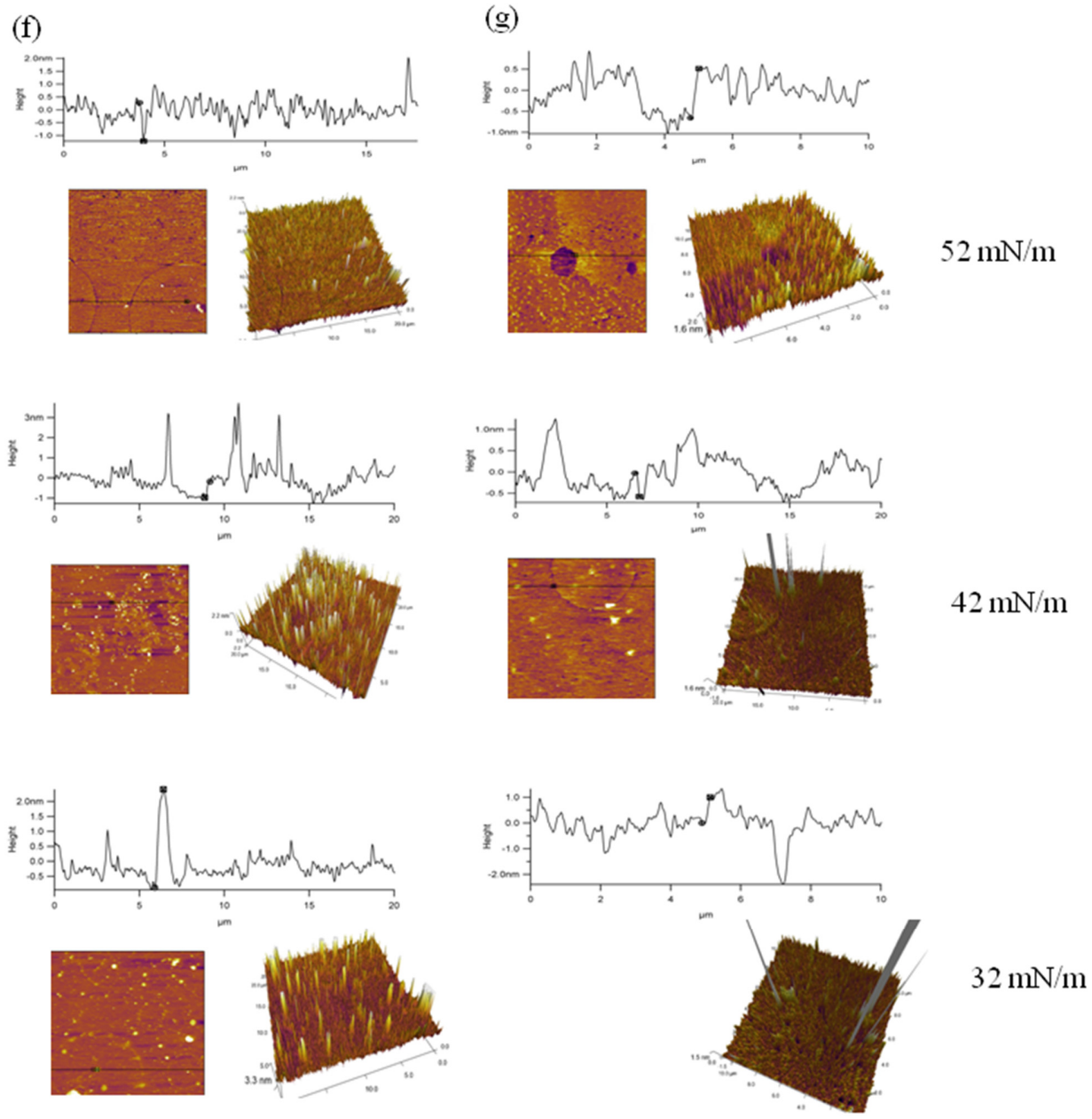

Figure S3. Height differences (section analysis) between the gel and fluid phases of the AFM image of BLES + additive films at γ 52, 42, and 32 mN/m for (a) pure BLES and BLES with (b) 10wt% serum, (c) 20wt% serum, (d) 10wt% cholesterol, (e) 20wt% cholesterol, (f)10wt% LDL and (g) 20wt% LDL. Both three dimensional (3D) and sectional analysis

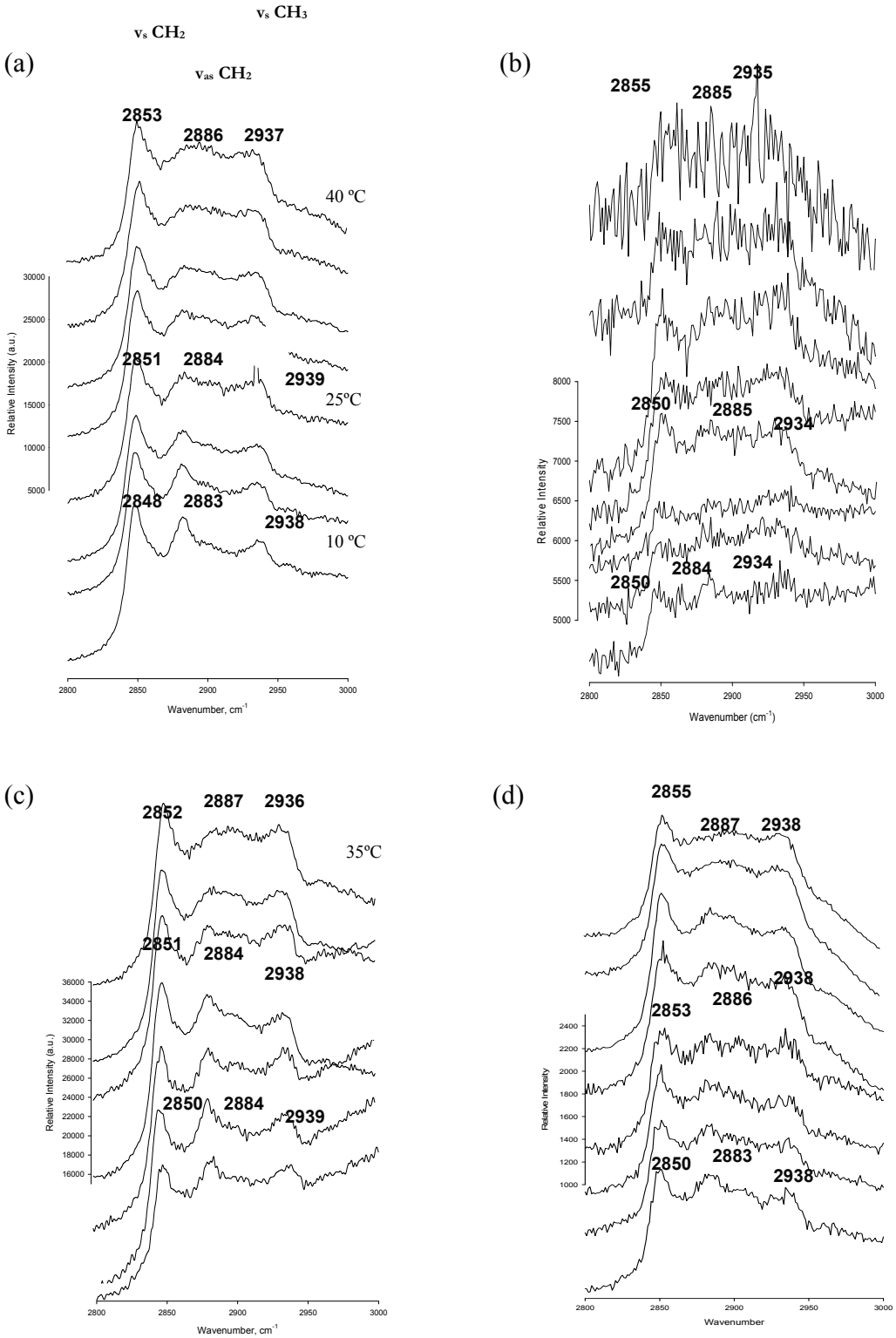
(a)
ν_s CH_3
ν_s CH_2
ν_{as} CH_2
2853
2886
2937
40 ºC
2851
2884
2939
25ºC
2848
2883
2938
10 ºC
Relative Intensity (a.u.)
Wavenumber, cm^{-1}
(b)
2855
2935
2885
2850
2885
2934
2884
2934
2850
Relative Intensity
Wavenumber (cm^{-1})
(c)
2852
2887
2936
35ºC
2851
2884
2938
2850
2884
2939
Relative Intensity (a.u.)
Wavenumber, cm^{-1}
(d)
2855
2887
2938
2938
2886
2853
2850
2883
2938
Relative Intensity
Wavenumber

Figure S4: Raman spectra of the 2800-3000 cm^{-1} range for (a) BLES, (b) BLES + 10wt% serum, (c) BLES +10wt% cholesterol, and (d) BLES + 10wt% LDL. Each graph is a representative of three different experimental trials. Similar trends were shown for BLES and BLES + 20wt% serum, 20wt% cholesterol, and 20wt% LDL samples. Temperature range indicated from 10^0C-40^0C, and was chosen, since BLES shows a broad thermotropic (gel to liquid crystalline) phase transition between the range as well as a midpoint of transition at 27^0C as determined previously by Raman and scanning calorimetry (Nag *et al*., 2002). Note the shift of the 2848 cm^{-1} band at 10^0C to 2855 cm^{-1} at 40^0C. The shift is characteristic of the BLES system, melting from gel to liquid crystalline phase. The spectra in (b) had a large noise to signal ratio, which was similar to the ones observed for serum. This could be due to protein auto-fluorescence from the serum soluble proteins.

RSC Advances

PAPER

View Article Online
View Journal | View Issue

Cite this: *RSC Adv.*, 2015, **5**, 26061

Physicochemical studies on local anaesthetic loaded second generation nanolipid carriers†

Prasant Nahak,[a] Gourab Karmakar,[a] Biplab Roy,[a] Pritam Guha,[a] Manish Sapkota,[b] Suraj Koirala,[b] Chien-Hsiang Chang[c] and Amiya Kumar Panda*[a]

Received 15th December 2014
Accepted 2nd March 2015

DOI: 10.1039/c4ra16434b

www.rsc.org/advances

This study aimed to investigate the effect of hydrocarbon chain length of nonionic surfactants, Tween 40 and Tween 60, on the physicochemical properties of nanostructured lipid carriers (NLCs). Two local anaesthetics, lidocaine (LIDO) and procaine hydrochloride (PRO·HCl), were incorporated in the NLCs. NLC formulations were prepared using sorbitantristearate (Span 65), soy lecithin (SLC) and stearic acid (SA) in a 2 : 2 : 1 mole ratio employing the hot homogenization technique. The systems were characterized by combined dynamic light scattering (DLS), transmission electron microscopy (TEM), differential scanning calorimetry (DSC) and spectroscopic studies. The formulations were found to be stable up to 60 days when kept at 4 °C. NLCs stabilized by Tween 60 were superior to the corresponding Tween 40 based formulations. A spherical morphology with smooth surfaces was evidenced by TEM measurements. DSC and polarity studies indicated that LIDO altered the crystallinity of the lipid matrices as it could insert into the core of the NLC. Entrapment efficiency (EE) and loading content (LC) studies revealed that Tween 60 stabilized NLCs have better drug loading capability than the Tween 40 based formulation. Controlled and prolonged drug release was experienced by Tween 60 stabilized drug loaded NLCs as studied by *in vitro* release kinetics. The developed NLCs could thus be considered to have prospects as novel drug carriers for controlled/sustained release to improve the time duration of anaesthesia, especially for topical application.

1. Introduction

For decades, attempts have been made to develop promising drug carriers associated with improved bioavailability, increased therapeutic activities and sustained release using lipid and polymeric nanoparticles.[1–5] However, it has not yet been possible to develop a single suitable drug delivery system with all the advantages. Different types of drug carriers have been designed using polymers, lipids and/or their composites; each one having its own merits and demerits.[4,6–14] Attempts towards developing efficient drug delivery systems experienced limited success in the pharmaceutical markets. The present day drug delivery systems include nanoemulsion,[13] polymeric nanoparticle,[8] liposome,[9] solid lipid nanoparticle (SLN)[15] and nanostructured lipid carrier (NLC), a modified form of SLN.[5] Hecht *et al.* and associates researchers have made a significant contribution in developing different drug delivery systems. These include the polymeric nanoparticles,[16] micellar nanoparticles,[17] peptides,[18] disaccharides moieties of bleomycin,[19,20] *etc.* It has been found that some other peptide based drug delivery systems, however, endure poor intracellular delivery and target specific selectivity.[18,21] The major drawbacks associated with nanoemulsions include its physical wavering due to the partitioning of drug into the aqueous phase. Besides, the controlled release cannot be assured due to the high mobility of drug incorporated in the system.[12,13,22] Polymeric nanoparticles suffer from its precincts, *viz.*, cytotoxicity during internalization and degradation inside the cell, non feasibility of large scale production, *etc.*[16,17,23] Also the polymer based drug delivery systems are susceptible to some chemical transformations, *viz.*, hydrolysis during storage and the resulted metabolites may be responsible for some serious toxicity.[8,10,24,25] Although the aforementioned limitations could successfully be overcome with the advent of small molecule based drug delivery systems and liposomes, however, such systems suffer from limitations like the physical unsteadiness, drug leakage, non-specific clearance, cellular penetration efficiency, selectivity and high cost of the excipients, *etc.*[9,19,20,25,26]

Since 1990, solid lipid nanoparticles (SLNs) have extensively been explored as potential drug carriers.[2,15,27,28] SLNs are typically spherical particles with an average size between 100–1000 nm.[29] The components of SLNs are biocompatible and

[a]*Department of Chemistry, University of North Bengal, Darjeeling-734013, West Bengal, India. E-mail: akpanda1@yahoo.com*

[b]*Department of Pharmaceutics, Himalayan Pharmacy Institute, Majhitar, Rangpo, East Sikkim-737136, India*

[c]*Department of Chemical Engineering, National Cheng Kung University, Tianan, 70101, Taiwan*

† Electronic supplementary information (ESI) available. See DOI: 10.1039/c4ra16434b

biodegradable under physiological conditions that minimize the risk of toxicity. The lipids used are solid under physiological condition. It has been reported that the SLNs are capable to act as suitable drug carrier, stable in gastrointestinal fluids and provide improved bioavailability to the drugs.[1,2] SLNs form highly crystalline lattice due to structurally (hydrocarbon chain) similar lipids which subsequently can afford limited space to drug molecules; this eventually results in the rapid drug expulsion during storage. Such limitation of SLNs could be overcome with the introduction of its modified form, known as nanostructured lipid carriers (NLCs). NLCs usually comprise structurally dissimilar lipidic components; the mismatch in the hydrocarbon chain results in the generation of multicrystalline lipid matrices. Presence of imperfection/void spaces can accommodate significant amount of drug. Subsequently, NLCs can have high entrapment efficiency, loading content, controlled drug release, long term physical stability, preserved chemical degradation of drug during storage, *etc.*[5,14,30–33] It has also been reported that NLCs can act as suitable carriers for both hydrophilic and lipophilic drugs.[34] Because of their unique particle size (100–1000 nm), internalization of such drug delivery systems into the cells become efficient; this facilitates site specific delivery of therapeutic agents.[35,36] Research on NLCs have thus gained significant importance because of their perspective, yet unexplored application potentials as drug delivery systems for the different routes of administration with an aim to improve the biodistribution and therapeutic efficacy.[5,31]

Different types of monoglycerides, diglycerides, triglycerides, waxes, phospholipids and fatty acids have extensively been used to develop NLCs.[29] However, use of sorbitan tristearate (Span 65) as one of the lipidic component in preparing NLCs is not common in literature, in spite of its biocompatibility.[37] It is not unexpected that imperfection/void spaces in the NLC matrices would exist if it is used in combination with soy lecithin and stearic acid. Hydrocarbon chain of the stabilizers also has pronounced effect on creating imperfections. The effect of stabilizers on the solution phase behavior and thermal properties of NLC such as temperature of maximum heat flow (T_m), peak width at half maxima ($\Delta T_{1/2}$), change in enthalpy (ΔH), heat capacity (ΔC_p) and crystallinity index (C.I.) have not meticulously been investigated. The hydrocarbon chain mismatch is expected to make the formulation as a novel carrier for lipophilic, hydrophilic as well as amphiphilic drug molecules. The study related to drug location in NLC is exceptional in literature and more investigations are warranted in this regard. Location of the drugs in the NLC could be predicted with the help of spectroscopic as well as thermal investigations. In addition, influence of hydrocarbon chain length on the entrapment efficiency, loading content and release kinetics are not well established for this type of small molecules loaded in NLC. Our present study is intended to explore such systems on the basis of detailed physicochemical characterization.

Lidocaine (LIDO) and procaine hydrochloride (PRO·HCl) are frequently used as local anaesthetics for topical application.[24,38,39] Both LIDO and PRO·HCl are frequently used in order to get relieves from pain itching, burn and cutaneous inflammation, *etc.*[40] They induce pain relief by blocking fast voltage-gated sodium channels in the cell membrane of post-synaptic neurons. Thus they prevent depolarization and inhibit the generation and propagation of nerve impulses.[41] LIDO and PRO·HCl are marketed as Xylocaine® and Novocaine® respectively.[38,42] While considering the aforementioned dermal applications, it is one of the essential condition that the drug should preferably remain on the skin surface, thus minimizing its side effects.[43,44] Besides, in case of topical formulation, it should be ensured that there should be adequate localization of drug,[40] as well as sustained release.[38] In spite of a number of available reports on local anaesthetics loaded drug delivery systems, however, no such single system have been found to be completely prudent in terms of topical applications. The major drawbacks of local anaesthetics in topical applications are characterized by cutaneous lesions, urticaria, edema, *etc.*[43,44] However, the major concern using LIDO or PRO·HCl is its penetration through skin which subsequently increase the plasma level in blood.[45] Studies demonstrated by different researchers[24,38,40] suggest that the severe side effects can drastically be reduced when loaded in suitable drug delivery system. Carafa *et al.*[40] have made a comparative study on the permeability of LIDO and its protonated form (LIDO·HCl). They have found that for classical liposome formulations permeability of hydrochloride derivative (LIDO·HCl) was less than the corresponding free base. It was rationalized on the basis that the free base, being more lipophilic, could permeate through the hydrophobic membrane bilayer than the hydrochloride derivative. We tried to ensure the validity of this rationalism for NLC formulation using LIDO and PRO·HCl. In order to prolong the anaesthetic effect and reduce dose frequency as well as the skin irritation caused by the high dose of anaesthetics, such formulations are considered worthy to be investigated.

The present study endeavours to investigate the effect of hydrocarbon chain length of the stabilizers (herein Tween 40 and Tween 60) on the formulation and physicochemical properties of NLC. NLCs were prepared by mixing sorbitan tristearate (Span 65), soy lecithin and stearic acid by way of hot homogenization technique in the absence and presence of varying amount of two local anaesthetics, LIDO and PRO·HCl. Dynamic light scattering studies were performed to determine the hydrodynamic diameter (d_h), polydispersity index (PDI) and zeta potential (Z.P.) of the NLCs. Thermal behaviour and the associated parameters, *viz.*, temperature of maximum heat flow (T_m), crystallinity index (CI), enthalpy change (ΔH) and heat capacity change (ΔC_p) of the lipid matrices in the absence and presence of the anaesthetics were evaluated by differential scanning calorimetry (DSC). Location and subsequent state of polarity of the drugs were investigated by UV-visible absorption spectroscopy. Furthermore, entrapment efficiency (EE), loading content (LC) and *in vitro* release kinetics of the drugs from the NLCs were studied. It is believed that the limitations of LIDO and PRO·HCl can be circumvented by incorporating them in NLC which are expected to release the anaesthetic in controlled and prolonged fashion at the site of action, even when present in high dose.

2. Experimental section

2.1. Materials

Sorbitan tristearate (Span 65, 99%) was purchased from S. D. Fine-Chem Ltd., India. [(2*R*)-2,3-Di(tetradecanoyloxy)propyl]-2-(trimethylazaniumyl) ethyl phosphate (soy lecithin, SLC, 98%) was a product from Calbiochem, Germany. Stearic acid (99%) as well as the nonionic surfactants polyoxyethylene (20) sorbitanmonopalmitate (Tween 40) and polyoxyethylene (20) sorbitanmonostearate (Tween 60), all of 98% purity, were purchased from Sisco Research Laboratory, India. Lidocaine (LIDO, 98%), procaine hydrochloride (PRO·HCl, 97%) and the dialysis bag (12 kDa MWCO) were obtained from Sigma-Aldrich Chemicals, USA. All the materials were used as received. HPLC grade solvents from Merck, India were used. Double distilled water with a specific conductance of 2–4 μS (at 25 °C) was used throughout the experiment.

2.2. Methods

2.2.1. Preparation of NLCs. Nanostructured lipid carriers (NLCs) were prepared by hot homogenization method followed by ultrasonication.[14,46] Quantitative amount of Span 65, SLC and SA (2 : 2 : 1 M/M/M) was taken in a round bottom flask and was dissolved in chloroform–methanol mixture (3 : 1, v/v). A thin film was generated in a rotary evaporator. The homogenized thin film was then heated at 70 °C (5–10 °C above the melting point of all the lipidic components). Aqueous Tween solution (10 mM, preheated was stirred at 1000 rpm using a magnetic stirrer. The coarsely at same temperature) was then added to the molten lipid mixture and emulsified dispersion was then exposed to ultrasonication for an hour (Takashi U250, Tokyo, Japan). The clear medium was then cooled down to room temperature whereby the stable NLC formulation was achieved. The total lipid concentration for all the formulations was kept constant at 5 mM and 10 mM nonionic surfactants (Tween 40 and Tween 60) were used separately as the stabilizers. Different formulations were prepared as either blank-NLC and LIDO or PRO·HCl loaded NLC whereby the drug concentration was varied in the range of 0.5–2.5 mM.

2.2.2. Instrumentation. The mean particle size, polydispersity index (PDI) and zeta potential (Z.P.) of the NLCs in the absence and presence of the two drugs were investigated by dynamic light scattering (DLS) studies (Zetasizer Nano ZS90, ZEN 3690, Malvern Instrument Ltd., U.K.). Data were recorded at 90° using a He–Ne laser (632.8 nm). Prior to measurement all the samples were filtered using 0.45 μm cellulose nitrate membrane. Considering apparent spherical geometry, surface area of the NLC was calculated. Taking into account of the average molecular cross sectional area of the individual lipidic components, the NLC concentration was found to be of the order of 25 nM for an overall 5 mM lipid concentration. It is also assumed that at this fairly dilute concentration the inter particle interaction was insignificant. Shape and morphology of the NLCs were investigated by transmission electron microscopy (TEM, Hitachi, Japan). UV-visible absorption spectra of drug loaded NLCs were recorded by a UV-visible spectrophotometer (UVD-2950, Labomed Inc., USA) in the range of 200–400 nm; corresponding NLC without the drug was used as reference. Thermal analyses were carried out using a differential scanning calorimeter, DSC 1 STAR^e system (Mettler Toledo, Switzerland). Samples were sealed in 40 μL standard aluminum pans and were quickly equilibrated in the temperature range of 15–80 °C within 15 min. DSC scan was performed with a scan rate of 2 °C min^{-1} in the temperature range 15–80 °C under nitrogen purge for both heating and cooling cycles. Corresponding surfactant, used as stabilizer for NLC preparation, was used in the reference pan. Thermal parameters, *viz.*, temperature of maximum heat flow (T_m), peak width at half maximum ($\Delta T_{1/2}$), changes in enthalpy (ΔH) and specific heat capacity (ΔC_p) were evaluated using DSC-STAR^e software. Entrapment efficiency (E.E.) and loading content (L.C.) of both LIDO and PRO·HCl loaded NLCs were evaluated by measuring the free drug concentration in the continuous phase of the NLC dispersion.[47] Briefly, 10 mL of drug loaded NLC dispersion was centrifuged at 10 000 rpm for 1 h at 4 °C (REMI, India). The drug loaded NLC thus got precipitated. The amount of free drug in the supernatant was quantified by measuring the absorbance at 264 nm and 293 nm for LIDO and PRO·HCl respectively (absorbance maxima of the drug in the Tweens). Entrapment efficiency (E.E.) and loading content (L.C.) were subsequently calculated by the following equation:[47,48]

$$\%\ \text{E.E.} = \frac{\text{weight}_{\text{intotal}} - \text{weight}_{\text{freedrug}}}{\text{weight}_{\text{intotal}}} \times 100 \quad (1)$$

$$\text{Loading content}\%\ (\text{LC}) = \left(\frac{W_a - W_s}{W_a + W_s - W_l}\right) \times 100\% \quad (2)$$

where, W_a, W_s and W_l were the weight of drug added in the NLC, analyzed weight of drug in supernatant and weight of lipid added in NLC, respectively. *In vitro* release kinetics was monitored by conventional dialysis bag method using aqueous surfactant solution as the release medium.[14] Dialysis bag (MWCO12 kDa) was soaked in the corresponding release medium overnight. Freshly prepared 10 mL drug loaded NLC dispersion was placed in the dialysis bag sealed and immersed in a beaker containing 50 mL of release medium with constant stirring. 2 mL of the aliquot was withdrawn at different time interval and was replaced by 2 mL of fresh release medium to maintain the sink condition. Quantification of LIDO and PRO·HCl was made colorimetrically at 264 and 293 nm respectively.

All the experiments, except the calorimetric studies, were carried out at controlled room temperature (25 °C). An average of three measurements has been reported for each set of studies.

3. Results and discussions

3.1. DLS studies

Hydrodynamic diameter (d_h), polydispersity index (PDI) and zeta potential (Z.P.) values are some of the stability indicators of NLC formulation.[49] Effect of hydrocarbon chain length of the Tweens and drug payload on d_h, PDI and Z.P. values of different

NLC formulations were studied by DLS technique. d_h–time profiles for different NLC formulations in the absence and presence of the drugs have been presented in Fig. 1. d_h values were found to be dependent on the type of Tween surfactant as well as on the nature and concentration of the local anaesthetics. NLC formulations were stable upto 60 days, after which phase separation of the components was noticed. Size of the blank NLCs depended on the hydrocarbon chain length of Tween. In case of Tween 40 stabilized NLC, size varied in the range of 250–475 nm; for Tween 60 the values were in the range of 43–75 nm. In both the cases d_h values increased with time. Increase in hydrodynamic diameter was due to the structural reorganization of the lipidic components as well as the Ostwald ripening process, common for the colloidal dispersions.[50,51] Size constriction, in case of Tween 60 stabilized systems, compared to Tween 40, can be rationalized by considering the insertion of the hydrocarbon chain of Tweens into the NLC matrices, as proposed in Scheme 1. Because of its similarity in the hydrocarbon chain length with the other lipidic components (stearic acid and Span 65, both having C_{18} hydrocarbon chains), Tween 60 could get inserted in a better way than Tween 40. Size of the drug loaded NLC formulations depended on type of the Tweens used as well as the anaesthetics and its concentration. While LIDO led to an overall increase in the size of the NLC formulations, for PRO·HCl loaded systems, the effects were less significant. PRO·HCl, being ionic in nature, is expected to reside on the palisade layer of the NLCs. On the contrary, LIDO, being more lipophilic, is expected to get inserted into the lipidic core to higher extent, which subsequently results in the size enhancement of the NLCs. However, insertion of LIDO into the NLC core resulted in an increase in polydispersity as well. In fact, similar observations were experienced while considering the PDI values of the formulations. Results are shown in Fig. S1 in the ESI.† It was observed that for PRO·HCl loaded NLCs PDI values were lower than the LIDO loaded systems. Results clearly suggest that PRO·HCl comprising systems were more homogeneous than the other. It was also observed that in case of PRO·HCl the PDI values did not appreciably change with time, however for LIDO loaded systems significant increase in PDI value with time was noticed. Size of the NLCs decreased with increasing LIDO concentration for Tween 40 stabilized systems. On the contrary increasing concentration of LIDO resulted in the size enhancement for Tween 60. This can further be rationalized on the basis of hydrocarbon packing of the Tweens in the NLC core. The drug LIDO, being amphiphilic in nature, enhances the adsolubilization of Tween 40 over the NLC surface. However, in case of Tween 60, addition of LIDO, which prefers to get deeply inserted into the NLC, will result in the swelling of the NLC core; subsequently sizes of the formulations were enhanced. Almost similar effect was noticed in case of PRO·HCl.

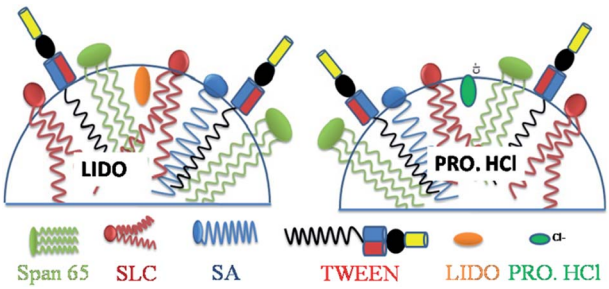

Scheme 1 Proposed model for the organization of lipids and drugs in the NLC formulations stabilized by Tweens.

Like other colloidal dispersions, NLC formulations are also charged which impart the kinetic stability.[52] Effects of drug concentration on the magnitude of zeta potential are graphically shown in Fig. 2. In all the cases zeta potential values were negative, due to the presence of the dissociated form of stearic acid. Magnitude of negative zeta potential values were higher in case of Tween 60 stabilized systems, suggesting higher

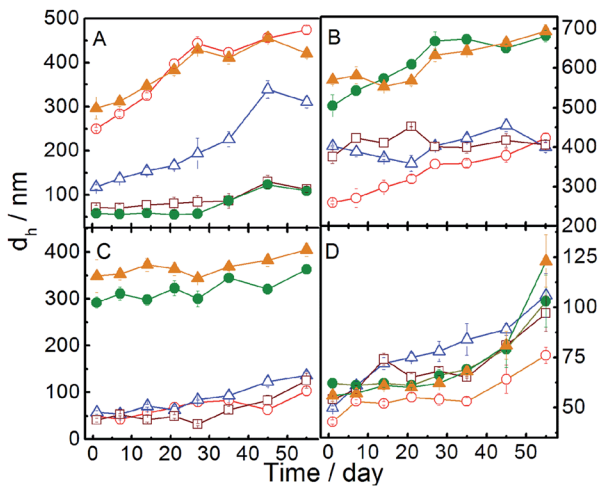

Fig. 1 Hydrodynamic diameter (d_h)–time profile of NLCs (Span 65 + SLC + SA, 2 : 2 : 1 M/M/M) dispersed in Tweens in presence of varying concentration of drugs. Panel A: LIDO loaded NLC in Tween 40; panel B: PRO·HCl loaded NLC in Tween 40; panel C: LIDO loaded NLC in Tween 60 and panel D: PRO·HCl loaded NLC in Tween 60. 5 mM NLC was dispersed in 10 mM Tweens in each case. Drug concentration (mM): ○, 0; △, 0.5; □, 1; ●, 2 and ▲, 2.5. Temp. 25 °C.

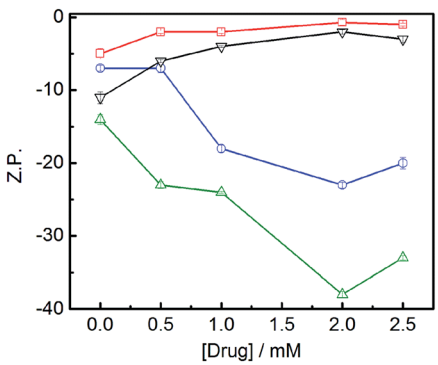

Fig. 2 Influence of LIDO and PRO·HCl on the (Z.P.) of NLCs (Span 65 + SLC + SA, 2 : 2 : 1 M/M/M) dispersed in Tweens. Systems: ○, LIDO-Tween 40; △, LIDO-Tween 60; □, PRO·HCl-Tween 40 and ▽, PRO. HCl-Tween 60. Temp. 25 °C. 5 mM lipid in the absence and presence of the drug was dispersed in 10 mM aqueous Tween solution.

dissociation of the fatty acid. In case of Tween 60, NLC surface is less masked by the hydrophobic environment because of its better insertion capability (as proposed earlier). Subsequently dissociation of the fatty acid becomes easier compared to Tween 40. Magnitude of the negative zeta potential increased with increasing LIDO concentration. LIDO being amphiphilic in nature results in the adsolubilization of the lipidic components for which the dissociation of the fatty acid becomes easier.

In case of PRO·HCl, as it is positively charged, it is not unexpected that it will mask the zeta potential through interfacial adsorption and charge neutralization. However such systems were found to be equally stable as the LIDO loaded systems. Steric stabilization by the Tweens could prevent the agglomeration of such NLC formulations.

3.2. Transmission electron microscopy (TEM) study

Shape and morphology of the NLCs were checked by TEM in order to get more information about particle size and shape. Spherical and smooth surface morphology of the NLCs were observed (Fig. 3).

NLCs were almost spherical in shape within 100–500 nm range, which were reflected with the size data determined by DLS. Smaller size, as obtained by the TEM studies, was probably due to the drying phenomena during sample preparation.

3.3. Differential scanning calorimetric (DSC) studies

Results on the DSC studies are presented in Fig. 4–6, Table S2 and Fig. S2 (ESI†) respectively. Fig. S2 (ESI†) demonstrates the general pattern of the endothermic and exothermic peaks during heating and cooling scans respectively for LIDO loaded NLC dispersed in Tween 60 aqueous solution. While the heating curve was broader and shallow, the cooling curve was well defined, more pronounced, narrow and sharp. This kind of observation is not uncommon in the literature.[53] As the exothermic peaks were more prominent, hence the cooling curves were taken into account for further data analyses. The exothermic peaks of the drug free as well as drug loaded NLC formulations were comparatively broader compared to the previously reported systems.[39] DSC cooling curves for different NLC formulations in the absence and presence of drugs are shown in Fig. 4. In case of drug free systems, significant

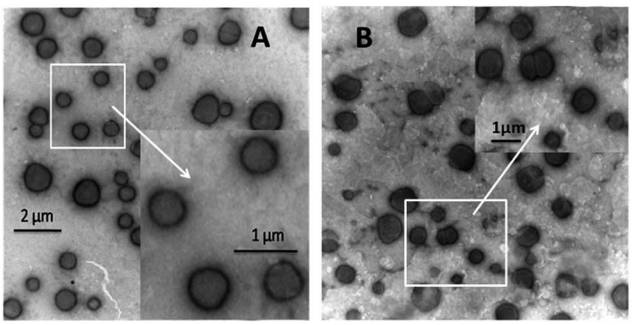

Fig. 3 Representative TEM images of LIDO loaded NLC dispersion in Tween 40 (A) and PRO·HCl loaded NLC dispersion in Tween 40 (B).

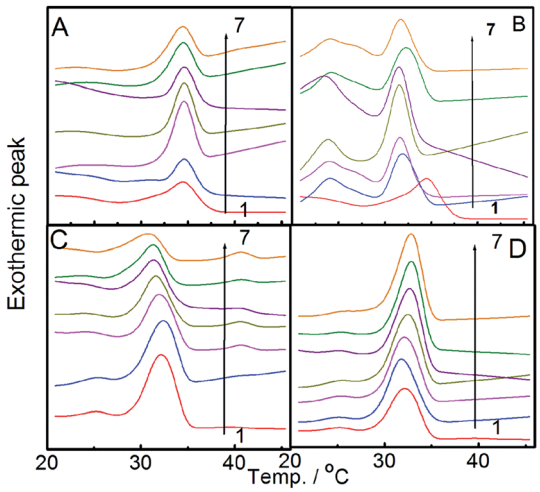

Fig. 4 DSC cooling curves of LIDO (panel A) and PRO·HCl (panel B) loaded NLC dispersed in Tween 40; LIDO (panel C) and PRO·HCl (panel D) loaded NLC dispersed in Tween 60. 5 mM NLC with Span 65 + SLC + SA, 2 : 2 : 1 M/M/M, was dispersed in 10 mM aqueous Tween solution. Concentration of drug (mM): 1, 0; 2, 0.2; 3, 0.5; 4, 1.0; 5, 1.5; 6, 2.0 and 7, 2.5. Scan rate 2 °C min^{-1}.

difference in the T_m values were noted between Tween 40 and Tween 60 stabilized NLCs. T_m values were 35.61 °C and 32.58 °C for Tween 40 stabilized system, and Tween 60 stabilized systems respectively. Decrease in the T_m value with decreasing size could be explained by Thomson proposition.[47,54–56] It has already been observed from the DLS studies that the NLCs stabilized by Tween 40 were larger than the Tween 60 stabilized systems. Therefore it is not unexpected that the smaller entities would have lower melting temperature than the larger particles.

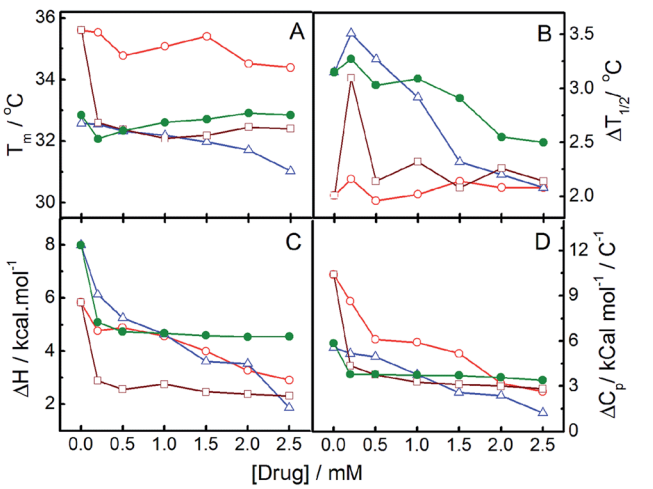

Fig. 5 Effects of drugs on the temperature of maximum heat flow (T_m, panel A), width of half peak height ($\Delta T_{1/2}$, panel B), change in enthalpy (ΔH, panel C) and heat capacity (ΔC_p, panel D) of NLCs (Span65 + SLC + SA, 2 : 2 : 1 M/M/M). 5 mM lipid was dispersed in 10 mM aqueous Tween solution. System ○; LIDO loaded in Tween 40: △; LIDO loaded Tween 60: □; PRO·HCl loaded Tween 40: and ●; PRO·HCl loaded Tween 60.

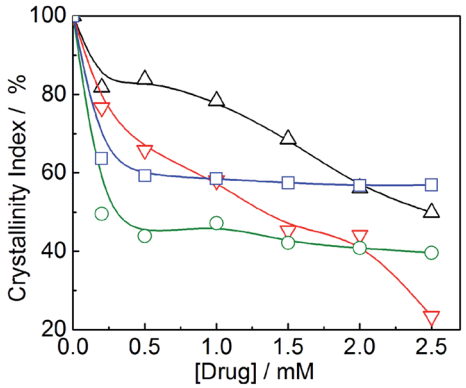

Fig. 6 Effects of drug concentration on the degree of crystallinity of NLC (5 mM, Span 65 + SLC + SA, 2 : 2 : 1 M/M/M). Systems: △, LIDO-Tween 40; ▽, LIDO-Tween 60; ○, PRO·HCl-Tween 40 and □, PRO·HCl-Tween 60.

T_m values progressively decreased with increasing LIDO concentration (Fig. 5 panel A). The effect was less pronounced for Tween 40 comprising systems than the Tween 60. Blank NLC formulations with Tween 60 exhibited lower T_m values and it continued for the LIDO loaded systems. In case of PRO·HCl, the T_m value did not change appreciably with varying drug. Difference in the T_m values among LIDO and PRO·HCl loaded systems could be rationalized by the same proposition as mentioned in the DLS studies. LIDO, being amphiphilic in nature, can have higher penetration into the NLC core than PRO·HCl. Thus the melting point are expected to decrease due to the added drug. For PRO·HCl, as the drug resides preferably on the NLC surface, hence it could not significantly perturb the packing of hydrocarbon chains in the NLCs. Studies on the thermal behaviour of the drug loaded NLC formulations thus could shed light on the location of the drugs.

Wide peaks indicate the presence of multicrystalline entities in the NLC formulation. Effect of drug on the thermal behaviour of NLCs were further scrutinized through the $\Delta T_{1/2}$–drug concentration profile (Fig. 5 panel B). Herein $\Delta T_{1/2}$ represents the peak width (thermal scan) at half maximum. Higher $\Delta T_{1/2}$ indicates multicrystallinity or crystal imperfection as well as the mismatch/adsolubilization of the lipidic components, especially induced by drugs. Panel B of Fig. 5 implies that the $\Delta T_{1/2}$ values were higher for Tween 60 stabilized systems. Also for this surfactant, the $\Delta T_{1/2}$ value for both the drugs decreased with the increasing drug concentration. For Tween 40 based formulations, variation in the $\Delta T_{1/2}$ values with drug concentration was less significant. Results further support our proposition as already mentioned previously. Adsolubilization of the lipidic core by LIDO resulted in the lowering of $\Delta T_{1/2}$ values. In case of PRO·HCl loaded systems, as the drug was only adsorbed onto the NLC surface, addition of this drug could not significantly alter the $\Delta T_{1/2}$ values.

Changes in enthalpy values for the drug free systems were higher than the corresponding drug loaded NLC formulations (shown in the panel C of Fig. 5). However the ΔH–drug concentration profiles were different for LIDO and PRO·HCl. While for LIDO loaded NLCs, the ΔH values decreased monotonously, however in case of PRO·HCl the ΔH values did not change appreciably with added drug. Increase in multicrystallinity with increasing drug concentration would effectively result in decreased ΔH value. As LIDO is capable of perturbing the lipid core structure, its progressive addition would result in the decrease of ΔH values. On the other hand, PRO·HCl predominantly resides on the NLC surface; hence its impact on the hydrocarbon chain packing was less prominent. Similar trend in the ΔC_p *vs.* drug concentration profile (panel D, Fig. 5) further supports this proposition.[57]

Crystallinity index (CI) is another DSC derived thermal parameter which can highlight the effect of drug on the molecular packing of the NLC components. Usually percentage of crystallinity index is compared with respect to the drug free system (blank NLCs are considered to be 100% crystalline). CI value can be derived from the DSC data using the following equation:[58–60]

$$\mathrm{CI}(\%) = \frac{\mathrm{enthalpy}_{(\mathrm{NLC})} \times 100}{\mathrm{enthalpy}_{(\text{blank NLC})} \times \text{concentration lipidphase } (\%)} \times 100 \quad (3)$$

Effects of LIDO and PRO·HCl on different formulations are shown in Fig. 6. NLC crystallinity (with respect to the corresponding blank formulation) progressively decreased with increasing LIDO concentration. This was due to the adsolubilization of the lipidic components by LIDO; which resulted in the softening of the packed lipidic components. In case of PRO·HCl although the CI values decreased initially, however as the drug predominantly resides on the NLC surface, it hardly could alter the molecular packing of the lipidic components.

3.4. UV-visible absorption spectral studies

UV-visible spectral study is a simple yet informative approach to understand the localization of the drug loaded in NLCs. State of polarity of the drugs and the local environment of the NLCs were evaluated by spectroscopic analysis whereby the drug molecules themselves were used as molecular probes. Absorption spectra of drug loaded NLCs were recorded in the wavelength range 200–400 nm. Polarity of the local environment of a drug incorporated in NLC can greatly affect its spectral behavior;[61,62] spectra of the drugs were also recorded in solvents of different polarities to make comparisons. UV-visible spectra of the drugs loaded in NLC as well as in different solvents are shown in Fig. 7. Absorption maxima of the drugs were found to be dependent on the polarity of the medium, as shown in Fig. S3 (ESI†). Spectra were suitably processed to determine the E_T (30) value (details are provided in the ESI†)[63] of the continuous medium (both the different solvents and drug loaded NLCs). There occurred a blue shift in the absorption maxima of both the drugs with decreasing solvent polarity. In case of LIDO loaded NLCs, the absorption maximum (λ_{max}) appeared at 239 nm, very close to that of LIDO in *n*-hexane. It suggests that LIDO being more lipophilic in nature could reside in the NLC core. In

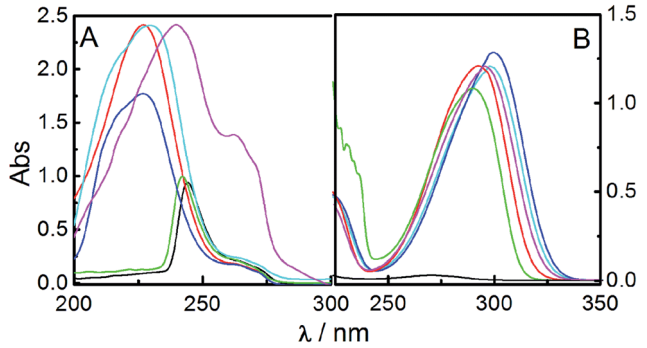

Fig. 7 UV-visible absorption spectra of 1 mM LIDO (panel A) and PRO·HCl (panel B) loaded in NLC as well as solvents of different polarity; at 25 °C. Systems: ▬, *n*-hexane; ▬, acetonitrile; ▬, chloroform; ▬, ethanol; ▬, methanol and ▬, drug loaded NLC respectively.

case of PRO·HCl the λ_{max} value appeared at 291 nm, which was in between the λ_{max} of PRO·HCl in methanol and ethanol. This confirms the localization of the drug on a more hydrophilic environment, herein on the surface of the NLCs.

3.5. Entrapment efficiency (EE) and loading content studies

Efficiency of an NLC formulation in terms of its use as a drug vehicle depends on its ability to incorporate/load/entrap the quantity of a drug. Results are summarized in Fig. 8. Tween 60 stabilized NLCs exhibited superior entrapment efficiency and loading content compared to the Tween 40 stabilized systems. Such a phenomenon could be explained on the proposition as mentioned earlier.[47,54,55] Because of ionicity, efficiency in entrapping PRO·HCl was less than LIDO in both the NLC formulations (Tween 40 and Tween 60). While considering the effect of drug concentration it was observed that the entrapment efficiency increased upto 0.5 mM, beyond which it did not change appreciably. This was due to the saturation of NLCs with respect to the drugs. There was no significant difference in the drug loading content among the different formulations. The drug loading content increased almost linearly with the added drug concentration (panel B). However, to address this issue in a better way, further studies are warranted using other drugs which is considered to be one of the future perspectives.

3.6. *In vitro* release kinetics

Release kinetics of an entrapped drug from the NLC matrix need to be investigated in order to assess the efficacy of the formulation. Drug release kinetics studies were performed by the conventional dialysis bag method, where the membrane retained the drug bound to the NLC and allowed the free drug to diffuse out into the release medium.[1] *In vitro* release behavior of the drugs loaded the NLC matrices have been demonstrated as the percentage of cumulative release in Fig. 9 and 10. LIDO and PRO·HCl showed 95.63% and 100% of release within 144 and 5 h respectively in Tween 60 solution. Parallel measurements were carried out using the anaesthetics separately in the absence of NLC. It has been proposed by Carafa *et al.*[40] that the diffusion of drug across the dialysis membrane was not the limiting step of the overall diffusion process. Release of both the drugs in presence of NLC was retarded compared to the same in absence of NLC as also reported by others.[64,65] Initial burst release, followed by a sustained/prolonged for both the drugs loaded in NLCs are not uncommon.[24] Thus, NLC systems could be considered to have potential application for sustaining the release of both the anaesthetics. Results revealed that the release rate of LIDO was slower as compared to that of PRO·HCl. This could be accountable to the fact that LIDO, being more lipophilic in nature, is inserted into the lipid core. On the contrary, PRO·HCl is interfacially adsorbed on the NLC surface owing to its ionic nature. While considering the initial burst release, it was observed that the process was complete when about 43% and 30% of PRO. HCl was released from the NLC in Tween 40 and Tween 60 respectively. The corresponding time was found to be 40 min. In case of LIDO, the values were 9% in Tween 40 and 6% in Tween 60 comprising systems respectively. In both Tween 40 and Tween 60, the initial burst

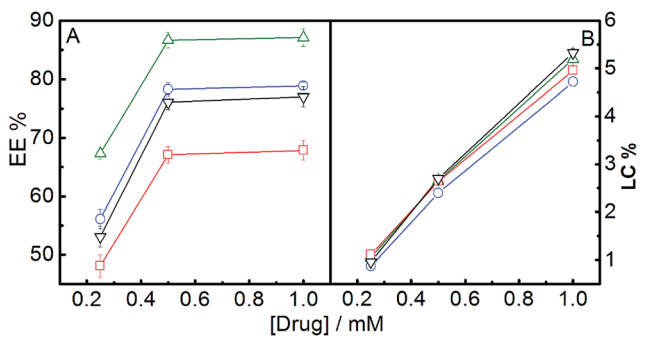

Fig. 8 Dependence of entrapment efficiency (E.E.) (panel A) and loading content (L.C.) (panel B) of NLC (5 mM, Span 65 + SLC + SA, 2 : 2 : 1 M/M/M) on the concentration of drugs. LIDO loaded NLCs dispersed in: ○, Tween 40; △, Tween 60; and PRO·HCl dispersed in □, Tween 40 and ▽, Tween 60. Each value represents the mean ± (S.D.) (n = 3). Temp. 4 °C.

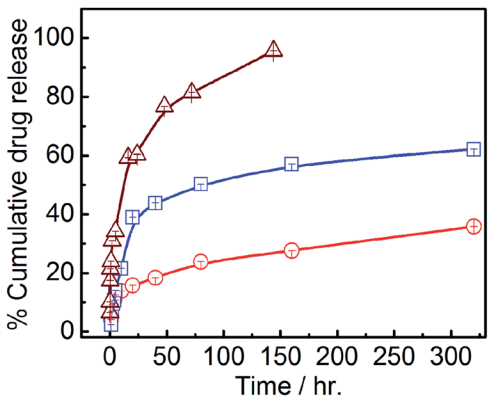

Fig. 9 *In vitro* cumulative LIDO release from NLC (5 mM, Span 65 + SLC + SA, 2 : 2 : 1 M/M/M). System: LIDO loaded NLC dispersion in Tween 40 (○), Tween 60 (□) and free LIDO in Tween 60 (△). Each point represents the mean ± (S.D.) (n = 3). Drug concentration was kept constant at 0.5 mM in each case. Temp. 25 °C.

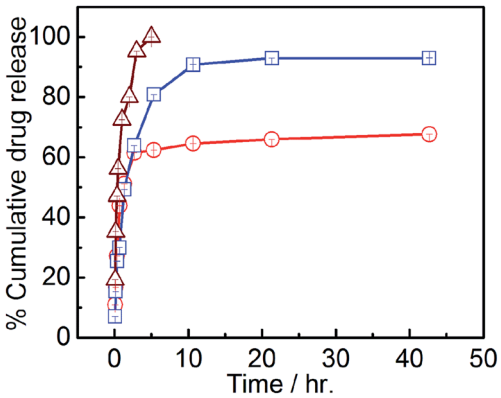

Fig. 10 *In vitro* cumulative PRO·HCl release from NLC (5 mM, Span 65 + SLC + SA, 2 : 2 : 1 M/M/M). Systems: PRO·HCl loaded dispersion in Tween 40 (○), Tween 60 (□) and free PRO·HCL in Tween 60 (△). Each point represents the mean ± (S.D.) ($n = 3$). Drug concentration was kept constant at 0.5 mM in each case. Temp. 25 °C.

release was complete within 2 h. Results further support better stabilization of LIDO in the NLC than the PRO·HCl which may be considered on the basis of its higher lipophilicity than PRO·HCl. Amount of the released drugs depended on the type of Tween surfactant. In case of Tween 40 stabilized system, 35–67% of the entrapped drug was released compared to 62–93% release for Tween 60 stabilized system. Higher loading capacity and larger imperfections for Tween 60 stabilized NLCs (in terms of hydrocarbon chain packing) compared to Tween 40, were responsible for this phenomenon.[47,54,60]

Data of the drug release profile were suitably processed and scrutinized for different release kinetics models such as First order, Higuchi, Korsemeyer–Peppas, Hixson–Crowell models. No formulations followed pseudo first order kinetics as reflected through the non-linear variation in the release profiles (Fig. 9 and 10). The obtained data were fitted into following drug release models by using DDSolver 1.0, and Add-In program for modeling and comparison of drug dissolution profiles:[66]

$$\text{Higuchi model: } F = k_{\mathrm{H}} t^{0.5} \quad (4)$$

$$\text{Korsemeyer–Peppas model: } F = k_{\mathrm{k}} t^{n} \quad (5)$$

$$\text{Hixson–Crowell model: } F = 100[1 - (1 - k_{\mathrm{HC}} t)^3] \quad (6)$$

$$\text{First order model: } F = 100(1 - \mathrm{e}^{-k_1 t}) \quad (7)$$

where, F is the percentage of the drug released, k_{H}, k_{k}, k_{HC} and k_1 are the release rate constants of Higuchi, Korsemeyer–Peppas, Hixson–Crowell and First order model respectively, t represents the time lag of the dissolution process, and n is the release exponent obtained from Korsemeyer–Peppas model. Among all the four models, the best-fit model was decided based on the highest regression values (r^2) for all the formulations. The release rate constant was calculated from the slope of the appropriate plots and regression co-efficient were accordingly determined. The results are summarized in Table S2 (ESI†). Release kinetics for both the drugs followed Korsemeyer–Peppas model. The regression coefficient (r^2) values of Korsemeyer–Peppas model for LIDO loaded in Tween 40 and Tween 60 were 0.99 and 0.95 respectively. In case of PRO·HCl, the (r^2) values were 0.99 and 0.94 respectively. The release exponent (n) determined from Korsemeyer–Peppas model for LIDO and PRO·HCl in both Tween 40 and Tween 60 stabilized NLCs were found to be less than 0.5 indicating release mechanisms being controlled by Fickian diffusion in all the systems. Values of release rate constants of LIDO loaded in NLCs for the Korsemeyer–Peppas model were 6.84 h^{-1} and 10.25 h^{-1} for Tween 40 and Tween 60 respectively. However in case of PRO·HCl, release rate constants were found to be 40.03 h^{-1} and 41.93 h^{-1} in NLCs stabilized with Tween 40 and Tween 60 respectively.

4. Summary and conclusion

Nanostructured lipid carriers (NLCs) were formulated by using Span 65, soy lecithin and stearic acid dispersed in aqueous Tween 40 or Tween 60 solution. Tween 60 provided better stabilization than Tween 40 because of its longer hydrocarbon chain. Hydrocarbon chains of Tween 60 could penetrate to greater extent than Tween 40 into the NLC matrices. TEM study confirmed the spherical morphology of the NLCs with smooth surface. Higher amount of LIDO could be encapsulated into the NLC than PRO·HCl. LIDO resides in the core of the NLC for its relatively higher hydrophobic nature. PRO·HCl, being ionic, preferentially adsorbs over the NLC surface. Apart from the DLS studies, DSC and spectroscopic investigations on the drug loaded NLC further supported such proposition. Because of its larger lipophilicity LIDO could be entrapped to greater extent compared to PRO·HCl. *In vitro* drug release study revealed that the lipidic matrices could act as promising vehicles for two most widely used local anaesthetics with controlled and prolonged release. Biphasic release behaviour was experienced by all the combinations. In order to further explore the viability, the formulations may be subjected to *in vitro* studies under biological condition. Besides, the *in vivo* studies as well as some clinical trials are warranted which are considered as the future perspectives.

Acknowledgements

Financial support in the form of a research grant (SR/S1/PC/32/2011) from the Department of Science and Technology, Govt. of India, New Delhi is sincerely acknowledged. P.N. acknowledges the receipt of a research fellowship from the University Grant Commission, New Delhi under the Rajiv Gandhi National Fellowship for disabled (no. F./2012-13/RGNF-2012-13D-GEN-CHH-51106/31-Oct-2013).

Notes and references

1 H. Dang, M. Meng, H. Zhao, J. Iqbal, R. Dai, Y. Deng and F. Lv, *J. Nanopart. Res.*, 2014, **16**, 1–10.

2 P. Dwivedi, R. Khatik, K. Khandelwal, I. Taneja, K. S. R. Raju, Wahajuddin, S. K. Paliwal, A. K. Dwivedi and P. R. Mishra, *Int. J. Pharm.*, 2014, **466**, 321–327.
3 L. B. Jensen, E. Magnussson, L. Gunnarsson, C. Vermehren, H. M. Nielsen and K. Petersson, *Int. J. Pharm.*, 2010, **390**, 53–60.
4 J. Madan, R. S. Pandey, V. Jain, O. P. Katare, R. Chandra and A. Katyal, *Nanomedicine*, 2013, **9**, 492–503.
5 M. Muchow, P. Maincent, R. H. Müller and C. M. Keck, *Drug Dev. Ind. Pharm.*, 2011, **37**, 8–14.
6 A. O. Elzoghby, *J. Controlled Release*, 2013, **172**, 1075–1091.
7 P. K. Gaur, S. Mishra, M. Bajpai and A. Mishra, *BioMed Res. Int.*, 2014, **2014**, 9.
8 A. K. Jain, N. K. Swarnakar, C. Godugu, R. P. Singh and S. Jain, *Biomaterials*, 2011, **32**, 503–515.
9 A. R. Mohammed, V. W. Bramwell, D. J. Kirby, S. E. McNeil and Y. Perrie, *Eur. J. Pharm. Biopharm.*, 2010, **76**, 404–412.
10 D. Narayanan, M. G. Geena, H. Lakshmi, M. Koyakutty, S. Nair and D. Menon, *Nanomedicine*, 2013, **9**, 818–828.
11 Y. R. Neupane, M. D. Sabir, N. Ahmad, M. Ali and K. Kohli, *Nanotechnology*, 2013, **24**, 0957–4484.
12 S. Shafiq-un-Nabi, F. Shakeel, S. Talegaonkar, J. Ali, S. Baboota, A. Ahuja, R. Khar and M. Ali, *AAPS PharmSciTech*, 2007, **8**, E12–E17.
13 F. Shakeel, S. Baboota, A. Ahuja, J. Ali and S. Shafiq, *J. Drug Targeting*, 2008, **16**, 733–740.
14 E. B. Souto, S. A. Wissing, C. M. Barbosa and R. H. Müller, *Int. J. Pharm.*, 2004, **278**, 71–77.
15 X. Huang, Y. J. Chen, D. Y. Peng, Q. L. Li, X. S. Wang, D. L. Wang and W. D. Chen, *Colloids Surf., B*, 2013, **102**, 391–397.
16 H. Xiao, R. Qi, S. Liu, X. Hu, T. Duan, Y. Zheng, Y. Huang and X. Jing, *Biomaterials*, 2011, **32**, 7732–7739.
17 H. Xiao, J. F. Stefanick, X. Jia, X. Jing, T. Kiziltepe, Y. Zhang and B. Bilgicer, *Chem. Commun.*, 2013, **49**, 4809–4811.
18 Y. Huang, Y. Jiang, H. Wang, J. Wang, M. C. Shin, Y. Byun, H. He, Y. Liang and V. C. Yang, *Adv. Drug Delivery Rev.*, 2013, **65**, 1299–1315.
19 Z. Yu, R. M. Schmaltz, T. C. Bozeman, R. Paul, M. J. Rishel, K. S. Tsosie and S. M. Hecht, *J. Am. Chem. Soc.*, 2013, **135**, 2883–2886.
20 B. R. Schroeder, M. I. Ghare, C. Bhattacharya, R. Paul, Z. Yu, P. A. Zaleski, T. C. Bozeman, M. J. Rishel and S. M. Hecht, *J. Am. Chem. Soc.*, 2014, **136**, 13641–13656.
21 H. Gao, Q. Zhang, Z. Yu and Q. He, *Curr. Pharm. Biotechnol.*, 2014, **15**, 210–219.
22 T. P. Sari, B. Mann, R. Kumar, R. R. B. Singh, R. Sharma, M. Bhardwaj and S. Athira, *Food Hydrocolloids*, 2015, **43**, 540.
23 K. R. Pawar and R. J. Babu, *Crit. Rev. Ther. Drug Carrier Syst.*, 2010, **27**, 419–459.
24 M. Polakovic, T. Gorner, R. Gref and E. Dellacherie, *J. Controlled Release*, 1999, **60**, 169–177.
25 W. Zhou, X. An, J. Wang, W. Shen, Z. Chen and X. Wang, *Colloids Surf., A*, 2012, **395**, 225–232.
26 J. Hurler, S. Žakelj, J. Mravljak, S. Pajk, A. Kristl, R. Schubert and N. Škalko-Basnet, *Int. J. Pharm.*, 2013, **456**, 49–57.
27 A. C. Silva, A. Kumar, W. Wild, D. Ferreira, D. Santos and B. Forbes, *Int. J. Pharm.*, 2012, **436**, 798–805.
28 J. You, F. Wan, F. de Cui, Y. Sun, Y.-Z. Du and F. Q. Hu, *Int. J. Pharm.*, 2007, **343**, 270–276.
29 S. A. Wissing, O. Kayser and R. H. Muller, *Adv. Drug Delivery Rev.*, 2004, **56**, 1257–1272.
30 K. Bhaskar, C. Krishna Mohan, M. Lingam, V. Prabhakar Reddy, V. Venkateswarlu and Y. Madhusudan Rao, *Drug Dev. Ind. Pharm.*, 2008, **34**, 719–725.
31 S. Khurana, N. K. Jain and P. M. Bedi, *Life Sci.*, 2013, **93**, 763–772.
32 H. Yuan, L.-L. Wang, Y.-Z. Du, J. You, F.-Q. Hu and S. Zeng, *Colloids Surf., B*, 2007, **60**, 174–179.
33 X.-G. Zhang, J. Miao, Y.-Q. Dai, Y.-Z. Du, H. Yuan and F.-Q. Hu, *Int. J. Pharm.*, 2008, **361**, 239–244.
34 M. Schäfer-Korting, W. Mehnert and H.-C. Korting, *Adv. Drug Delivery Rev.*, 2007, **59**, 427–443.
35 W. N. Charman, *J. Pharm. Sci.*, 2000, **89**, 967.
36 C. J. H. Porter and W. N. Charman, *Adv. Drug Delivery Rev.*, 2001, **50**, 61.
37 H. S. Kim, T. H. Shin, M. Yoon, M. J. Kang and J. Lee, *Tissue Eng. Regener. Med.*, 2008, **5**, 798–803.
38 P. Pathak and M. Nagarsenker, *AAPS PharmSciTech*, 2009, **10**, 985–992.
39 C. Puglia, M. G. Sarpietro, F. Bonina, F. Castelli, M. Zammataro and S. Chiechio, *J. Pharm. Sci.*, 2011, **100**, 1892–1899.
40 M. Carafa, E. Santucci and G. Lucania, *Int. J. Pharm.*, 2002, **231**, 21–32.
41 K. R. Courtney and G. R. Strichartz, in *Local Anaesthetics*, 1987, vol. 81, pp. 53–94.
42 O. V. Bobreshova, A. V. Parshina, K. Y. Yankina, E. Y. Safronova and A. B. Yaroslavtsev, *Nanotechnol. Russ.*, 2013, **8**, 743–750.
43 M. Nagarsenker and A. Joshi, *Drug Dev. Ind. Pharm.*, 1997, **23**, 1159–1165.
44 M. H. Schmid and H. C. Korting, *Adv. Drug Delivery Rev.*, 1996, **18**, 335–342.
45 L. Labedzki, H. R. Ochs, D. R. Abernethy and D. J. Greenblatt, *Klin. Wochenschr.*, 1983, **61**, 379–380.
46 A. C. Silva, E. Gonzalez-Mira, M. L. Garcia, M. A. Egea, J. Fonseca, R. Silva, D. Santos, E. B. Souto and D. Ferreira, *Colloids Surf., B*, 2011, **86**, 158–165.
47 A. P. Nayak, W. Tiyaboonchai, S. Patankar, B. Madhusudhan and E. B. Souto, *Colloids Surf., B*, 2010, **81**, 263–273.
48 F.-Q. Hu, S.-P. Jiang, Y.-Z. Du, H. Yuan, Y.-Q. Ye and S. Zeng, *Colloids Surf., B*, 2005, **45**, 167–173.
49 X. Yang, L. Zhao, L. Almasy, V. M. Garamus, A. Zou, R. Willumeit and S. Fan, *Int. J. Pharm.*, 2013, **450**, 225–234.
50 H. Bunjes, M. Drechsler, M. Koch and K. Westesen, *Phase separation within solid lipid nanoparticles loaded with high amounts of ubidecarenone (Q10)*, CRS Press, Paris, 2000, vol. 27.
51 T. J. Wooster, M. Golding and P. Sanguansri, *Langmuir*, 2008, **24**, 12758–12765.
52 A. Kovacevic, S. Savic, G. Vuleta, R. H. Müller and C. M. Keck, *Int. J. Pharm.*, 2011, **406**, 163–172.

53 S. H. Jin, S. H. Kim, H. N. Cho and S. K. Choi, *Macromolecules*, 1991, **24**, 6050–6052.
54 V. Jenning, A. F. Thunemann and S. H. Gohla, *Int. J. Pharm.*, 2000, **199**, 167–177.
55 V. Teeranachaideekul, P. Boonme, E. B. Souto, R. H. Muller and V. B. Junyaprasert, *J. Controlled Release*, 2008, **128**, 134–141.
56 V. Teeranachaideekul, E. B. Souto, V. B. Junyaprasert and R. H. Müller, *Eur. J. Pharm. Biopharm.*, 2007, **67**, 141–148.
57 H. Ali, K. El-Sayed, P. W. Sylvester and S. Nazzal, *Colloids Surf., B*, 2010, **77**, 286–297.
58 M. A. Schubert and C. C. Müller-Goymann, *Eur. J. Pharm. Biopharm.*, 2005, **61**, 77–86.
59 B. Siekmann and K. Westesen, *Colloids Surf., B*, 1994, **3**, 159–175.
60 V. Teeranachaideekul, E. B. Souto, V. B. Junyaprasert and R. H. Muller, *Eur. J. Pharm. Biopharm.*, 2007, **67**, 141–148.
61 M. Chakraborty and A. K. Panda, *Spectrochim. Acta, Part A*, 2011, **81**, 458–465.
62 E. M. Kosower, *J. Am. Chem. Soc.*, 1958, **80**, 3253–3260.
63 C. Reichardt, *Chem. Rev.*, 1994, **94**, 2319–2358.
64 N. A. Estes 3rd, A. S. Manolis, D. J. Greenblatt, H. Garan and J. N. Ruskin, *Am. Heart J.*, 1989, **117**, 1060–1064.
65 B. R. Kuhnert, P. M. Kuhnert, E. H. Philipson, C. D. Syracuse, C. J. Kaine and C. H. Yun, *Anesth. Analg.*, 1986, **65**, 273–278.
66 Y. Zhang, M. Huo, J. Zhou, A. Zou, W. Li, C. Yao and S. Xie, *AAPS J.*, 2010, **12**, 263–271.

Electronic Supplementary Material (ESI) for RSC Advances.

Table S 1. Temperature for maximum heat flow (T_m), the width at half peak height ($\Delta T_{1/2}$), change in enthalpy (ΔH), heat capacity (ΔC_p) and percentage of crystallinity (C.I.) of blank as well as LIDO and PRO.HCl loaded NLC (5mM; Span 65+SLC+SA, 2:2:1 M/M/M).

[Drug]/ mM	T_m/ ºC	$\Delta T_{1/2}$/ ºC	ΔH/kcal.mol^{-1}	ΔC_p/kcal.mol^{-1}C^{-1}	CI (%)
Lidocaine loaded NLC in Tween 40					
0.0	35.61	2.01	5.83	10.40	100
0.2	35.53	2.16	4.77	8.63	81
0.5	34.77	1.96	4.89	6.12	83
1.0	35.07	2.02	4.57	5.95	78
1.5	35.40	2.14	4.00	5.18	68
2.0	34.51	2.08	3.27	3.18	56
2.5	34.39	2.08	2.91	2.65	49
Lidocaine loaded NLC in Tween 60					
0.0	32.58	3.15	8.00	5.85	100
0.2	32.55	3.51	6.13	5.18	76
0.5	32.33	3.27	5.26	4.95	65
1.0	32.18	2.92	4.64	3.78	58
1.5	31.97	2.32	3.62	2.58	45
2.0	31.71	2.20	3.53	2.38	44
2.5	31.02	2.08	1.87	1.23	23
Procaine hydrocloride loaded NLC in Tween 40					
0.0	35.61	2.01	5.83	10.40	100
0.2	32.60	2.02	2.89	4.36	49
0.5	32.38	2.00	2.56	3.76	43
1.0	32.08	2.34	2.75	3.28	47
1.5	32.18	2.10	2.46	3.12	42
2.0	32.45	2.02	2.38	3.01	40
2.5	32.40	2.01	2.31	2.83	39
Procaine hydrocloride loaded NLC in Tween 60					
0.0	32.58	3.15	8.99	5.85	100
0.2	32.07	4.09	5.09	3.79	63
0.5	32.34	3.68	4.74	3.79	59
1.0	32.61	3.49	4.68	3.74	58
1.5	32.71	3.29	4.59	3.72	57
2.0	32.91	3.24	4.54	3.58	56
2.5	32.85	3.29	4.55	3.40	56

DSC measurements were performed on day one of sample preparation.

Table S 2. Drug release kinetics profiles of LIDO and PRO.HCl loaded NLCs.

Formulation	Korsemeyer-Peppas			Higuchi		Hixson-Crowell		First order	
	r^2	k	n	r^2	k	r^2	k	r^2	k
LIDO-T40	0.99	6.84	0.283	0.98	2.35	0.93	0.001	0.93	0.002
LIDO-T60	0.95	10.25	0.333	0.91	4.47	0.87	0.002	0.90	0.007
PRO.HCL-T40	0.99	40.03	0.178	0.75	15.51	0.76	0.031	0.93	0.393
PRO.HCl-T60	0.94	41.93	0.256	0.86	0.271	0.90	0.036	0.92	0.446

*r^2=regression coefficient, k= release rate constant, n=diffusional exponent.

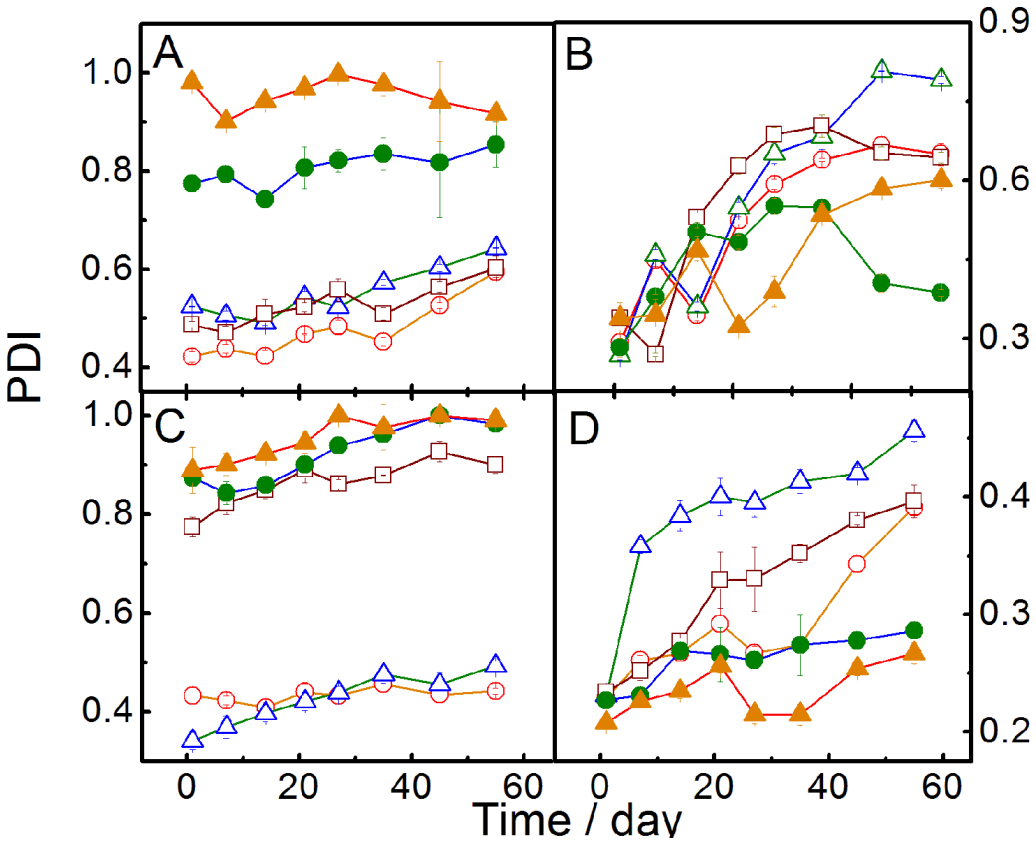

Figure S 1. Variation in the polydispersity index (PDI) of NLCs (Span 65 + SLC + SA, 2:2:1 M/M/M) with time in presence of varying concentration of drugs. Panel A: LIDO loaded NLC in Tween 40; panel B: PRO.HCl loaded NLC in Tween 40; panel C: LIDO loaded NLC in Tween 60 and panel D: PRO.HCl loaded NLC in Tween 60. 5 mM NLC was dispersed in 10 mM Tween in each case. Drug concentration (mM) : O, 0; Δ , 0.5; □, 1; ●, 2 and ▲, 2.5 . Temp. 25 ºC.

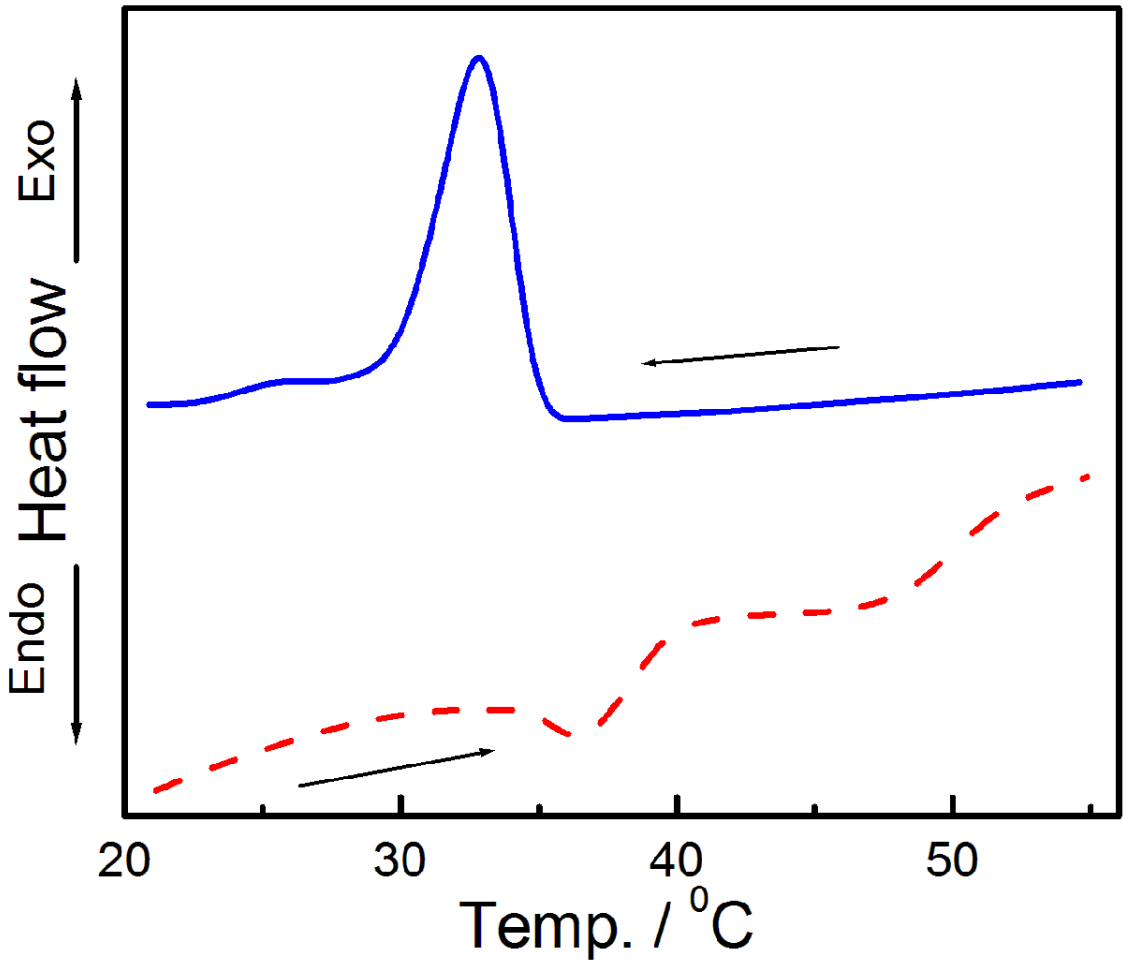

Figure S 2. DSC heating (- - - -) and cooling (——) thermogram of 2.5 mM LIDO loaded NLC (5 mM, Span 65+SLC+SA, 2:2:1 M/M/M) dispersed in Tween 60 (10mM). Scan rate: 2 ºC/min.

E_T (30) value is defined as the molar electronic transition energy (E_T) of dissolved probe molecule measured in kCal/mol at room temperature(25 ºC) and normal pressure (1bar). It is expressed by the equation:

$$E_T(30) = 28591/\lambda_{max}$$

where, λ_{max} is the wavelength of maximum absorption

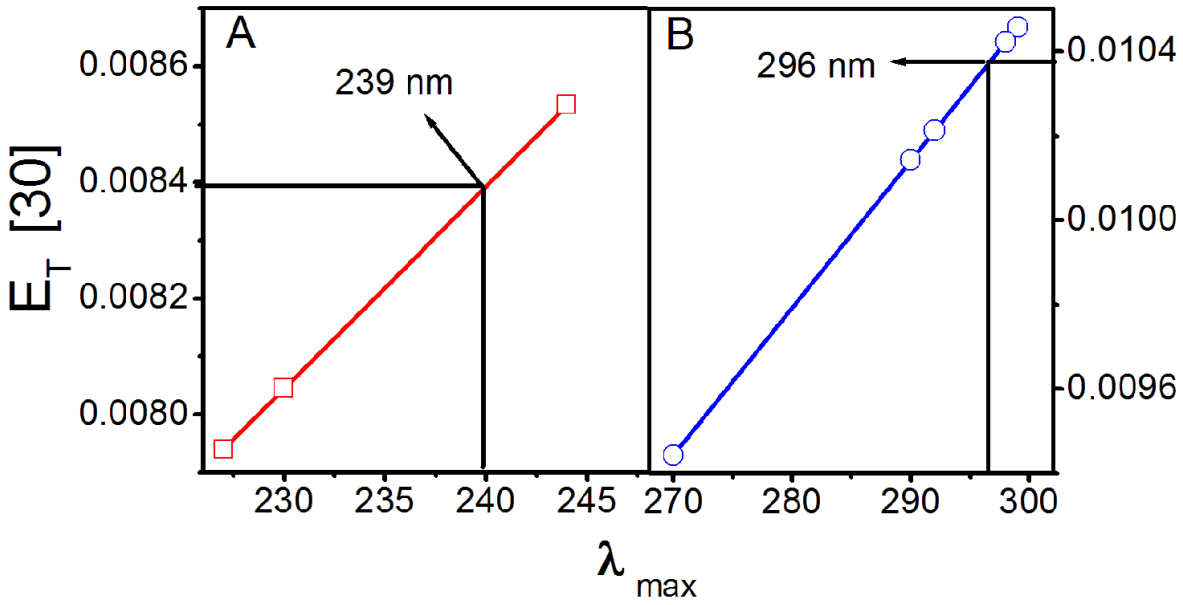

Figure S 3. Dependence of absorption maxima (λ_{max}) of LIDO (panel A) and PRO.HCl (panel B) on the E_T30 scale of medium at 25 ºC.

LANGMUIR

Article

pubs.acs.org/Langmuir

Influence of Lipid Core Material on Physicochemical Characteristics of an Ursolic Acid-Loaded Nanostructured Lipid Carrier: An Attempt To Enhance Anticancer Activity

Prasant Nahak,[†] Gourab Karmakar,[†] Priyam Chettri,[‡] Biplab Roy,[†] Pritam Guha,[†] Shila Elizabeth Besra,[§] Anjana Soren,[§] Alexey G. Bykov,[∥] Alexander V. Akentiev,[∥] Boris A. Noskov,[∥] and Amiya Kumar Panda*[,⊥]

[†]Department of Chemistry, University of North Bengal, Darjeeling 734 013, West Bengal, India

[‡]Department of Biotechnology, University of North Bengal, Darjeeling 734 013, West Bengal, India

[§]Cancer Biology and Inflammatory Disorder Division, CSIR-Indian Institute of Chemical Biology, 4, Raja S. C. Mullick Road, Kolkata 700032,West Bengal, India

[∥]Department of Colloid Chemistry, St. Petersburg State University, Universitetsky pr. 26, 198504 St. Petersburg, Russia

[⊥]Department of Chemistry and Chemical Technology, Vidyasagar University, Midnapore 721 102, West Bengal, India

Supporting Information

ABSTRACT: The impact of saturation and unsaturation in the fatty acyl hydrocarbon chain on the physicochemical properties of nanostructured lipid carriers (NLCs) was investigated to develop novel delivery systems loaded with an anticancer drug, ursolic acid (UA). Aqueous NLC dispersions were prepared by a high-pressure homogenization−ultrasonication technique with Tween 80 as a stabilizer. Mutual miscibility of the components at the air−water interface was assessed by surface pressure−area measurements, where attractive interactions were recorded between the lipid mixtures and UA, irrespective of the extent of saturation or unsaturation in fatty acyl chains. NLCs were characterized by combined dynamic light scattering, transmission electron microscopy (TEM), atomic force microscopy (AFM), differential scanning calorimetry, drug encapsulation efficiency, drug payload, *in vitro* drug release, and *in vitro* cytotoxicity studies. The saturated lipid-based NLCs were larger than unsaturated lipids. TEM and AFM images revealed the spherical and smooth surface morphology of NLCs. The encapsulation efficiency and drug payload were higher for unsaturated lipid blends. *In vitro* release studies indicate that the nature of the lipid matrix affects both the rate and release pattern. All UA-loaded formulations exhibited superior anticancer activity compared to that of free UA against human leukemic cell line K562 and melanoma cell line B16.

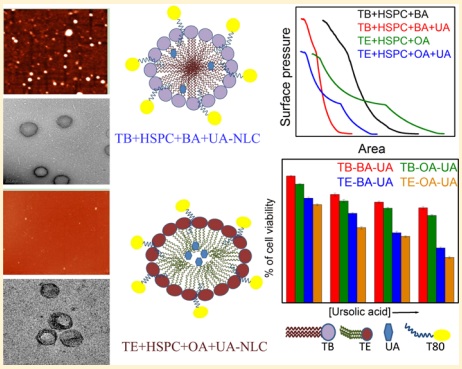

INTRODUCTION

Cytotoxic anticancer drugs are more reactive, more unstable, and more diverse in terms of molecular structure and physicochemical properties than other drug classes. At the same time, their poor specificity and tendency to induce drug resistance hinder the optimal performance in the case of conventional chemotherapy. Cancer cells exercise a variety of defense mechanisms at the cellular level to diminish the activities of chemotherapeutic agents to which they are exposed. These defense mechanisms are known as "cellular" drug resistance. The most notable is the multidrug resistance (MDR) phenotype, which involves active efflux of a broad range of cytotoxic drug molecules out of the cytoplasm by membrane-bound transporters.[1−3] In recent years, it has become more evident that the mere development of novel drugs is insufficient to guarantee progress in drug therapy.

Nanodimensional drug delivery systems possess important properties such as the increasing solubility of hydrophobic drugs and the improvement of their bioavailability.[4,5] Solid lipid nanoparticles (SLNs) combine the advantages of emulsions, liposomes, and polymeric nanoparticles; other favorable qualities of SLNs include biocompatibility,[6] improved solubility, high bioavailability, controlled drug release,[7,8] targeting effect on brain,[9] accessibility to large scale production,[10] etc. It is therefore not surprising that this relatively new class of drug carriers is quickly being adopted for the delivery of various anticancer compounds as the SLNs, comprising physiological lipids, can minimize potential toxicity and enhance efficiency.[11] However, because of the highly crystalline nature of pure solid lipids or blends of solid lipids, drugs tend to be excluded, leading to low loading capacity and drug expulsion during storage. To overcome the limitations of SLNs, nanostructured lipid carriers (NLCs) have evolved as alternatives. NLCs are usually prepared from a mixture of spatially incompatible solid

Received: June 28, 2016
Revised: August 16, 2016
Published: September 2, 2016

DOI: 10.1021/acs.langmuir.6b02402
Langmuir 2016, 32, 9816−9825

and liquid lipids. Assimilation of liquid lipids increases the imperfections in the solid lipid matrix; furthermore, liquid lipids can elevate the level of drug solubilization, allowing superior accommodation for the hydrophobic drugs, which eventually enhances the drug payload and reduces the level of expulsion of the drug during storage.[12−15] A blend of solid and liquid lipids can form a stable NLC that remains in the solid state at body temperature; thus, the drug release profile can be easily modulated by varying the lipid matrix composition.[16,17] More important is the faster internalization of lipid nanoparticles into cancerous cells, leading to greater potential in cancer therapy.[18−20]

NLCs comprising a mixture of saturated (solid) and unsaturated (liquid) triglycerides, phospholipids, and fatty acids may be considered as an interesting alternative to conventional combinations such as fatty acid and triglyceride, as the blends are usually polycrystalline in nature and can enhance physical stability, encapsulation efficiency, release behavior, therapeutic efficiency, etc.[17,19,21,22] Although a number of reports about NLCs comprising saturated (solid) and unsaturated (fluid/liquid) lipids are available in the literature,[12−14,23] comparative studies describing the effect of unsaturated lipids and saturated lipids on the physicochemistry of NLCs are scarce. Thus, there has been ample research in the field of NLCs, with special reference to the use of different combinations of saturated and unsaturated lipids.

Ursolic acid (UA, 3β-hydroxy-urs-12-en-28-oic acid), a natural pentacyclic triterpenoid found in different plant species,[24] possesses a wide range of bioactivities, viz., antitumor, anti-inflammatory, antioxidant, antibacterial, antiviral, and hepatoprotective effects.[25−29] Recent studies have shown that UA has potential antitumor effects and cytotoxic activity toward various types of cancer cell lines.[30−33] In spite of such potential, the clinical application of UA is limited because of its poor aqueous solubility, resulting in its low bioavailability and poor *in vivo* pharmacokinetics. During the past decade, many approaches have been developed to improve the solubility of UA using polymeric nanoparticles,[32−35] micronization,[36] lipidic nanoparticles,[37,38] liposomes,[30,39] salt formation,[40] solid dispersions,[40] inclusion complexes,[41,42] microemulsions and nanocrystals, etc.[31] In spite of different attempts, it has not yet been possible to develop a single optimal delivery system. Therefore, the search for novel drug delivery systems is highly warranted to improve the solubility, payload, and oral bioavailability of UA. The aim of this study was to evaluate and compare the saturated and unsaturated lipid comprising NLCs to determine if differences in composition can alter the performance of these systems. Saturated lipid [tribehenin (TB) and 2,3-di(docosanoyloxy)propyl docosanoate], unsaturated lipid (trierucin (TE) and 2,3-bis{[(*Z*)-docos-13-enoyl]oxy}propyl (*Z*)-docos-13-enoate], saturated fatty acid [behenic acid (BA), docosanoic acid], and unsaturated fatty acid [oleic acid (OA), (9*Z*)-9-octadecenoic acid] were used for these studies, keeping the molar proportion of HSPC (hydrogenated soy phosphatidylcholine) constant for all the systems. Because the major drawbacks of ursolic acid are lower drug loading and poor water solubility, another objective was the development of UA-encapsulated NLCs comprising different lipid matrices to enhance drug loading, improve solubility, and increase oral bioavailability.

Surface pressure−area isotherm studies of the pure and mixed lipids as well as with ursolic acid in different combinations were conducted to determine the nature of the interactions between the lipids and the drug. Such studies can also predict the location of the drug molecules. If UA molecules prefer to stay at the interface of the NLCs, they would definitely alter the surface pressure−area isotherm of the lipid mixture. On the other hand, if the drug molecules prefer to stay in the core of the NLCs, they would hardly have any impact on the surface pressure−area isotherm of lipid mixtures. To address this issue, surface pressure−area isotherms of the lipid mixtures with varying amounts of UA were determined. The influence of different lipids on the size, polydispersity index, and ζ potential of NLCs was investigated in the absence and presence of UA. Calorimetric studies of different formulations in the absence and presence of UA were conducted with the intention of determining the impact of the composition of lipids as well as UA on the thermal behavior of NLCs. To investigate the impact of saturated and unsaturated lipids on UA entrapment efficiency (EE), loading content (LC) and release kinetics of UA-loaded formulations were also assessed. Finally, anticancer activities against human leukemic cell line K562 and melanoma cell line B16 were evaluated to determine the anticancer potential of UA-loaded NLCs. It is believed that such a comprehensive study would eventually lead to the formulation of novel drug delivery systems in the treatment of cancer and to a clearer understanding of the fundamental properties of NLCs.

MATERIALS AND METHODS

Materials. Ursolic acid (UA), tribehenin (TB), trierucin (TE), behenic acid (BA), and oleic acid (OA) were purchased from TCI Chemicals. Hydrogenated soy phosphatidylcholine (HSPC), a dialysis bag (12 kDa molecular weight cutoff), DMEM, and RPMI 1640 medium with L-glutamine (Gibco), fetal calf serum, sodium pyruvate, HEPES, MTT [3-(4,5-dimethylthiazol-2-yl)-2,5-diphenyltetrazolium bromide], and trypsin were obtained from Sigma-Aldrich. Tween 80 was purchased from Sisco Research Laboratory. AR grade disodium hydrogen phosphate ($Na_2HPO_4{\cdot}2H_2O$), sodium dihydrogen phosphate ($NaH_2PO_4{\cdot}2H_2O$), and sodium chloride (NaCl) were the products of Merck Specialties Pvt. Ltd. Penicillins/streptomycin (Biowest), gentamycin (Nicholas), dimethyl sulfoxide (DMSO), sodium bicarbonate, and other chemicals/reagents were of analytical grade and purchased from local firms. All the chemicals used were stated to be ≥99% pure and used as received. Doubly distilled water and high-performance liquid chromatography grade water were used throughout the study. Human leukemic cell line K562 and mouse melanoma cell line B16 were purchased from the National Facility for Animal Tissue and Cell Culture (Pune, India). The K562 cells were maintained in RPMI 1640, and B16 cells were maintained in DMEM supplemented with 10% heat-inactivated FCS, 100 units/mL penicillin, 100 mg/mL streptomycin, and 100 μg/mL gentamycin. Both cultures were maintained at 37 °C in a humidified atmosphere containing 5% CO_2. Mouse melanoma B16 cells are adherent in nature. During subculturing of the cells, this adherence can be diminished by adding a 1× trypsin solution to the cell. In all the experiments, untreated leukemic and melanoma cells were termed the control group.

Methods. Surface pressure (π)−area (A) isotherms of pure as well as mixed monolayers (solvent spread) were obtained using a Langmuir surface balance (Micro Trough X, Kibron, Helsinki, Finland). A monolayer was generated by spreading an appropriate quantity of a lipid solution dissolved in a 3:1 (v/v) chloroform/methanol mixture at the air−water interface with a Hamilton microsyringe. The solvent was allowed to evaporate for 15 min. After the generation and equilibration of the monolayer film, the barriers were compressed at a rate of 5 mm/min.

NLCs were prepared by the hot homogenization−ultrasonication method as previously described.[43] Briefly, quantitative amounts of lipids (2:2:1 TB/TE:HSPC:OA/BA molar ratio) were dissolved in a 3:1 (v/v) chloroform/methanol mixture; the solvent was removed

DOI: 10.1021/acs.langmuir.6b02402
Langmuir 2016, 32, 9816−9825

using a rotary evaporator. The thin film thus obtained was melted at 95 °C and dispersed in the preheated aqueous surfactant (Tween 80) solution. The coarse emulsion was exposed to high-speed dispersion for 1 h; the obtained pre-emulsion was sonicated for a period of 1 h with a probe sonicator (Takashi U250, Takashi Electric) at 150 W/kHz, maintaining the same temperature to produce nanoemulsions that were allowed to cool to room temperature to produce the NLCs, which were stored at 4 °C for further study. In the case of the drug-loaded formulation, UA was premixed with the lipids while the thin film was being generated. The total lipid concentration in the dispersion was maintained at 5 mM in a 2:2:1 TB/TE:HSPC:OA/BA molar ratio, and a 10 mM aqueous nonionic (Tween 80) surfactant solution was used as a stabilizer. Different formulations, drug free or loaded, were prepared. The drug concentrations were 0.125, 0.25, and 0.5 mM for all cases.

The mean particle size, population distribution, polydispersity index, and ζ potential of the NLCs were measured in a dynamic light scattering spectrometer using a Malvern Zetasizer Nano Series ZS90 instruments (Malvern Instruments, Malvern, U.K.) at 25 °C. The shape, morphology, and surface topology of the NLCs were investigated by transmission electron microscopy (TEM) (Hitachi, Tokyo, Japan) and tapping mode atomic force microscopy (AFM) (Nanoscope III, Bruker) studies.[43] Calorimetric measurements were performed using a differential scanning calorimetry (DSC) 1 STAR^e system (Mettler Toledo). The DSC studies were performed in the temperature range of −30 to 100 °C with a scan rate of 2.5 °C/min. The phase transition temperature and other relevant thermal parameters were evaluated from the obtained DSC thermograms of respective samples using STAR^e Software version 11.00. The entrapment efficiency (EE) and drug loading (DL) were determined by the standard methods as reported previously.[44] The UA content was estimated with a UV spectrophotometer, measuring the absorbance at 214 nm. The entrapment efficiency (EE) and drug loading (DL) capacity of NLCs were calculated using the following equations:

$$\mathrm{EE\%} = \frac{W_{TC} - W_{FC}}{W_{TC}} \times 100 \quad (1)$$

$$\mathrm{DL\%} = \frac{W_{TC} - W_{FC}}{W_{TC} - W_{FC} + W_{TL}} \times 100 \quad (2)$$

where W_{TC}, W_{FC}, and W_{TL} represent total amounts of UA, free UA, and lipid, respectively. *In vitro* release of UA from the NLCs was assessed using the standard dialysis bag method under sink conditions over a 96 h period.

***In Vitro* Cytotoxicity Study of UA-Loaded NLCs.** Log phase K562 and B16 cells (1×10^5 cells, 100 μL cell suspensions) were seeded in 96-well tissue culture plates. They were treated with freshly prepared UA-loaded NLCs at different concentrations and different incubation times at 37 °C in a humidified atmosphere containing 5% CO_2. Untreated cells served as the control. The cytotoxicity studies were performed using the MTT assay, and the absorbance of the colored solution was measured at a wavelength of 492 nm for K562 and at 570 nm for B16 cells by a microplate manager (reader type, model 680 XR from Bio-Rad Laboratories Inc.). IC_{50} values were obtained at 24 and 48 h for UA-loaded NLCs.

RESULTS AND DISCUSSION

Interfacial Behavior of Monomolecular Films. Surface pressure (π)−area (A) isotherms were constructed for pure components, mixed lipids, and mixed lipids in combination with UA. In the case of the mixed lipid and UA combinations, the lipid mixture was considered component 1 while UA was considered component 2. Lift-off areas of TB, TE, HSPC, BA, OA, and UA appeared at 75.14, 164.02, 93.61, 51.22, 78.87, and 106.17 nm^2 molecule^{-1}, respectively. Representative isotherms are shown in Figure 1and Figure S1.

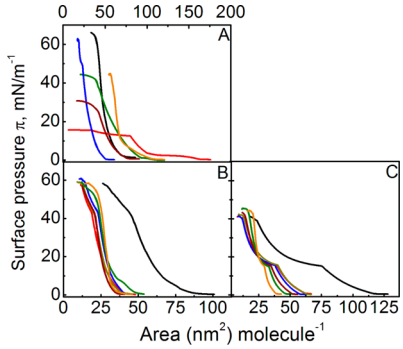

Figure 1. Surface pressure (π)−area (A) isotherms of (A) (black) tribehenin, (red) trierucin, (green) HSPC, (blue) behenic acid, (brown) oleic acid, and (orange) ursolic acid; (B) a TB/HSPC/BA mixture; and (C) a TE/HSPC/OA mixture. Panels B and C describe the π−A isotherm of the mixed monolayer in the absence and presence of ursolic acid using water as the subphase. The mole percents of ursolic acid with respect to the lipid mixture were (black) 0, (red) 2.5, (blue) 5, (brown) 10, (maroon) 30, (green) 50, and (orange) 70. The temperature was 25 °C.

Addition of UA resulted in a downshift in the lift-off area of the mixed monolayers; the downshift was more significant for fluid lipids (TE/HSPC/OA and TE/HSPC/BA). The condensing effect of UA, analogous to that of cholesterol,[45−48] was due to the strong attractive hydrophobic and/or van der Waals interactions between the lipids and UA molecules.

Monolayer mechanical properties can easily be assessed by calculating the elasticity modulus (C_s^{-1}), which is the inverse of the film compressibility defined according to the following relation[49]

$$C_s^{-1} = -A\left(\frac{d\pi}{dA}\right)_T \quad (3)$$

The profiles of the elasticity modulus versus the percent of compressed area are shown in Figure 2.

For lipid mixtures in the absence of UA, maximal values were observed at 85, 79, 46, and 37 mN m^{-1} for TB/HSPC/BA, TB/HSPC/OA, TE/HSPC/BA, and TE/HSPC/OA mixtures, respectively. C_s^{-1} values for UA/lipid mixed monolayers reveal a major reduction in the maximum, ranging from 120 to 67 mN m^{-1}, from 95 to 65 mN m^{-1}, from 75 to 30 mN m^{-1}, and from

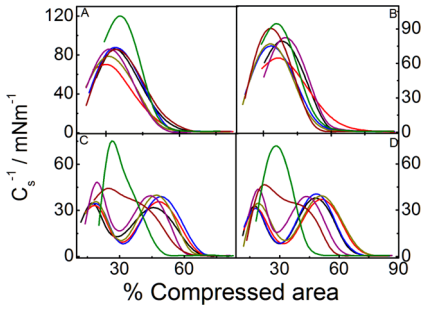

Figure 2. Variation of the inelasticity modulus (C_s^{-1}) with the percent of compressed area for mixed monolayer systems: (A) TB/HSPC/BA, (B) TB/HSPC/OA, (C) TE/HSPC/BA, and (D) TE/HSPC/OA. The lipid mixture was component 1 [2:2:1 (m/m/m)], and ursolic acid was component 2. The mole percents of ursolic acid with respect to the lipid mixture were (black) 0, (red) 2.5, (blue) 5, (brown) 10, (purple) 30, (maroon) 50, and (green) 70. The temperature was 25 °C.

DOI: 10.1021/acs.langmuir.6b02402
Langmuir 2016, 32, 9816−9825

72 to 35 mN m^{-1} for TB/HSPC/BA, TB/HSPC/OA, TE/HSPC/BA, and TE/HSPC/OA mixtures, respectively. Such a decrease indicates a fluidizing effect of UA or the decreased elasticity of the mixed lipid monolayer; the lower the maximal value of the elasticity modulus, the higher the fluidity of the monolayer.[50] An alteration of the molecular area of the UA molecule occupied in the monolayer, a change in the molecular packing effectiveness, and/or a change in the membrane fluidity may induce such modifications in the thermodynamic parameters.

To gain further information about the interactions between the lipids and UA molecules, the excess area (A_{ex}), changes in the excess free energy of mixing (ΔG_{ex}), and changes in the free energy of mixing (ΔG_{mix}) of the lipid/UA monolayers were calculated from the π–A isotherms at different surface pressures. The excess area determines if the mixing is ideal or nonideal. The ideal area of mixing is calculated using eq 4:[50]

$$A_{id} = x_1A_1 + x_2A_2 \tag{4}$$

where x_1 and x_2 are the mole fractions and A_1 and A_2 the areas per molecule of components 1 and 2, respectively. To estimate the deviation from the ideal behavior, the excess area (A_{ex}) was calculated as[50]

$$A_{ex} = A_{12} - A_{id} \tag{5}$$

where A_{12} represents the experimentally obtained mean molecular area. The A_{ex} value of the pseudobinary monolayer was calculated at different surface pressures (from 5 to 30 mN m^{-1} with an interval of 5 mN m^{-1}), as shown in Figure 3.

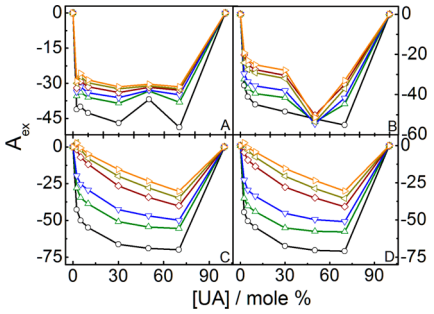

Figure 3. Dependence of the excess molecular area (A_{ex}) on the relative proportion of ursolic acid in the (A) TB/HSPC/BA, (B) TB/HSPC/OA, (C) TE/HSPC/BA, and (D) TE/HSPC/OA mixed monolayer systems. The lipid mixture was component 1 [2:2:1 (m/m/m)], and ursolic acid was component 2. The mole percents of ursolic acid with respect to the lipid mixture were 0, 2.5, 5, 10, 30, 50, 70, and 100 at surface pressures of (○) 5, (△) 10, (▽) 15, (◇) 20, (left-pointing triangles) 25, and (right-pointing triangles) 30 mN m^{-1}. The temperature was 25 °C.

Negative deviations from the ideality for A_{ex} values were recorded for all the lipids and for all mole percents of UA in the entire studied surface pressure range, which indicate attractive interactions among the components. The magnitudes of the negative deviations were higher for the unsaturated lipid (TE) than for the saturated lipid (TB), indicating better incorporation of UA into the mixed monolayer containing unsaturated lipids.

The excess free energy that determines the degree of deviation from the ideally mixed monolayer was calculated using the following expression:[50]

$$\Delta G_{ex}^{\circ} = \int_0^{\pi} [A - (x_1A_1 + x_2A_2)]\, d\pi \tag{6}$$

Changes in the free energy of mixing determine the thermodynamic stability of the monolayers. It can be computed from the excess free energy and the ideal free energy (ΔG_{id}) using eqs 7 and 8:[50]

$$\Delta G_{mix} = \Delta G_{ex} + \Delta G_{id} \tag{7}$$

where the ideal free energy (ΔG_{id}) is given by

$$\Delta G_{id} = RT(x_1 \ln x_1 + x_2 \ln x_2) \tag{8}$$

where R is the universal gas constant and T is the absolute temperature. Negative ΔG_{ex} values, as shown in Figure 4,

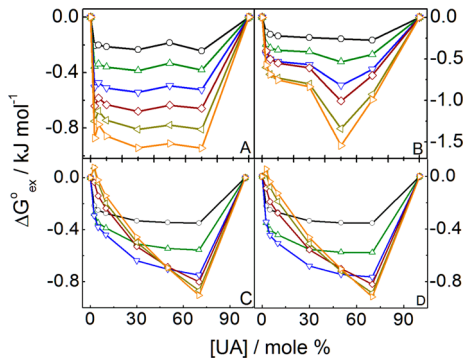

Figure 4. Dependence of the change in excess free energy (ΔG_{ex}°) on the relative proportion of ursolic acid in the (A) TB/HSPC/BA, (B) TB/HSPC/OA, (C) TE/HSPC/BA, and (D) TE/HSPC/OA mixed monolayer systems. The lipid mixture was component 1 [2:2:1 (m/m/m)], and ursolic acid was component 2. The mole percents of ursolic acid with respect to the lipid mixture were 0, 2.5, 5, 10, 30, 50, 70, and 100 at surface pressures of (○) 5, (△) 10, (▽) 15, (◇) 20, (left-pointing triangles) 25, and (right-pointing triangles) 30 mN m^{-1}. The temperature was 25 °C.

indicate spontaneity in the mixing processes between the components.[47,50−52] ΔG_{ex} values were more negative at higher surface pressures. The minimal ΔG_{ex} value was identified at 19, 52, 67, and 69 mol % UA for TB/HSPC/BA, TB/HSPC/OA, TE/HSPC/BA, and TE/HSPC/OA mixtures, respectively, at a π of 10 mN/m. These compositions, therefore, correspond to the most stable lipid/UA mixed films. The surface pressure increase in the loose packing density regimes, $\pi \leq 10$ mN/m (LE and LE/LC phase transitions), caused the ΔG_{ex} values of all the lipid mixtures to become more negative, because of the increase in the level of intermolecular attractive van der Waals forces.

The decrease in the ΔG_{ex} with an increasing mole percent of UA indicates the dependence of the packing of lipid molecules on the relative proportion of UA. A negative ΔG_{mix} value implies spontaneity in the mixing processes and strong interactions between the interfacial components, as shown in Figure S2. Negative ΔG_{mix} values were observed at all surface pressures, thus suggesting spontaneous mutual miscibility among the components. The minimal ΔG_{mix} value was obtained at 50 mol % UA and a surface pressure of 10 mN m^{-1}, corresponding to the composition of the monolayer with the maximal thermodynamic stability.

The dipole moment of the film-forming materials and the change in orientation of head or tail groups in the lipid monolayer as well as of the water molecules in the subphase

DOI: 10.1021/acs.langmuir.6b02402
Langmuir 2016, 32, 9816−9825

Table 1. Mean Sizes (d_h), PDIs, Potentials, Entrapment Efficiencies (EE%), and Loading Capacities (LC%) of Empty and Ursolic Acid-Loaded NLCs[a]

formulation	[UA] (mM)	size (nm)	PDI	ZP (mV)	EE%	LC%
TB/HSPC/BA	0.000	207 ± 2	0.34 ± 0.01	−16 ± 0.4		
	0.125	208 ± 1	0.34 ± 0.009	−17 ± 0.6	78.38 ± 1.9	3.78 ± 0.04
	0.250	210 ± 3	0.35 ± 0.001	−17 ± 0.5	83.55 ± 1.3	3.99 ± 0.09
	0.500	235 ± 5	0.37 ± 0.003	−18 ± 0.4	83.63 ± 0.8	3.99 ± 0.03
TB/HSPC/OA	0.000	196 ± 3	0.38 ± 0.013	−19 ± 0.8		
	0.125	184 ± 5	0.38 ± 0.009	−15 ± 0.7	80.08 ± 0.9	3.88 ± 0.03
	0.250	190 ± 7	0.38 ± 0.006	−17 ± 0.5	85.33 ± 1.5	4.09 ± 0.07
	0.500	191 ± 4	0.40 ± 0.012	−18 ± 0.1	85.56 ± 1.7	4.09 ± 0.04
TE/HSPC/BA	0.000	174 ± 2	0.34 ± 0.009	−19 ± 0.4		
	0.125	183 ± 3	0.35 ± 0.013	−19 ± 0.3	92.97 ± 1.9	4.42 ± 0.07
	0.250	191 ± 7	0.35 ± 0.024	−18 ± 0.7	94.05 ± 1.5	4.53 ± 0.02
	0.500	180 ± 2	0.35 ± 0.005	−18 ± 0.2	94.36 ± 1.7	4.59 ± 0.06
TE/HSPC/OA	0.000	147 ± 5	0.31 ± 0.016	−20 ± 0.2		
	0.125	171 ± 3	0.34 ± 0.009	−20 ± 0.4	97.14 ± 1.8	4.67 ± 0.09
	0.250	185 ± 7	0.35 ± 0.023	−20 ± 0.5	99.92 ± 1.3	4.76 ± 0.07
	0.500	182 ± 4	0.31 ± 0.008	−19 ± 0.3	99.38 ± 1.5	4.76 ± 0.02

[a]$N = 3$ (mean ± SD). Abbreviations: HSPC, hydrogenated soy phosphatidylcholine (common in all the systems); TB, tribehenin; TE, trierucin; BA, behenic acid; OA, oleic acid; LC, loading capacity. Drug concentrations of 0.125, 0.25, and 0.5 mM.

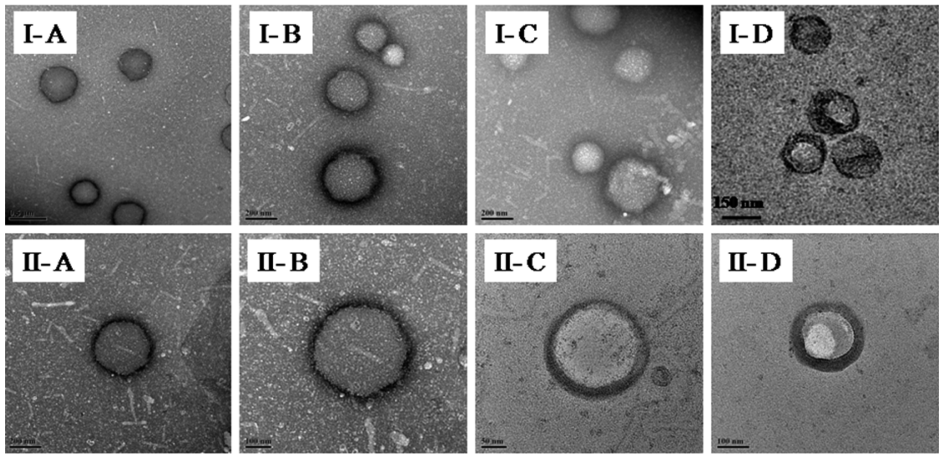

Figure 5. TEM images of (A) TB/HSPC/BA, (B) TB/HSPC/OA, (C) TE/HSPC/BA, and (D) TE/HSPC/OA NLC formulations. I and II denote blank NLCs and ursolic acid-loaded NLCs, respectively.

during compression give the value of surface potential. The surface potential−area measurements have been obtained to gain information about the orientation of the film constituents. Surface potential isotherms of pure components are shown in Figure S3; the formation of mixed lipid monolayers on a subphase containing pure water with and without varying concentrations of UA is shown in Figure S4. The surface potential−area profiles were more or less similar to the surface pressure−area isotherms, further supporting the aforementioned propositions.

Dispersions and Solution Behavior of the NLCs. *Dynamic Light Scattering (DLS) Studies.* The hydrodynamic diameter (d_h), polydispersity index (PDI), and ζ potential (ZP) are some of the markers of colloidal dispersion determining its stability as well as giving insight into the *in vivo* performance of NLCs. NLCs comprising triglyceride, phospholipid, and fatty acids were TB/HSPC/BA, TB/HSPC/OA, TE/HSPC/BA, and TE/HSPC/OA mixtures. The TB/TE:HSPC:BA/OA molar ratio was kept fixed at 2:2:1; the overall lipid concentration was 5 mM dispersed in 10 mM aqueous Tween 80. The size of NLCs ranged from 140 to 230 nm with unimodal distributions. NLC formulations were studied up to 100 days (Figure S5). Particles were found to be fairly monodisperse, as revealed from the size distribution curves (data not shown) as well as from the PDI values (Figure S6). The sizes of TB/HSPC/BA, TB/HSPC/OA, TE/HSPC/BA, and TE/HSPC/OA NLCs were found to be 220 ± 8, 190 ± 7, 174 ± 4, and 147 ± 5 nm, respectively, with size increasing in the following order: TE/HSPC/OA < TE/HSPC/BA < TB/HSPC/OA < TB/HSPC/BA [where the percentages of unsaturation in the fatty acyl hydrocarbon chains were 60, 40, 20, and 0, respectively (Table 1)]. Stronger association among the lipidic components in the case of unsaturated lipid and fatty acid resulted in size constriction compared to that in the saturated lipids.[53,54] The DLS results thus could be correlated with the monolayer studies; the extents of negative deviation from ideality were higher among fluid lipids. An increasing amount of UA increased the size of TB/HSPC/BA and TE/HSPC/BA NLCs (Figure S5A,C). The lower multicrystallinity in the case of the lipid systems with lower degrees of unsaturation restricts the drug molecules mostly to reside on the palisade layer of the NLC, which subsequently results in the

DOI: 10.1021/acs.langmuir.6b02402
Langmuir 2016, 32, 9816−9825

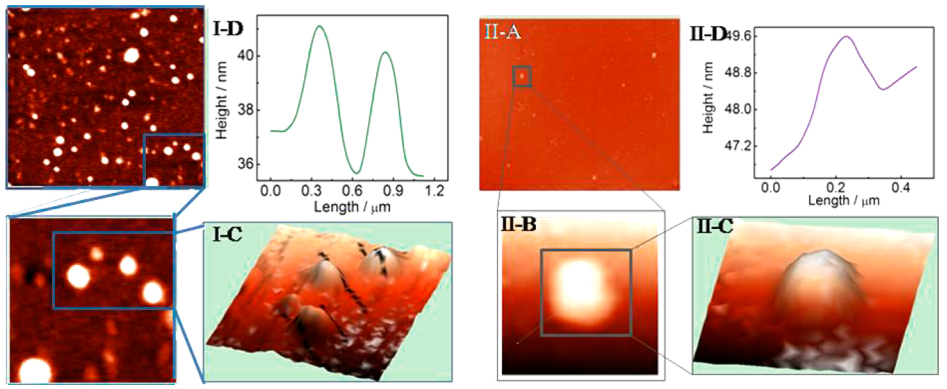

Figure 6. Representative AFM images of (I) TB/HSPC/BA and (II)TE/HSPC/OA NLC formulations. (A and B) Two-dimensional images, (C) three-dimensional images, and (D) and section analysis.

swelling of the NLC leading to an increase in d_h. On the other hand, in the case of more fluidic combinations (TB/HSPC/OA and TE/HSPC/OA), there was an initial increase in size with the addition of drug; the effect became insignificant with size variation at higher drug concentrations (Figure S5B,D).

Better incorporation and drug solubilization in the case of liquid lipids direct the drug to the core of the NLC, resulting in a significant influence of the added drug on d_h. In all cases, the size of the NLC formulations increased with time probably because of the tendency of the NLC formulations to coagulate. PDI values of <0.5 indicate homogeneity of the NLC formulation (Figure S6). A negative ZP was due to the dissociation of fatty acid in NLCs (Figure S7). The extent of dissociation of the incorporated fatty acid was higher for fluid lipids, for which negative values of ZP were recorded. In addition, the liquid lipid reduced d_h and consequently decreased the effective NLC surface area; thus, the ZP values for the systems having larger amounts of liquid lipids were higher. The effect of UA on the ZP of NLCs was not significant because of its nonionic nature. In all cases, the magnitude of ZP decreased with storage time (Figure S7), which was due to the structural modification of lipidic components as well as the Ostwald ripening/coagulation process, common for colloidal dispersions.[55]

Morphological Studies. The size of NLCs, as evaluated from TEM studies (Figure 5), could be well correlated with particle size as determined by DLS measurements. NLCs were spherical with a smooth surface in the case of TB/HSPC/BA and TB/HSPC/OA formulations. While good contrast and distinct images were visualized in the former category, however, in the case of TE/HSPC/BA and TE/HSPC/OA formulations, contrast and distinctness were somehow reduced. It might be due the presence of a larger amount of liquid lipid in the NLC formulation. The existence of individual and distinct particles also indicates the monodisperse nature of the formulations, as was also observed by DLS.[56,57]

Representative AFM images of TB/HSPC/BA and TE/HSPC/OA NLCs are shown in Figure 6. NLCs were found to be spherical with a smooth surface. NLCs were separated from each other, indicating the absence of aggregated species. The observed particle sizes (200−230 nm) were comparable to those of the DLS and TEM studies. The particles were very distinct (Figure 6, II-A and II-B), unlike TE/HSPC/OA NLCs, whose size was found to be in the range of 160−200 nm, with less contrast and distinctiveness. The TB/HSPC/BA and TE/HSPC/OA NLC systems showed the observed vertical dimension to be as large as 4.1 and 2.9 nm, respectively. This could be explained by the presence of larger amounts of unsaturated lipid in the second category of NLCs than in the former.

Di erential Scanning Calorimetric (DSC) Studies. Phase transition temperatures (T_m) of tribehenin, trierucin, behenic acid, oleic acid, hydrogenated soy phosphatidylcholine, and the drug ursolic acid were found to be 82.9, 30.1, 81.4, 14.3, and 283.7 °C, respectively, as shown in Figure S8. The main rationale of this study was to perceive whether the crystallinity differed in the lipid matrices due to the presence of saturation and unsaturation in their mixed states in the form of NLCs. In case of the physical mixtures (where the components were dissolved in organic solvents and subsequently dried under vacuum), the sharp peak of UA, which appeared at 283.7 °C in its pure state, disappeared (data not shown).

This indicates complete solubilization of the amorphous state of ursolic acid in the lipid matrix.[58] The thermal behavior of the physical mixture of lipids and UA with lipids was also assessed (Figure S9). T_m values of the TB/HSPC/BA, TB/HSPC/OA, TB/HSPC/BA/UA, and TB/HSPC/OA/UA physical mixtures appeared at 80.1, 80.4, 77.5, and 77.8 °C, respectively (Figure S9A). T_m values of the TE/HSPC/BA, TE/HSPC/OA, TE/HSPC/BA/UA, and TE/HSPC/OA/UA physical mixtures were 27.9, 19.6, 27.8, and 20.0 °C, respectively (Figure S9B). Table 2 describes the combined thermodynamic parameters, derived from the DSC thermograms. The T_m value of the UA/lipid mixture, however, decreased significantly upon loading of UA into saturated lipid, which indicates a decrease in the crystallinity of the lipid matrix; this may be attributed to UA entrapment in the case of NLCs. On the other hand, the T_m values of the UA/lipid mixture did not change much with loading of UA into unsaturated lipid, although the peak was broader compared to that of the corresponding physical mixture of lipid, which may be attributed to the entrapment of UA in the NLCs. The endothermic and exothermic peaks of the physical mixtures of TB/HSPC/OA NLCs were shifted from 80 to 64 °C and from 30 to 32 °C, respectively, in the presence of UA (Figure S10). This shift was a combined effect of the inclusion of Tween 80 (on the palisade layer) as well as the drug into the core of NLCs. The endothermic peaks were taken into account to derive other associated thermal parameters, viz., changes in enthalpy (ΔH), heat capacity (ΔC_p), and width of the melting peak at half-maxima ($\Delta T_{1/2}$). DSC heating curves of different lipid matrices, viz., TB/HSPC/

DOI: 10.1021/acs.langmuir.6b02402
Langmuir 2016, 32, 9816−9825

Table 2. Temperatures for Maximal Heat Flow (T_m), Widths at Half-Peak Height ($T_{1/2}$), and Changes in Enthalpy (H) and Heat Capacity (C_p) of Blank and UA-Loaded NLCs

formulation	[UA] (mM)	T_m (°C)	$\Delta T_{1/2}$ (°C)	ΔH (kcal mol^{-1})	ΔC_p (kcal mol^{-1} C^{-1})
TB/HSPC/BA	0.000	30.0	2.5	1.49	0.61
	0.125	35.4	2.5	1.81	0.71
	0.250	34.7	2.7	2.62	0.96
	0.500	34.5	2.9	3.72	1.28
TB/HSPC/OA	0.000	29.7	4.9	1.22	0.25
	0.125	30.0	6.6	4.42	0.67
	0.250	29.1	6.9	2.40	0.35
	0.500	26.6	7.5	1.61	0.22
TE/HSPC/BA	0.000	8.0	3.0	1.93	0.65
	0.125	8.6	3.2	3.39	1.06
	0.250	5.9	3.4	7.97	2.32
	0.500	4.0	4.4	9.79	2.21
TE/HSPC/OA	0.000	2.2	4.9	1.92	0.39
	0.125	4.0	5.3	2.55	0.49
	0.250	3.9	5.6	2.55	0.45
	0.500	3.7	5.8	2.52	0.43

BA, TB/HSPC/OA, TE/HSPC/BA, and TE/HSPC/OA NLCs, in the presence and absence of UA are given in Figure 7.

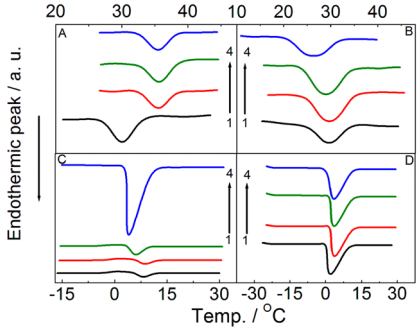

Figure 7. DSC heating curves of ursolic acid-loaded NLCs: (A) TB/HSPC/BA, (B) TB/HSPC/OA, (C) TE/HSPC/BA, and (D) TE/HSPC/OA. Ursolic acid concentrations of (1) 0, (2) 0.125, (3) 0.25, and (4) 0.5 mM. The scan rate was 2.5 °C/min.

Considering the drug free systems, significant changes in the T_m values were noted between saturated and unsaturated lipids as well as fatty acids. The T_m values were 80.1 and 80.4 °C for TB/HSPC/BA and TB/HSPC/OA formulations, respectively, but were 27.9 and 19.6 °C for TE/HSPC/BA and TE/HSPC/OA formulations, respectively. The decrease in T_m with a decrease in the size of NLCs could be explained by the Thomson proposition.[43] It has already been observed from the DLS studies that the NLCs formulated by saturated lipid and fatty acid were larger than the NLCs comprising unsaturated lipid and fatty acid. It is not unexpected that the smaller entities would have melting temperatures lower than those of the larger particles.

In the case of TE/HSPC/OA and TB/HSPC/BA NLCs, the phase transition temperature passed through maxima with an increasing UA concentration. These results indicate that at lower concentrations the drug molecules reside on the surface of NLCs and at higher concentrations the drug molecules are partitioned into the NLC core. In case of TE/HSPC/BA and TB/HSPC/OA NLCs, a progressive decrease in the phase transition temperature was observed with an increase in drug concentration. Increased multicrystallinity, contributed by the added drug, reduces the lowering of phase transition temperature. The liquid lipids further help the drug molecules become introduced into the core and enhance the multicrystallinity, as further supported by the increasing $\Delta T_{1/2}$ with increasing UA concentration. Incorporation of UA also increases ΔH and ΔC_p. The higher multicrystallinity led to the formation of aggregated clusters; consequently, ΔH and ΔC_p increase. In the case of TB/HSPC/OA NLCs, the extent of cluster formulation is lower because of the rigidity of NLCs. Hence, significant enhancement of the phase transition enthalpy and heat capacity was observed at the higher drug concentration for the said NLC formulation.

Determination of UA Entrapment E ciency and Drug Loading Capacity. Entrapment efficiency (EE) and drug loading (DL) capacity values, to estimate the quantity of UA incorporated into the NLCs, are summarized in Table 1 along with other data. The entrapment efficiency decreased in the following order: TE/HSPC/OA > TE/HSPC/BA > TB/HSPC/OA > TB/HSPC/BA (in accordance with the lipophilicity and stronger associative interaction between drugs and lipid molecules). Incorporation of the liquid fatty acid into solid lipids causes a reduction in crystallinity, consequently resulting in more imperfections in the lipid matrix and providing more space for UA molecules.[16,54,59,60] Thus, the proposition of the DSC studies was further supported by such results. The entrapment efficiency and drug loading results are well correlated with monolayer studies. With an increasing concentration of UA, a marked increase in the percentage of encapsulated drug up to 0.25 mM was recorded, beyond which it did not change appreciably.

In Vitro Release Kinetics for Release of Ursolic Acid from NLCs. The cumulative percentage releases of UA from NLC dispersions over 96 h are shown in Figure 8.

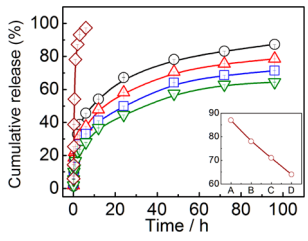

Figure 8. *In vitro* cumulative release of ursolic acid from NLCs. Composition of NLCs: (green triangles) TB/HSPC/BA, (blue squares) TB/HSPC/OA, (red triangles) TE/HSPC/BA, (black circles) TE/HSPC/OA, and (maroon diamonds) free UA in PBS (pH 7.4) and 1% (v/v) Tween 80 at 37 ± 0.1 °C. Error bars represent the standard deviation (SD) of three different release experiments.

Values for the release of UA from the TE/HSPC/OA, TE/HSPC/BA, TB/HSPC/OA, and TB/HSPC/BA formulations of 87, 78, 71, and 64%, respectively, were recorded, as presented in the inset of Figure 8. The release of UA from NLC was dependent on NLC composition.[61] A larger amount of UA was released from the unsaturated lipid blends than from the blends of saturated lipids.[62] Native UA (without any NLC, control) showed more rapid release than UA-loaded NLC, indicating sustained release of UA incorporated into NLC

DOI: 10.1021/acs.langmuir.6b02402
Langmuir 2016, 32, 9816−9825

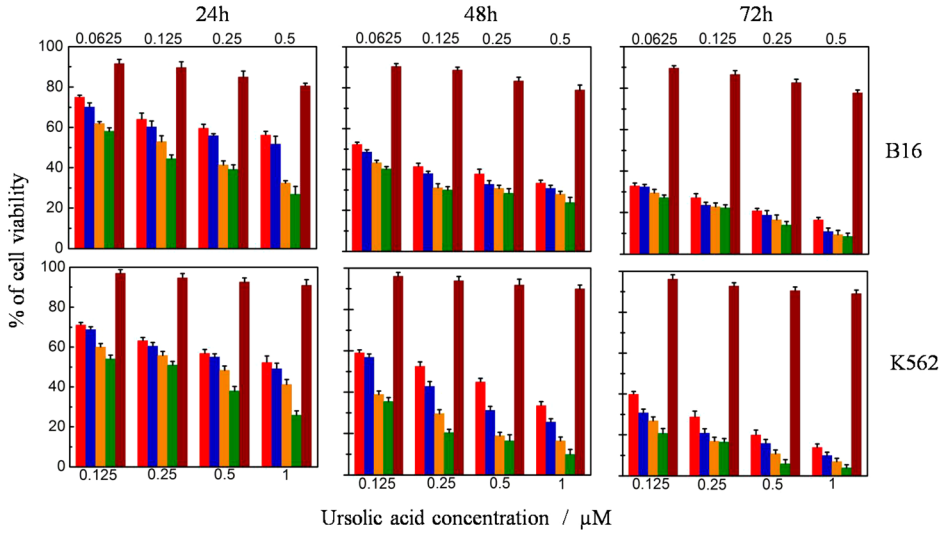

Figure 9. *In vitro* cytotoxicity activity of free ursolic acid (brown) and ursolic acid loaded with different NLCs, TB/HSPC/BA (red), TB/HSPC/OA (blue), TE/HSPC/BA (orange), and TE/HSPC/OA (green), on the viability of B16 and K562 cells. Cells were grown and treated for 24, 48, and 72 h. Experiments were performed in triplicate, with the results showing the mean and standard deviation of the triplicate of each group. The experiments were repeated three times with similar results.

compared to that of native UA. Thus, the NLC dispersion could be a useful carrier with better control of UA release.

The two-step release was observed for UA loaded in all NLCs, as evidenced by the initial burst release within 3 h (39, 31, 26, and 23%) followed by a sustained release up to 96 h (87, 79, 71, and 64%). This could account for the fact that the drug encapsulation efficiency in these NLCs (i.e., matrix type or reservoir type) and surface properties both could affect the release behavior of UA-loaded NLCs.[16] The initial burst release can be explained on the basis of the release of UA enriched in the outer shell of NLCs.

In Vitro Cytotoxicity Studies. *In vitro* cytotoxicity assays were conducted on human melanoma cell line B16 and leukemic cell line K562 by performing the MTT assay for UA upon administration in free forms or loaded in different NLCs, as shown in Figure 9. Blank NLCs did not show any significant cytotoxicity.

IC_{50} values at 24 h for free UA and UA loaded in TE/HSPC/OA and TE/HSPC/BA NLCs were 7.7, 0.041, and 0.10 μM for the B16 cell line and 224.38, 0.14, and 0.23 μM for the K562 cell line, respectively. However, the IC_{50} values of UA at 48 h when it is loaded in TB/HSPC/OA and TB/HSPC/BA NLCs were 0.062, 0.052, 0.09, and 0.19 μM for B16 and K562 cell lines, respectively. Lower IC_{50} values of UA-loaded NLCs, compared to that of free UA, suggest superior activity of the drug-loaded NLC compared to that of the free drug. Cytotoxicities of different UA-loaded NLCs comprising lipid matrices are also important attributes because UA loaded in TE/HSPC/OA and TE/HSPC/BA NLCs showed cytotoxicity higher than that in TB/HSPC/OA and TB/HSPC/BA NLCs in terms of concentration of UA and incubation time. The minimal IC_{50} values, lower incubation times, and higher cytotoxicities for TE/HSPC/OA and TE/HSPC/BA NLCs against both the cell lines could be attributed to the fact that the higher encapsulation efficiency, faster release, and smaller size of the unsaturated lipid led to better internalization of the drug into the cell.

Furthermore, the capability of the formulations increased when either the concentration of UA-loaded NLCs was increased or the incubation time was extended for UA-loaded NLCs. The results indicated that the anticancer activity of UA against both types of cells occurred in a concentration- and time-dependent manner. This dominance may mainly be caused by better internalization of the UA-loaded NLCs and the sustained release of UA inside the cancer cells.[32] It is worth mentioning that UA-loaded NLCs showed remarkable anticancer activities against K562 cells, which is otherwise a multidrug resistant cell line. UA-loaded NLCs thus hold the promise of overcoming multidrug resistance, and this aspect should be extensively exploited in cancer treatment.

CONCLUSIONS

In this study, NLCs comprising saturated and unsaturated lipids and containing pentacyclic triterpenoid ursolic acid were successfully formulated. The findings reveal the influence of saturated and unsaturated lipids and fatty acids on the particle size, polydispersity index, ζ potential, drug encapsulation efficiency, *in vitro* release behavior, and *in vitro* cytotoxicity of the formulation. The studies of surface pressure (π)−area (A) isotherms of pure components, mixed lipids, and mixed lipids with ursolic acid suggest that ursolic acid alters the interfacial organization of lipids. The spherical morphology of NLCs with a smooth surface was observed for all the formulations. Significant differences in crystal structure between NLCs comprising saturated and unsaturated lipids were noted, whereby the crystallinity of UA was lost because of its incorporation into the NLCs. Release of the drug was sustained for all the NLCs; unsaturated lipids exhibited drug release faster than that of saturated components. The most useful finding from this report is the significant difference between the cytotoxicity of free UA and UA-loaded NLCs, which demonstrates the superiority of UA-loaded NLCs over free UA in penetrating the cell membrane. UA in saturated and unsaturated lipids and fatty acid comprising NLCs showed comparable cytotoxicity in human leukemic cell line K562 and melanoma cell line B16 and enhanced anticancer activity. Conclusively, both saturated and unsaturated lipid-containing

DOI: 10.1021/acs.langmuir.6b02402
Langmuir 2016, 32, 9816−9825

NLCs formulated in this study may be used as potential delivery systems for UA with improved anticancer activity.

■ ASSOCIATED CONTENT

Supporting Information

The Supporting Information is available free of charge on the ACS Publications website at DOI: 10.1021/acs.langmuir.6b02402.

Additional findings (PDF)

■ AUTHOR INFORMATION

Corresponding Author

*Department of Chemistry and Chemical Technology, Vidyasagar University, Midnapore 721 102, West Bengal, India. E-mail: akpanda@mail.vidyasagar.ac.in. Phone: +919433347210. Fax: +91322275329/297.

Notes

The authors declare no competing financial interest.

■ ACKNOWLEDGMENTS

Financial support in the form of a research grant (SR/S1/PC/32/2011) from the Department of Science and Technology, Government of India, New Delhi, is sincerely acknowledged. P.N. acknowledges the receipt of a research fellowship from the University Grant Commission, New Delhi, under the Rajiv Gandhi National Fellowship for the disabled (F./2012-13/RGNF-2012-13D-GENCHH-51106/31-Oct-2013). B.A.N. and A.K.P. sincerely acknowledge the support from the Indo-Russian Collaborative research project, funded by the Department of Science and Technology, Government of India (Project INT/RUS/RFBR/P-220), and the Russian Foundation of Basic Research (RFBR N° 15-53-45043_IND_a). A.G.B., A.V.A., and B.A.N. acknowledge St. Petersburg State University for Research Grant 12.38.241.2014. P.N. sincerely acknowledges the valuable guidance from Dr. B. Achari of the CSIR-Indian Institute of Chemical Biology, Kolkata, India.

■ REFERENCES

(1) Baird, R. D.; Kaye, S. B. Drug resistance reversal–are we getting closer? *Eur. J. Cancer* **2003**, *39* (17), 2450–61.

(2) Gieseler, F.; Rudolph, P.; Kloeppel, G.; Foelsch, U. R. Resistance mechanisms of gastrointestinal cancers: why does conventional chemotherapy fail? *Int. J. Colorectal Dis.* **2003**, *18* (6), 470–80.

(3) Schilsky, R. L.; Milano, G. A.; Ratain, M. J. *Principles of Antineoplastic Drug Development and Pharmacology*; Taylor & Francis: New York, 1996; pp 457–486.

(4) Junyaprasert, V. B.; Morakul, B. Nanocrystals for enhancement of oral bioavailability of poorly water-soluble drugs. *Asian J. Pharm. Sci.* **2015**, *10* (1), 13–23.

(5) Khadka, P.; Ro, J.; Kim, H.; Kim, I.; Kim, J. T.; Kim, H.; Cho, J. M.; Yun, G.; Lee, J. Pharmaceutical particle technologies: An approach to improve drug solubility, dissolution and bioavailability. *Asian J. Pharm. Sci.* **2014**, *9* (6), 304–316.

(6) Müller, R.; Petersen, R.; Hommoss, A.; Pardeike, J. Nanostructured lipid carriers (NLC) in cosmetic dermal products. *Adv. Drug Delivery Rev.* **2007**, *59* (6), 522–530.

(7) Dang, H.; Meng, M. H. W.; Zhao, H.; Iqbal, J.; Dai, R.; Deng, Y.; Lv, F. Luteolin-loaded solid lipid nanoparticles synthesis, characterization, & improvement of bioavailability, pharmacokinetics in vitro and vivo studies. *J. Nanopart. Res.* **2014**, *16* (4), 2347.

(8) Gaur, P. K.; Mishra, S.; Bajpai, M.; Mishra, A. Enhanced Oral Bioavailability of Efavirenz by Solid Lipid Nanoparticles: In Vitro Drug Release and Pharmacokinetics Studies. *BioMed Res. Int.* **2014**, *2014*, 9.

(9) Kaur, I. P.; Bhandari, R.; Bhandari, S.; Kakkar, V. Potential of solid lipid nanoparticles in brain targeting. *J. Controlled Release* **2008**, *127* (2), 97–109.

(10) Mehnert, W.; Mäder, K. Solid lipid nanoparticles: production, characterization and applications. *Adv. Drug Delivery Rev.* **2001**, *47* (2), 165–196.

(11) Wong, H. L.; Bendayan, R.; Rauth, A. M.; Li, Y.; Wu, X. Y. Chemotherapy with anticancer drugs encapsulated in solid lipid nanoparticles. *Adv. Drug Delivery Rev.* **2007**, *59* (6), 491–504.

(12) Hu, F.-Q.; Jiang, S.-P.; Du, Y.-Z.; Yuan, H.; Ye, Y.-Q.; Zeng, S. Preparation and characteristics of monostearin nanostructured lipid carriers. *Int. J. Pharm.* **2006**, *314* (1), 83–89.

(13) Shen, J.; Sun, M.; Ping, Q.; Ying, Z.; Liu, W. Incorporation of liquid lipid in lipid nanoparticles for ocular drug delivery enhancement. *Nanotechnology* **2010**, *21* (2), 025101.

(14) Pardeike, J.; Weber, S.; Haber, T.; Wagner, J.; Zarfl, H. P.; Plank, H.; Zimmer, A. Development of an Itraconazole-loaded nanostructured lipid carrier (NLC) formulation for pulmonary application. *Int. J. Pharm.* **2011**, *419* (1–2), 329–338.

(15) Teeranachaideekul, V.; Souto, E. B.; Junyaprasert, V. B.; Müller, R. H. Cetyl palmitate-based NLC for topical delivery of Coenzyme Q 10–Development, physicochemical characterization and in vitro release studies. *Eur. J. Pharm. Biopharm.* **2007**, *67* (1), 141–148.

(16) Souto, E. B.; Wissing, S. A.; Barbosa, C. M.; Müller, R. H. Development of a controlled release formulation based on SLN and NLC for topical clotrimazole delivery. *Int. J. Pharm.* **2004**, *278* (1), 71–77.

(17) Yuan, H.; Wang, L.-L.; Du, Y.-Z.; You, J.; Hu, F.-Q.; Zeng, S. Preparation and characteristics of nanostructured lipid carriers for control-releasing progesterone by melt-emulsification. *Colloids Surf., B* **2007**, *60* (2), 174–179.

(18) Goutayer, M.; Dufort, S.; Josserand, V.; Royère, A.; Heinrich, E.; Vinet, F.; Bibette, J.; Coll, J.-L.; Texier, I. Tumor targeting of functionalized lipid nanoparticles: assessment by in vivo fluorescence imaging. *Eur. J. Pharm. Biopharm.* **2010**, *75* (2), 137–147.

(19) Teskač, K.; Kristl, J. The evidence for solid lipid nanoparticles mediated cell uptake of resveratrol. *Int. J. Pharm.* **2010**, *390* (1), 61–69.

(20) Yuan, H.; Miao, J.; Du, Y.-Z.; You, J.; Hu, F.-Q.; Zeng, S. Cellular uptake of solid lipid nanoparticles and cytotoxicity of encapsulated paclitaxel in A549 cancer cells. *Int. J. Pharm.* **2008**, *348* (1–2), 137–145.

(21) Chen, C.-C.; Tsai, T.-H.; Huang, Z.-R.; Fang, J.-Y. Effects of lipophilic emulsifiers on the oral administration of lovastatin from nanostructured lipid carriers: physicochemical characterization and pharmacokinetics. *Eur. J. Pharm. Biopharm.* **2010**, *74* (3), 474–482.

(22) Müller, R.; Radtke, M.; Wissing, S. Nanostructured lipid matrices for improved microencapsulation of drugs. *Int. J. Pharm.* **2002**, *242* (1), 121–128.

(23) Teeranachaideekul, V.; Müller, R. H.; Junyaprasert, V. B. Encapsulation of ascorbyl palmitate in nanostructured lipid carriers (NLC) effects of formulation parameters on physicochemical stability. *Int. J. Pharm.* **2007**, *340* (1), 198–206.

(24) Laszczyk, M. N. Pentacyclic triterpenes of the lupane, oleanane and ursane group as tools in cancer therapy. *Planta Med.* **2009**, *75* (15), 1549–60.

(25) Checker, R.; Sandur, S. K.; Sharma, D.; Patwardhan, R. S.; Jayakumar, S.; Kohli, V.; Sethi, G.; Aggarwal, B. B.; Sainis, K. B. Potent anti-inflammatory activity of ursolic acid, a triterpenoid antioxidant, is mediated through suppression of NF-κB, AP-1 and NF-AT. *PLoS One* **2012**, *7* (2), e31318.

(26) Chiang, L.; Chiang, W.; Chang, M.; Ng, L.; Lin, C. Antiviral activity of Plantago major extracts and related compounds in vitro. *Antiviral Res.* **2002**, *55* (1), 53–62.

(27) Chung, P. Y.; Navaratnam, P.; Chung, L. Y. Synergistic antimicrobial activity between pentacyclic triterpenoids and antibiotics against Staphylococcus aureus strains. *Ann. Clin. Microbiol. Antimicrob.* **2011**, *10* (1), 25.

DOI: 10.1021/acs.langmuir.6b02402
Langmuir 2016, 32, 9816–9825

(28) Saravanan, R.; Viswanathan, P.; Pugalendi, K. V. Protective effect of ursolic acid on ethanol-mediated experimental liver damage in rats. *Life Sci.* **2006**, *78* (7), 713−718.
(29) Yan, S.-l.; Huang, C.-y.; Wu, S.-t.; Yin, M. -c., Oleanolic acid and ursolic acid induce apoptosis in four human liver cancer cell lines. *Toxicol. In Vitro* **2010**, *24* (3), 842−848.
(30) Caldeira de Araújo Lopes, S.; Vinícius Melo Novais, M.; Salviano Teixeira, C.; Honorato-Sampaio, K.; Tadeu Pereira, M.; Ferreira, L. A. M.; Braga, F. C.; Oliveira, M. C. Preparation, Physicochemical Characterization, and Cell Viability Evaluation of Long-Circulating and pH-Sensitive Liposomes Containing Ursolic Acid. *BioMed Res. Int.* **2013**, *2013*, 7.
(31) Song, J.; Wang, Y.; Song, Y.; Chan, H.; Bi, C.; Yang, X.; Yan, R.; Wang, Y.; Zheng, Y. Development and characterisation of ursolic acid nanocrystals without stabiliser having improved dissolution rate and in vitro anticancer activity. *AAPS PharmSciTech* **2014**, *15* (1), 11−19.
(32) Zhang, H.; Li, X.; Ding, J.; Xu, H.; Dai, X.; Hou, Z.; Zhang, K.; Sun, K.; Sun, W. Delivery of ursolic acid (UA) in polymeric nanoparticles effectively promotes the apoptosis of gastric cancer cells through enhanced inhibition of cyclooxygenase 2 (COX-2). *Int. J. Pharm.* **2013**, *441* (1−2), 261−8.
(33) Zhang, H.; Zheng, D.; Ding, J.; Xu, H.; Li, X.; Sun, W. Efficient delivery of ursolic acid by poly(N-vinylpyrrolidone)-block-poly (ε-caprolactone) nanoparticles for inhibiting the growth of hepatocellular carcinoma in vitro and in vivo. *Int. J. Nanomed.* **2015**, *10*, 1909−1920.
(34) Alvarado, H. L.; Abrego, G.; Garduno-Ramirez, M. L.; Clares, B.; Calpena, A. C.; Garcia, M. L. Design and optimization of oleanolic/ursolic acid-loaded nanoplatforms for ocular anti-inflammatory applications. *Nanomedicine* **2015**, *11* (3), 521−30.
(35) Jin, H.; Pi, J.; Yang, F.; Wu, C.; Cheng, X.; Bai, H.; Huang, D.; Jiang, J.; Cai, J.; Chen, Z. W. Ursolic acid-loaded chitosan nanoparticles induce potent anti-angiogenesis in tumor. *Appl. Microbiol. Biotechnol.* **2016**, *100*, 6643−6652.
(36) Yang, L.; Sun, Z.; Zu, Y.; Zhao, C.; Sun, X.; Zhang, Z.; Zhang, L. Physicochemical properties and oral bioavailability of ursolic acid nanoparticles using supercritical anti-solvent (SAS) process. *Food Chem.* **2012**, *132* (1), 319−325.
(37) Mandelli Almeida, M.; Nadia, A. B.-C.; Denise, C. J.; Mary, K. T.; Rolim, B. A.; Robles, V. M. V. Evaluation of physical and chemical stability of nanostructured lipid carries containing ursolic acid in cosmetic formulation. *J. Appl. Pharm. Sci.* **2013**, *3* (3), 5−8.
(38) Zhou, X. J.; Hu, X. M.; Yi, Y. M.; Wan, J. Preparation and body distribution of freeze-dried powder of ursolic acid phospholipid nanoparticles. *Drug Dev. Ind. Pharm.* **2009**, *35* (3), 305−10.
(39) Lopes, S. C.; Novais, M. V.; Ferreira, D. S.; Braga, F. C.; Magalhães-Paniago, R.; Malachias, A.; Oliveira, M. C. Ursolic acid incorporation does not prevent the formation of a non-lamellar phase in pH-sensitive and long-circulating liposomes. *Langmuir* **2014**, *30* (50), 15083−15090.
(40) de Oliveira Eloy, J.; Saraiva, J.; de Albuquerque, S.; Marchetti, J. M. Solid dispersion of ursolic acid in Gelucire 50/13: a strategy to enhance drug release and trypanocidal activity. *AAPS PharmSciTech* **2012**, *13* (4), 1436−45.
(41) Vyas, A. Preparation and characterization of the inclusion complex of ursolic acid with polymerized hydrophilic cyclodextrin. *Planta Med.* **2015**, *81* (05), PP20.
(42) Wei, Z.; Bi, S. M. The Preparation and Characterization of Inclusion Complex of Ursolic Acid with γ-Cyclodextrin. *Adv. Mater. Res.* **2011**, *403*−*408*, 712−716.
(43) Nahak, P.; Karmakar, G.; Roy, B.; Guha, P.; Sapkota, M.; Koirala, S.; Chang, C.-H.; Panda, A. K. Physicochemical studies on local anaesthetic loaded second generation nanolipid carriers. *RSC Adv.* **2015**, *5* (33), 26061−26070.
(44) Jain, A. K.; Jain, A.; Garg, N. K.; Agarwal, A.; Jain, A.; Tyagi, R. K.; Jain, S. A.; Jain, R. K.; Agrawal, H.; Agrawal, G. P. Adapalene loaded solid lipid nanoparticles gel: an effective approach for acne treatment. *Colloids Surf., B* **2014**, *121*, 222−229.
(45) Alwarawrah, M.; Dai, J.; Huang, J. A Molecular View of the Cholesterol Condensing Effect in DOPC Lipid Bilayers. *J. Phys. Chem. B* **2010**, *114* (22), 7516−7523.
(46) Nowotarska, S. W.; Nowotarski, K. J.; Friedman, M.; Situ, C. Effect of structure on the interactions between five natural antimicrobial compounds and phospholipids of bacterial cell membrane on model monolayers. *Molecules* **2014**, *19* (6), 7497−515.
(47) Panda, A. K.; Nag, K.; Harbottle, R. R.; Possmayer, F.; Petersen, N. O. Thermodynamic studies on mixed molecular langmuir films: Part 2. Mutual mixing of DPPC and bovine lung surfactant extract with long-chain fatty acids. *Colloids Surf., A* **2004**, *247* (1−3), 9−17.
(48) Yasmann, A.; Sukharev, S. Properties of Diphytanoyl Phospholipids at the Air−Water Interface. *Langmuir* **2015**, *31* (1), 350−357.
(49) Karmakar, G.; Nahak, P.; Guha, P.; Roy, B.; Chettri, P.; Sapkota, M.; Koirala, S.; Misono, T.; Torigoe, K.; Ghosh, S.; Panda, A. K. Effects of Fatty Acids on the Interfacial and Solution Behavior of Mixed Lipidic Aggregates Called Solid Lipid Nanoparticles. *J. Oleo Sci.* **2016**, *65* (5), 419−430.
(50) Guha, P.; Roy, B.; Karmakar, G.; Nahak, P.; Koirala, S.; Sapkota, M.; Misono, T.; Torigoe, K.; Panda, A. K. Ion-Pair Amphiphile: A Neoteric Substitute That Modulates the Physicochemical Properties of Biomimetic Membranes. *J. Phys. Chem. B* **2015**, *119* (11), 4251−4262.
(51) Chou, T.-H.; Chang, C.-H. Thermodynamic Characteristics of Mixed DPPC/DHDP Monolayers on Water and Phosphate Buffer Subphases. *Langmuir* **2000**, *16* (7), 3385−3390.
(52) Panda, A. K.; Nag, K.; Harbottle, R. R.; Possmayer, F.; Petersen, N. O. Thermodynamic studies of bovine lung surfactant extract mixing with cholesterol and its palmitate derivative. *J. Colloid Interface Sci.* **2007**, *311* (2), 551−555.
(53) Fang, J.-Y.; Fang, C.-L.; Liu, C.-H.; Su, Y.-H. Lipid nanoparticles as vehicles for topical psoralen delivery: Solid lipid nanoparticles (SLN) versus nanostructured lipid carriers (NLC). *Eur. J. Pharm. Biopharm.* **2008**, *70* (2), 633−640.
(54) Gaba, B.; Fazil, M.; Khan, S.; Ali, A.; Baboota, S.; Ali, J. Nanostructured lipid carrier system for topical delivery of terbinafine hydrochloride. *Bull. Fac. Pharm.* **2015**, *53* (2), 147−159.
(55) Wooster, T. J.; Golding, M.; Sanguansri, P. Impact of oil type on nanoemulsion formation and Ostwald ripening stability. *Langmuir* **2008**, *24* (22), 12758−65.
(56) Neupane, Y. R.; Srivastava, M.; Ahmad, N.; Kumar, N.; Bhatnagar, A.; Kohli, K. Lipid based nanocarrier system for the potential oral delivery of decitabine: Formulation design, characterization, ex vivo, and in vivo assessment. *Int. J. Pharm.* **2014**, *477* (1−2), 601−612.
(57) Sütö, B.; Berkó, S.; Kozma, G.; Kukovecz, Á.; Budai-Szücs, M.; Erös, G.; Kemény, L.; Sztojkov-Ivanov, A.; Gáspár, R.; Csányi, E. Development of ibuprofen-loaded nanostructured lipid carrier-based gels: characterization and investigation of in vitro and in vivo penetration through the skin. *Int. J. Nanomed.* **2016**, *11*, 1201−1212.
(58) Kashanian, S.; Rostami, E. PEG-stearate coated solid lipid nanoparticles as levothyroxine carriers for oral administration. *J. Nanopart. Res.* **2014**, *16* (3), 1−10.
(59) Jenning, V.; Thunemann, A. F.; Gohla, S. H. Characterisation of a novel solid lipid nanoparticle carrier system based on binary mixtures of liquid and solid lipids. *Int. J. Pharm.* **2000**, *199* (2), 167−77.
(60) Patel, D.; Dasgupta, S.; Dey, S.; Ramani, Y. R.; Ray, S.; Mazumder, B. Nanostructured Lipid Carriers (NLC)-Based Gel for the Topical Delivery of Aceclofenac: Preparation, Characterization, and In Vivo Evaluation. *Sci. Pharm.* **2012**, *80* (3), 749−764.
(61) Venishetty, V. K.; Chede, R.; Komuravelli, R.; Adepu, L.; Sistla, R.; Diwan, P. V. Design and evaluation of polymer coated carvedilol loaded solid lipid nanoparticles to improve the oral bioavailability: A novel strategy to avoid intraduodenal administration. *Colloids Surf., B* **2012**, *95*, 1−9.
(62) Carafa, M.; Santucci, E.; Lucania, G. Lidocaine-loaded non-ionic surfactant vesicles: characterization and in vitro permeation studies. *Int. J. Pharm.* **2002**, *231* (1), 21−32.

DOI: 10.1021/acs.langmuir.6b02402
Langmuir 2016, 32, 9816−9825

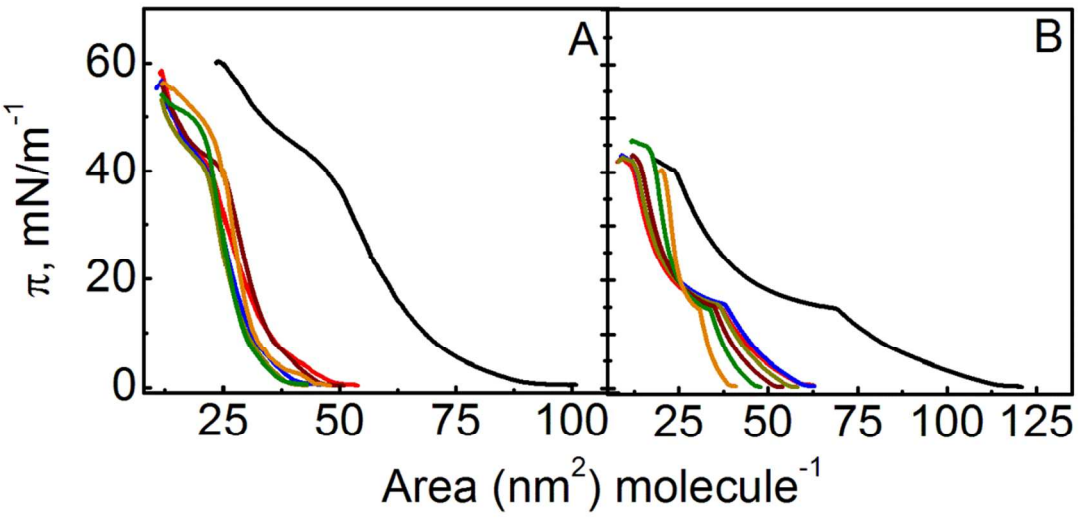

! " # $
% # & % ’ (
#) * + (, - .! , - /)0! , - 0! , - 1.!
, - 2.! , - 0.! , - 3.) /04)

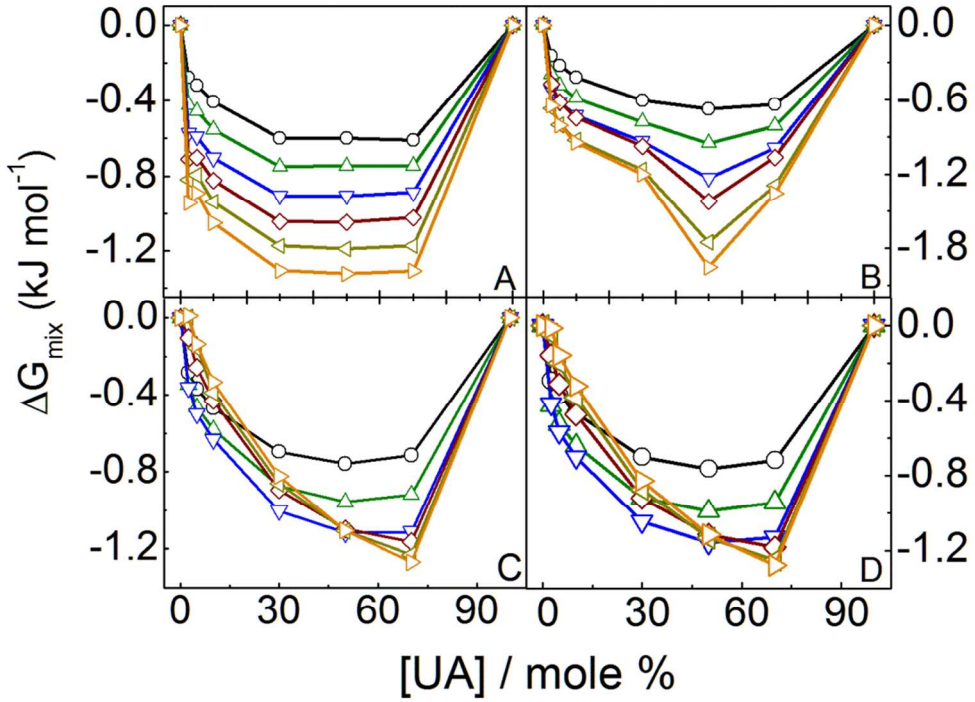

’ ’% ’ 56 &
% % ! !
" ! " 7 - - 1- / / 1-
*8*8* - /) * + (.-
/)0- 0- 1.- 2.- 0.- 3. 1.. 9 $1 :- 0! △- 1.! ▽ 10! ; /.! ◁-
/0 ▷- 2.)) /0 4)

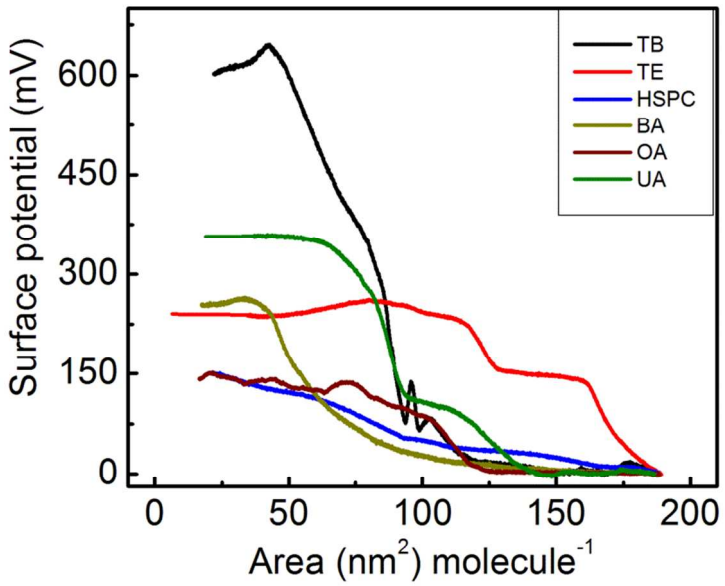

! %

’) ((#)) /0 4)

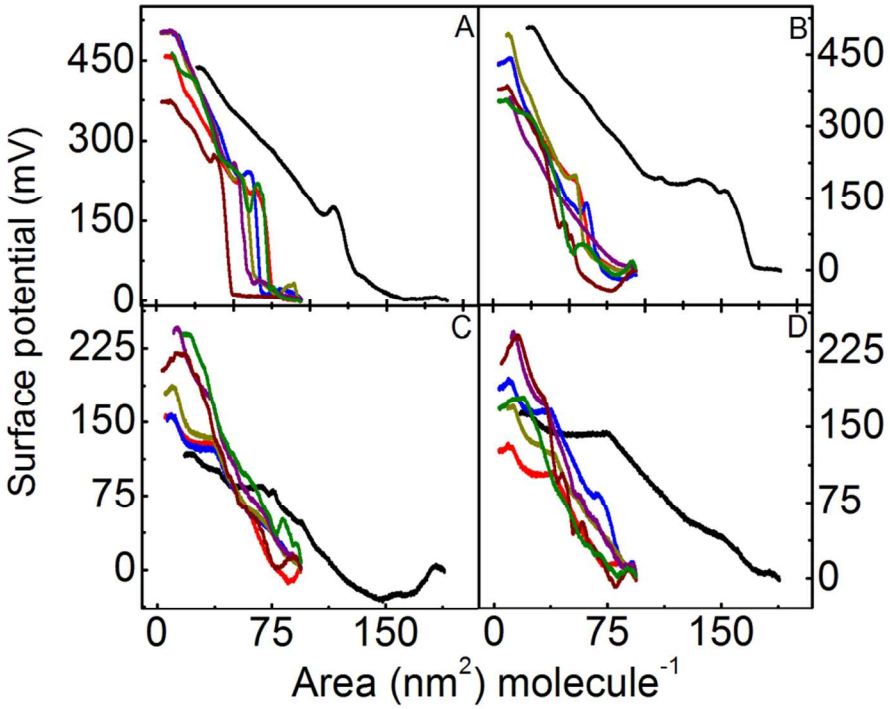

<

! ! " !

" 7 # % #

& % ’ (#) * + (

, .! , - /)0! , - 0! , - 1.! , - 2.! , - 0.! , - 3.)) /0 4)

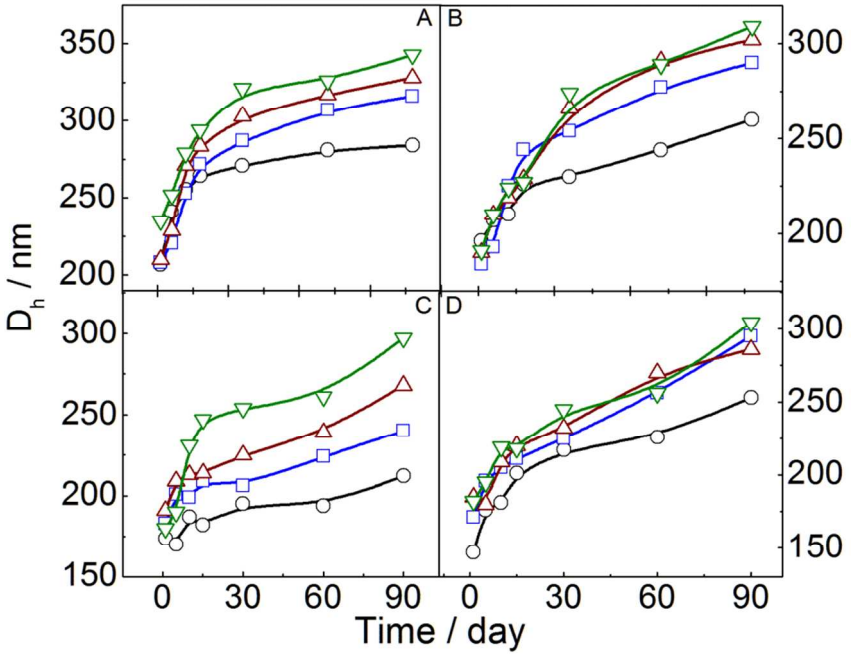

< % % 9=

! ! " 7

") 0 * 9= (1. * (>.) ?

* : - .! @ - .)1/0! △ - .)/0 ▽ - .)0)) /0 4)

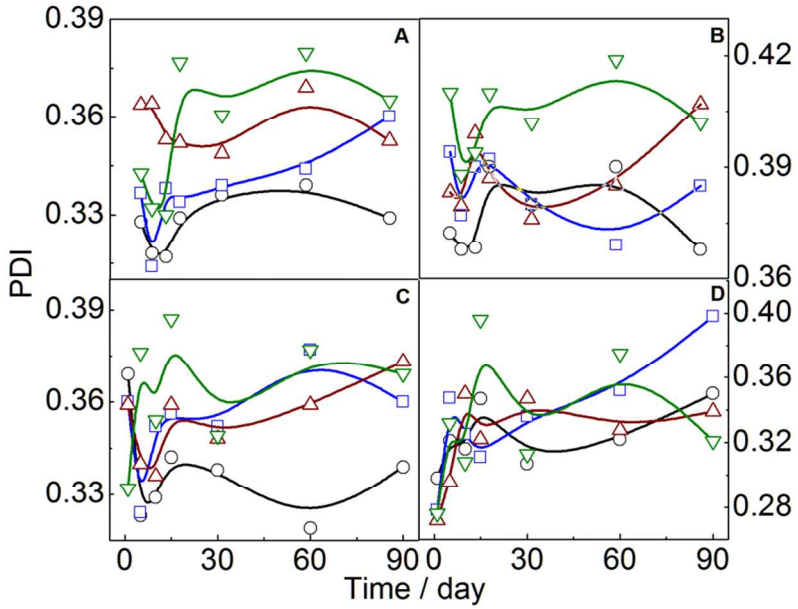

< % % 7A 9=

! ! " 7

") 0 * 9= (1. * (>.) ?

* : - .! @ - .)1/0! △ - .)/0 ▽ - .)0)) /0 4)

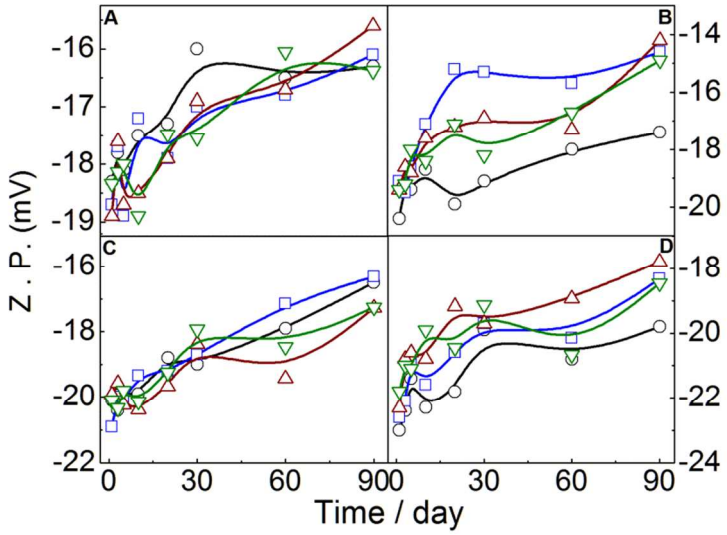

< B C)) 9= !
! " 7 ") 0 * 9=
(1. * (>.) ? * : - .! @ - .)1/0!
△ - .)/0 ▽ - .)0)) /0 4)

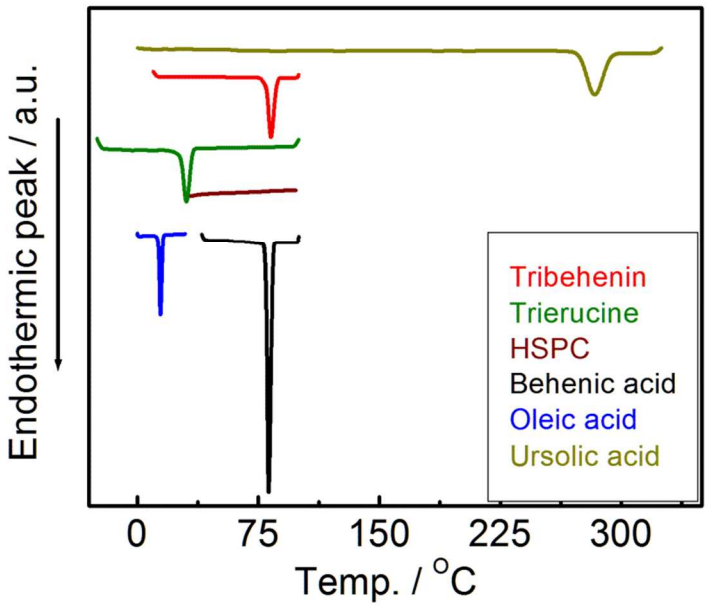

7 ’ ’ ? ! %
’) /)0 4 [$1])